ENHANCEMENT OF ULTRASONIC AND ULTRAVIOLET IRRADIATION WITH CHEMICAL OXIDANTS

Thesis by

Linda Weavers

In Partial Fulfillment of the Requirements

for the Degree of

Doctor of Philosophy

California Institute of Technology

Pasadena, CA

1998

(Submitted Dec. 2, 1997)

To my sister, Susie, who is always with me in spirit...

Acknowledgments

Help from more people than I ever imagined was needed to do this "independent" research. First and foremost is my advisor, Michael Hoffmann, who accepted me into his research group although I didn't even know what a pipette was. I am grateful for his patience in allowing me to pursue the projects that interested me. Steve Eisenreich got me here in the beginning by easing my anxieties about Caltech with his reply, "Well, maybe it is a *little* harder than the University of Minnesota." Also, I wish to thank my examining committee: Dr. Brennen, Dr. Hering, Dr. Hoffmann, and Dr. Morgan.

Being a frazzled and naive first-year, I was initiated into the lab by Inez Hua who became a friend as we traded recipes as well as glassware. Ralf Höchemer was a constant source of research ideas and laughs. Anne Johansen always had an ear to listen to my troubles, was constantly ready for beer breaks, and showed me more about the IC than I wanted to know. Although Scot Martin and I fought over my banana habits, he gave me useful advice on how to be a wise graduate student. My simple bubble model exploded into a major effort in the last weeks of my time at Caltech, which would not have been possible without A. J. Colussi's continual efforts to improve the model and understand bubble dynamics. I think I learned more about physical chemistry and thermodynamics from him than I could have in a year long course. I cannot forget the other members of the Hoffmann and Morgan groups who have helped along the way including: Weng-Ki Ching, Wonyong Choi, Yael Dubowski, Hui-Ming Hung, Janet Kesselman, Axel Kratel,

Pat Lang, Tom Lloyd, Simo Pehkonen, Nicole Peill, Ron Seifert, Steve Szczepankiewicz, and Dean Willberg.

The undergraduates who performed experiment, after experiment, after experiment cannot be forgotten. Frank Ling performed the majority of the experiments in Chapter 3. His zany nature livened up tedious lab work. Noah Malmstadt whirled into lab for 6 weeks and had no trouble learning all the experimental techniques necessary to "finish up" the experiments of Chapter 5. And Leah Foechterle helped along the way as well.

The support staff of Linda Scott, Fran Matzen, Andrea Wilson, Rayma Harrison, and Susan Leising were always happy to find anything I needed or solve any problem I had. Peter Green had useful advice on how to analyze any bizarre compound I could dream up and Yaniv Dubowski was a cheerful face and kept me from throwing computer equipment off the roof when I couldn't get things to work.

To Pat Chuang, I owe a special thanks. I may not have made it *to* the research effort of the Ph. D. if it were not for his patience and determination to make me understand PDE's, aerosols, and the finer points of complex variables when I had all but given up. I have been trying to pay him back with as many dinners and as much beer as possible.

Many other people have provided useful and necessary distractions over the last 5 years. Matt Fraser was always available for swimming, golfing, skiing, sledding, or other random diversions. Miriam Jackson provided a tennis partner as well as ridicule since she could beat me even though she was 8 months pregnant. Hali Forstner, Michelle Wild, Mike Kleeman, Lisa Thurston, Mike Hannigan, Chris Nolte, Don Collins, and Courtney Kennedy made life more bearable.

Although sometimes I seemed ungrateful, my parents' encouragement, guidance, and advice have helped make me the person I am today.

Finally, I cannot thank Paul Sivilotti enough for all of his support both intellectually and emotionally. We are defending one day apart, but he has still been more helpful and caring than I could imagine.

Abstract

The combination of ultrasound and ozone was used to study the degradation of nitrobenzene, 4-nitrophenol, 4-chlorophenol, cyclohexene, and pentachlorophenol in aqueous solutions. Using ultrasonic frequencies of 20 and 500 kHz revealed apparent enhancement at 20 kHz and antagonism at 500 kHz for the combined system although the first-order degradation rate constants in the absence of O_3 (ozone) was typically a factor of 10 larger at 500 kHz. A comparison of the first-order degradation rate constants for nitrobenzene, 4-nitrophenol, and 4-chlorophenol by sonication, ozonation, and the combination of sonication and ozonation revealed that the observed enhancement upon the combination of ultrasound and ozone is mainly the result of thermolytic decomposition of ozone in a collapsing cavitation bubble. A continuous flow reactor closed to the atmosphere, open to the atmosphere, and open to the atmosphere with gas bubbling was used to probe the effects of ultrasound on O_3 mass transfer. Enhanced mass transfer of O_3 appeared to be the result of rapid decomposition of O_3 in a cavitation bubble. The degradation of pentachlorophenol and observation of intermediates showed OH attack of the aromatic ring. A chemical kinetic model was developed to gain insight into the formation of radicals in various bubbles at 20 and 500 kHz with and without O_3 present. The model revealed O_3 pyrolysis slightly before the end of collapse followed rapid free-radical formation in the last nanoseconds due to H_2O and O_2 decomposition.

In addition, a new advanced oxidation process, photoactivated periodate, was

developed to investigate the decomposition of triethanolamine, its associated chemical oxygen demand, and the oxidation of an industrial wastewater. The optimal pH for COD degradation was determined to be pH 7.6 due to the combined effects of pH on the speciation of TEA and IO_4^-. Increasing the $[IO_4^-]_0/[TEA]_0$ ratio increased the degradation rate up to an apparent saturation value. Irradiation with a 1000 W Hg(Xe) lamp increased the pseudo first-order degradation rate constant of COD by a factor of 5.5 for synthetic TEA solutions and 2.3 for the industrial wastewater as compared to irradiation with a 1000 W Xe lamp.

Table of Contents

List of Figures

List of Tables

Chapter 1

Introduction and Motivation

Advanced oxidation processes (AOPs) such as ultrasonic and ultraviolet irradiation have been shown to be effective for the elimination of organic and inorganic pollutants from water (1-47). AOPs are generally grouped together because they all result in the in situ formation of radicals or more specifically, hydroxyl radicals, in sufficient quantity to affect water treatment (27,48). These processes are often needed when conventional approaches to water and wastewater treatment are ineffective. However, AOPs are often costly and sometimes ineffective for the degradation of contaminants in water or wastewater that contains a mixture of organic and inorganic compounds.

To overcome some of the deficiencies of traditional AOPs, chemical oxidants can add additional oxidizing power to reach target levels of water quality. Oxidants such as ozone and periodate have high oxidation potentials but are either selective, have large activation energies, or both. Combining these oxidants with ultrasound or ultraviolet irradiation broadens the range of compounds that can be degraded by the creation of reactive free radicals. Activation energies of free radical reactions with compounds are typically less than those of multi-electron oxidants. Depending on the cost of the oxidants, the overall cost of using AOPs may be decreased by reducing the time required for oxidations to occur.

The primary goal of this research was to explore rate enhancement with these oxidants and gain some understanding of the mechanisms of enhancement. With sonolytic ozonation or photoactivated periodate, significant generation of free radicals and catalytic cycle formation was observed via increased degradation rates of organic contaminants in these systems.

In the ultrasonic system, pyrolysis of O_3 in a cavitation bubble and subsequent formation of OH• was investigated by the degradation of three similar aromatic compounds, nitrobenzene (NB), 4-nitrophenol (4-NP), and 4-chlorophenol (4-CP) as explained in Chapter 3. Chapter 4 explored the various mass transfer mechanisms occurring during sonolytic ozonation by investigating the decomposition of ozone in a

continuously-stirred tank reactor (CSTR) mode under conditions closed to the atmosphere, open to the atmosphere, and open to the atmosphere with ozone gas bubbling. In Chapter 5, the decomposition of a refractory pollutant, pentachlorophenol, was investigated and reaction products were followed to determine the degradation pathway.

The principal objectives in the investigation of photoactivated periodate in Chapter 6, were to selectively destroy triethanolamine (TEA) and its associated chemical oxygen demand (COD). Optimal reaction conditions with respect to pH, $[IO_4^-]_0/[TEA]_0$, and light intensity were explored. Experiments were performed on industrial wastewater to evaluate the practical effectiveness of this treatment technology.

REFERENCES

1. Hoffmann, M. R.; Martin, S. T.; Choi, W.; Bahneman, D. W., *Chem. Rev.,* **1995**, *95*, 69-96.

2. Barbeni, M.; Pramauro, E.; Pelizzetti, E., *Chemosphere,* **1985**, *14*, 195-208.

3. Calvert, J. G.; Pitts, J. N. *Photochemistry*; John Wiley and Sons: New York, 1966.

4. Gerasimov, O. V.; Parmon, V. N.; Lymar, S. V., *J. Photochem. Photobiol. A: Chem.,* **1993**, *74*, 21-29.

5. Grätzel, C. K.; Jirousek, M.; Grätzel, M., *J. Mol. Catal.,* **1990**, *60*, 375-387.

6. Halmann, M., *J. Photochem. Photobiol. A: Chem.,* **1992**, *66*, 215-223.

7. Jardim, W. F.; Moraes, S. G.; Takiyama, M. M. K., *Wat. Res.,* **1997**, *31*, 1728-1732.

8. Legrini, O.; Oliveros, E.; Braun, A. M., *Chem. Rev.,* **1993**, *93*, 671-698.

9. Masten, S. J.; Davies, S. H. R. In *Environmental Oxidants*; J. O. Nriagu and M. S. Simmons, Eds.; John Wiley & Sons: New York, 1994; pp 517-547.

10. Mills, G.; Hoffmann, M. R., *Environ. Sci. Technol.,* **1993**, *27*, 1681-1689.

11. Minero, C.; Pelizzetti, E.; Malato, S.; Blanco, J., *Chemosphere,* **1993**, *26*, 2103-2119.

12. Peill, N. J.; Hoffmann, M. R., *Environ. Sci. Technol.,* **1996**, *30*, 2806-2812.

13. Pelizzetti, E.; Carlin, V.; Minero, C., *New J. Chem.,* **1991**, *15*, 351-359.

14. Peyton, G. R.; Huang, F. Y.; Burleson, J. L.; Glaze, W. H., *Environ. Sci. Technol.,* **1982**, *16*, 448-453.

15. Peyton, G. R.; Glaze, W. H., *Environ. Sci. Technol.,* **1988**, *22*, 761-767.

16. Sierka, R. A.; Amy, G. L., *Ozone Sci. Engng.,* **1985**, *7*, 47-62.

17. Barbier, P. F.; Pétrier, C., *J. Adv. Oxid. Technol.,* **1996**, *1*, 154-159.

18. Berlan, J.; Trabelsi, F.; Delmas, H.; Wilhelm, A. M.; Petrignani, J. F., *Ultrasonics Sonochemistry,* **1994**, *1*, S97-S102.

19. Bhatnagar, A.; Cheung, H. M., *Environ. Sci. Technol.,* **1994**, *28*, 1481-1486.

20. Chen, J. W., *Water,* **1972**, *69*, 61-70.

21. Cost, M.; Mills, G.; Glisson, P.; Lakin, J., *Chemosphere,* **1993**, *27*, 1737-1743.

22. Drijvers, D.; De Baets, R.; De Visscher, A.; Van Langenhove, H., *Ultrasonics Sonochemistry,* **1996**, *3*, S83-S90.

23. De Visscher, A.; Van Eenoo, P.; Drijvers, D.; Van Langenhove, H., *J. Phys. Chem.*, **1996**, *100*, 11636-11642.

24. Francony, A.; Pétrier, C., *Ultrasonics Sonochemistry,* **1996**, *3*, S77-S82.

25. Glaze, W. H.; Peyton, G. R., *Environ. Sci. Technol.*, **1982**, *16*, 454-458.

26. Glaze, W. H.; Kang, J. W.; Chapin, D. H., *Ozone Sci. Eng.*, **1987**, *9*, 335-352.

27. Glaze, W. H., *Environ. Sci. Technol.*, **1987**, *21*, 224-230.

28. Gurol, M. D.; Vatistas, R., *Wat. Res.*, **1987**, *21*, 895-900.

29. Hart, E. J.; Henglein, A., *J. Phys. Chem.*, **1985**, *89*, 4342-4347.

30. Hart, E. J.; Henglein, A., *J. Phys. Chem.*, **1986**, *90*, 3061-3061.

31. Hart, E. J.; Henglein, A., *J. Phys. Chem.*, **1987**, *91*, 3654-3656.

32. Hart, E. J.; Fischer, C. H.; Henglein, A., *J. Phys. Chem.*, **1990**, *94*, 284-290.

33. Hua, I.; Höchemer, R. H.; Hoffmann, M. R., *Environ. Sci. Technol.*, **1995**, *29*, 2790-2796.

34. Hua, I.; Höchemer, R. H.; Hoffmann, M. R., *J. Phys. Chem.*, **1995**, *99*, 2335-2342.

35. Hua, I.; Hoffmann, M. R., *Environ. Sci. Technol.,* **1996**, *30*, 864-871.

36. Hua, I.; Hoffmann, M. R., *Environ. Sci. Technol.,* **1997**, *31*, 2237-2243.

37. Kontronarou, A.; Mills, G.; Hoffmann, M. R., *J. Phys. Chem.,* **1991**, *95*, 3630-3638.

38. Kontronarou, A.; Mills, G.; Hoffmann, M. R., *Environ. Sci. Technol.,* **1992**, *26*, 2420-2428.

39. Kontronarou, A.; Mills, G.; Hoffmann, M. R., *Environ. Sci. Technol.,* **1992**, *26*, 1460-1462.

40. Makino, K.; Mossoba, M. M.; Riesz, P., *J. Phys. Chem.,* **1983**, *87*, 1369-1377.

41. Nagata, Y.; Hirai, K.; Bandow, H.; Maeda, Y., *Environ. Sci. Technol.,* **1996**, *30*, 1133-1138.

42. Okouchi, S.; Nojima, O.; Arai, T., *Wat. Sci. Tech.,* **1992**, *26*, 2053-2056.

43. Pétrier, C.; Jeunet, A.; Luche, J.-L.; Reverdy, G., *J. Am. Chem. Soc.,* **1992**, *114*, 3148-3150.

44. Pétrier, C.; Lamy, M.-F.; Francony, A.; Benahcene, A.; David, B., *J. Phys. Chem.,* **1994**, *98*, 10514-10520.

45. Pétrier, C.; David, B.; Laguian, S., *Chemosphere,* **1996**, *32*, 1709-1718.

46. Riesz, P.; Kondo, T.; Krishna, C. M., *Ultrasonics,* **1990**, *28*, 295-303.

47. Turai, L. L.; Rosario, F. d., *Appita,* **1982**, *35*, 407-411.

48. Peyton, G. R. In *Emerging Technologies in Hazardous Waste Management*1990; pp 100-118.

Chapter 2

Background

ULTRASOUND

Sound is a waveform consisting of density variations in an elastic medium. Three regimes of sound exist based on the frequency of the longitudinal wave; infrasonic ($f < 20$ Hz), sonic (20 Hz $< f <$ 20 kHz), and ultrasonic ($f >$ 20 kHz) (1,2). For sinusoidal waves the following relation between the speed of the wave (c), the frequency (f), and the wavelength (λ) is valid:

$$c = f\lambda \qquad (1)$$

Ultrasonic waves in aqueous solution where chemical effects are observed have wavelengths in the range of 0.2 to 7.5 cm (3).

Besides the freqeuncy of sound, the intensity, amplitude, and impedance of the waves are of particular interest for sonochemistry. The acoustic intensity is the average energy flux in the direction of propagation. For plane waves the intensity is:

$$I = \frac{P_A^2}{2Z} \qquad (2)$$

where P_A is the acoustic amplitude pressure, and Z is the acoustic impedance. From eqn. 2 it is clear that as more energy per unit area is added to the system, the pressure amplitude also increases. As the sound propagates through a medium it can lose energy to the medium by attenuation:

$$I = I_0 e^{-2\alpha d} \qquad (3)$$

where α is the attenuation coefficient and d is the distance from the source. The attenuation coefficient is a function of f^2. Therefore, lower frequency waves penetrate farther into the medium than higher frequency waves (1,2).

The acoustic impedance is analogous to the index of refraction in optics. Therefore, it is important for determining how a wave propagates from one medium to another. For plane waves it is dependent on the density (ρ_0) and speed of sound in the medium:

$$Z = \rho_0 c \tag{4}$$

If the acoustic impedance is matched, complete transmission of the wave occurs. However, mismatched configurations cause pressure or velocity doubling from in or anti-phase reflections which result in standing waves (2).

The use of ultrasound to enhance chemical reactions was first reported in 1927. Since that time, the study of sonochemistry has undergone a resurgence due to the development of ultrasonic equipment such as ultrasonic probes and baths. Ultrasound, when applied to a liquid, induces a variety of chemical reactions. However, ultrasonically induced reactions are not the result of direct interaction between the molecule and the energy of the wave as in photochemistry. Rather, the rarefaction and compression cycles of the wave create cavitation (3).

ACOUSTIC CAVITATION

Cavitation is the growth and collapse of gas bubbles. During a rarefaction cycle in the absence of gas nuclei and provided there is ample sound intensity, the average molecular distance between molecules increases to the point where it exceeds the critical distance necessary to hold the liquid intact. This tensile stress creates a vaporous bubble. As the liquid enters a compression cycle the bubble will shrink and possibly collapse. The bubble dynamics for a spherically oscillating bubble in an incompressible fluid can be described by the RPNNP equation named after the main contributers to its formulation: Rayleigh, Plesset, Noltingk, Neppiras, and Poritsky (1). However, it is commonly referred to as the Rayleigh-Plesset equation:

$$R\ddot{R}+\frac{3\dot{R}^2}{2}=\frac{1}{\rho}\left\{\left(p_0+\frac{2\sigma}{R_0}-p_v\right)\left(\frac{R_0}{R}\right)^{3\kappa}+p_v-\frac{2\sigma}{R}-\frac{4\eta\dot{R}}{R}-p_0-P(t)\right\} \quad (5)$$

where R = radius of the bubble, ρ = density of the fluid, p_0 = hydrostatic pressure, σ = surface tension, R_0 = initial radius, p_v = vapor pressure of the fluid, κ = ratio of heat capacities of the gas (the polytropic exponent): C_p/C_v, η = viscosity of the fluid, and $P(t) = P_A \sin\omega t$ is the acoustic pressure. This equation is derived from the conservation of energy. It assumes T_∞, η, and ρ are constant, the temperature and pressure in the bubble are uniform, and no mass transfer between the gas and surrounding liquid. However, it is unlikely that a bubble collapses symmetrically (4).

In real systems, bubble collapse is unstable allowing small perturbations to grow into major asymmetries. The presence of other cavitating bubbles, a wall, a free surface, a pressure gradient, a relative velocity, or a body force such as gravity or magnetic fields result in asymmetries for an initially spherical bubble. By conservation of momentum, as the bubble collapses, the mass of the bubble decreases and hence the linear velocity of the bubble wall increases. For the collapse to be spherical, the radial liquid velocity would need to be uniform in all directions. However, in the presence of an asymmetry, liquid access to the bubble varies across the surface, producing a faster collapsing bubble wall in a region of the bubble. As the bubble implodes a jet is formed on the side with the faster collapse which impinges the opposite side of the bubble and causes the bubble to fragment. Numerical estimates of the jet velocity range from 100 to 1000 m s^{-1} (5).

Cavitation is considered inertial (otherwise known as transient) when the bubble size oscillates by several orders of magnitude during an acoustic cycle (6). For a vaporous cavity the maximum radius reached is dependent on the density of the liquid, the applied frequency ($\omega = 2\pi f$) and the hydrostatic and acoustic pressure:

$$R_{max} = \frac{4}{3\omega}(P_A - p_0)\left(\frac{2}{\rho P_A}\right)^{1/2}\left(1 + \frac{2}{3p_0}(P_A - p_0)\right)^{1/3} \quad (6)$$

An inertial cavitation bubble generally exists for very few cycles after which it grows explosively and then collapses violently generating a shock wave and large temperatures and pressures regionally. Temperatures and pressures in a vaporous water bubble can reach several thousand Kelvin and hundreds of atmospheres, respectively (7). A collapsing cavitation bubble obtains the following pressure and temperature at collapse (3):

$$P_{max} = P\left(\frac{P_m(\kappa - 1)}{P}\right)^{\frac{\kappa}{\kappa-1}} \quad (7)$$

$$T_{max} = T_0\left(\frac{P_m(\kappa - 1)}{P}\right) \quad (8)$$

where $P_m = p_0 + P_A$, and κ = the ratio of heat capacities (the polytropic exponent): C_p/C_v. These equations indicate that higher pressures and temperatures will be reached at collapse with higher κ. Monoatomic gases typically have κ's of 1.67, as opposed to diatomic gases in which $\kappa \approx 1.4$.

Acoustic cavitation also produces stable cavitation bubbles that do not collapse entirely during the compression cycle. This is characterized by repetitive low energy pulsations about an equilibrium radius (6). Inertial cavitational bubble motion is dominated by the inertia of the liquid whereas stable cavitation is dominated by the stiffness of the gas. Stable cavitation lasts several cycles but can evolve into transient cavitation. This can occur by rectified diffusion or by coalescence. Figure 2.1 (1) shows a bubble oscillating over a few cycles (stable cavitation) then collapsing violently (inertial cavitation).

Rectified diffusion is a two part, nonlinear effect involving the mass transfer of gas between the bubble and liquid. The first effect is that of surface area. During the

compression cycle the bubble is compressed and gas diffuses from the bubble to the liquid. Then in the rarefaction cycle, the bubble expands and gas diffuses inward. However, the surface area in the rarefaction cycle is greater and the net effect is gas increase in the bubble. The other effect is due to the diffusion boundary layer. When the bubble expands, the boundary layer is thinner and gas transfer influx is enhanced more than the flux out in the compression cycle. The overall effect is bubble growth. Figure 2.2 (8) shows the thresholds for rectified diffusion and transient cavitation to occur with air-saturated bubbles at 20 kHz. P_T/P_o is the threshold acoustic pressure over the ambient hydrostatic pressure and R_o is the equilibrium bubble radius. AB is the threshold above which rectified diffusion occurs. Similarly, CD is the threshold for transient cavitation. S and T show the process of a bubble growing by rectified diffusion. In the case of S, it reaches the transient cavitation threshold and collapses into smaller bubbles. Some of the bubbles will be so small that they will enter area X and slowly dissolve. A bubble can also grow by rectified diffusion but not reach the cavitation threshold as seen with T. In this case the bubble will grow until the effects of buoyancy remove it (4,8).

Theoretically, for a cavity to form in a liquid in the presence of an acoustic field, the total tensile stress applied (pressure in the rarefaction cycle minus hydrostatic pressure) during the rarefaction cycle must exceed the tensile strength of the liquid. In pure water, cavitation inception theoretically occurs with an applied tension of 1500 atmospheres (1). However, cavitation is observed at pressures of less than 10 atmospheres. This is due to "weak spots" in the fluid. Weak spots are any type of inhomogeneity in the fluid and can be anything from particles to gas nuclei to cosmic radiation (3,4). It is impossible to remove all cavitation nuclei and it is often beneficial to add cavitation nuclei to reduce the acoustic pressure amplitude in which cavitation is first detected, the cavitation threshold.

The sound field, as defined by the frequency and pressure amplitude, affects how the bubble reacts under its influence. This is observed in eqn. (6) in which the maximum radius a bubble achieves is dependent on the pressure amplitude and the frequency. By

considering a gas bubble pulsating in a liquid as an oscillator, the natural frequency of the bubble was calculated by Minneart (9):

$$f = \frac{1}{2\pi R_0}\left(\frac{3\kappa p_0}{\rho}\right)^{1/2} \tag{9}$$

From this analysis, for an applied frequency, the bubble size at which maximum perturbations occur is determined. Since it is an inverse relationship between frequency and radius, smaller radii will be influenced more by higher frequency waves. Similarly, the collapse time of a bubble is also frequency dependent (3):

$$\tau = \left(\frac{\rho}{P_m}\right)^{1/2}\left(1 + \frac{P_g}{P_m}\right) \tag{10}$$

where P_g is the pressure in the bubble at R_{max}, and P_m is the applied pressure ($P_A + p_0$).

Besides the obvious bubble oscillations, ultrasound can have secondary effects on the bubbles. Important phenomena affecting mass transfer of gas into and out of either a bubble or a sonochemical reactor include, acoustic streaming, microstreaming, and Bjerknes forces.

Acoustic streaming is caused by an energy gradient in the direction of propagation of the acoustic wave resulting from the absorption of the acoustic wave by the medium. The energy gradient corresponds to a force which when acting on a liquid causes the liquid to accelerate in the direction of propagation (1):

$$\nabla p = \frac{F}{V} = \frac{2Ib}{c} \tag{11}$$

where ∇p is the gradient pressure, F/V is the force per unit volume, I is the intensity, b is the amplitude acoustic attenuation constant, and c is the speed of sound in the medium. Thus, larger acoustic intensity (power input/surface area of emitter) causes a larger force

and hence a larger acceleration of the liquid. This will result in more turbulence in the reactor and increased mixing of the solution. Since this is a mechanical effect, it is dependent on the reactor configuration.

The second type of streaming is called microstreaming. It occurs near small objects within the sound field. It arises from frictional forces that occur within the viscous boundary layer and medium carrying vibrations of circular frequency and results in shear stress near the boundary layer (6). This microstreaming creates circulation and results in greater efficiency of gas flux to and from a bubble and can also damage biological cells.

When a bubble is in a standing wave field, the pressure gradient oscillates as does the bubble volume. A primary Bjerknes force results from oscillations of the radius not in phase with oscillations of pressure, which occurs with bubbles far from the resonant size. Bubbles smaller than resonant size cluster at pressure antinodes. Similarly, bubbles larger than the resonant radius travel down pressure gradients to the pressure nodes. Secondary Bjerknes forces are attractive forces between two bubbles either below or above the resonant size since the bubble are acting in phase with each other. Therefore, at the nodes and anti nodes the bubbles coalesce due to primary and secondary Bjerknes forces, and if they are large enough they will be removed by buoyancy forces (1).

SONOCHEMISTRY

The collapse of cavitation bubbles in water generates a variety of chemical processes and reaction sites (10-38). Cavitating water is considered to have four main reactive regions as shown in Figure 2.3. First is the vapor bubble which pyrolyzes vaporous water molecules into hydroxyl radical and hydrogen atoms during collapse:

$$H_2O \xrightarrow{\Delta} H\bullet + OH\bullet \qquad (12)$$

Gases such as O_2 and high Henry's law solutes also exist in the vapor region and undergo direct pyrolysis reactions (3,10-14,16,17,19). Next is the interfacial sheath around the vapor. Here supercritical water exists (26) along with dissolved radicals from the bubble. This is the reaction site for nonvolatile solutes and also the site for liquid phase pyrolysis. Although it is not shown in Figure 2.3, it is also believed to be possible for liquid to be injected into the center of a cavitation bubble as it collapses asymmetrically, referred to as a spume (39). Similar to the interfacial sheath, it is where liquid phase pyrolsis is expected to occur. Finally, in the bulk phase there is an increase in metastable oxidants such as hydrogen peroxide which are formed from radical recombination reactions (3,17).

The physical properties of a solute are important in identifying its capability to be decomposed by sonication. The Henry's Law constant of a compound, which is its equilibrium air-water distribution, is defined by:

$$H = \frac{P_i}{C_w} \tag{13}$$

where H (Pa m^3 mol^{-1}) is the Henry's Law constant, P_i is the partial pressure of the chemical species i in the gas phase, and C_w is the aqueous phase concentration of the solute. This parameter characterizes relative amounts of a solute that will enter the vapor bubble. The octanol-water partitioning coefficient, K_{ow}, is another key parameter which approximates the hydrophobicity of a compound. It is defined by:

$$K_{ow} = \frac{C_o}{C_w} \tag{14}$$

where C_o is the concentration of the compound in the organic phase. This constant will give insight into the amount of surface excess at the cavitation bubble interface.

PHOTO INITIATORS WITH ULTRAVIOLET IRRADIATION

Unlike sonochemistry, in which sound does not directly interact with a molecule, photochemistry occurs when there is interaction between a light quantum, a photon, and a molecule. Two basic conditions must exist for a reaction between the photon and a molecule to proceed. First, the photon has a discrete amount of energy determined from its wavelength. Thus, for a photon to break a bond (>40 kcal mol^{-1}), it must have a wavelength corresponding to the energy of the bond, typically lower than 700 nm. Second, as the first law of photochemistry states (40): "*Only the light which is absorbed by a molecule can be effective in producing photochemical change in the molecule.*" Therefore, for a reaction to proceed the molecule must be able to absorb the wavelength of light irradiated.

The absorption of a photon by a molecule results in the formation of an excited state. As shown in Figure 2.4, this excitation can be dissipated by four mechanisms: radiative processes such as luminescence, radiationless processes, bimolecular deactivation, and dissociation of the molecule. Dissociation typically results in free radical formation (41). Utilizing light for the purpose of degrading compounds relies on dissociation and free radical formation.

A photo initiator is a compound which absorbs light and decomposes into free radicals. The use of a photo initiator such as periodate, TiO_2 semiconductor particles (42) or Fenton's reagent is often necessary since many organic contaminants do not absorb UV light strongly (43). A desirable photo initiator will absorb photons efficiently and decompose into reactive radicals. The radicals then react with the target compound. Due to symmetry and molecular geometry, the effectiveness of the photo initiator will vary depending on the characteristics of the solutes in the water.

CHEMICAL OXIDANTS WITH ADVANCED OXIDATION PROCESSES

Ozone (O_3) and periodate (IO_4^-) are very strong oxidants that can oxidize organic compounds to carbon dioxide and water. However, the kinetics of oxidation of most organic compounds with the groundstate oxidants are slow. Standard reduction potentials for half reactions of the reduction of the oxidant are shown in Table 2.1 (44-46). Standard conditions are when the concentrations of species in the reaction are at one molar, gases at one atmosphere and a temperature of 25 °C. Utilization of ultraviolet light with these oxidants has resulted in enhanced reaction rates (43,47-54). Although less studied, the combination of cavitation with these oxidants, also has potential. The generation of free radicals by these processes can significantly reduce times required for destruction of organic contaminants.

Ozone

Ozone has been the most widely studied oxidant for the degradation of aqueous contaminants. Ozone is being implemented at water and wastewater treatment plants in order to reduce trihalomethane formation resulting from chlorination (55). Ozone has resonance structures which allows it to act as an electrophile or a nucleophile. Although the molecule has a very high oxidation potential, ozone reactions are very selective, and limited to molecular sites with high electron density such as alkenes or sites where the carbon contains an electron withdrawing group. Ozone, however, is unstable and undergoes a chain decomposition in alkaline systems to liberate hydroxyl radicals (55). Hydroxyl radical is non-selective in its reactions allowing it to react with organic compounds either by H-atom abstraction, direct electron transfer, or insertion.

Another method of generating free radicals from ozone is the use of ultraviolet irradiation. Peyton and Glaze (54) found that hydrogen peroxide produced initially by irradiation of O_3, formed hydroxyl radicals by O_3 reactions with hydroperoxide anions. Another AOP which combines hydrogen peroxide and ozone directly, bypasses the need for UV light (56). H_2O_2/O_3 does not depend on the transmissivity of the solution in the

UV region where O_3 absorbs, it has wider applicability. However, O_3/UV systems are attractive in some situations, especially if the pollutant absorbs UV light.

The coupling of ultrasonic irradiation with ozonation provides another possible AOP. In this case, OH• is generated from the decomposition of ozone. However, ozone is decomposed thermolytically in the vapor phase of a cavitation bubble as follows (16,17):

$$O_3 \xrightarrow{\Delta} O_2 + O(^3P) \qquad (15)$$

The initiation reaction yields atomic oxygen which reacts with water to form hydroxyl radical:

$$O(^3P) + H_2O \longrightarrow 2\ OH\bullet \qquad (16)$$

The reaction sequence of eqs. 15 and 16 occurs in the vapor phase of cavitation bubbles. The products then migrate to the interfacial sheath of the bubble where they are transferred into the aqueous phase. The combination of O_3 and ultrasound should be an effective oxidation system since 2 OH• molecules are formed per O_3 molecule consumed. Hydrogen peroxide accumulation in the aqueous phase provides an indirect measure of OH• production in the vapor phase and in the interfacial region. Previous studies have measured increased H_2O_2 production by sonolytic ozonation over sonolysis of oxygen (15,16).

Previous studies of the combined process involving ultrasound and ozone have shown faster degradation rates for humic and fulvic acids, 4-nitrophenol, trinitrotoluene, and phenol than either system alone as well as very rapid decomposition of ozone due to an ultrasonic field (15-20,57-61). Sonolytic ozonation has also been investigated for the disinfection of water (58,62,63). In this case, ultrasound it thought to act on the bacteria and viruses directly by breaking up clusters and particulate organic matter as well as decomposing O_3.

Also, previous researchers have reported increased mass transfer coefficents, $k_L a$ (s^{-1}), of ozone diffusing into solution in the presence of ultrasound (20,58,59). k_L is the mass transfer velocity (cm s^{-1}) and a is the specific interfacial area for mass transfer (cm^2/cm^3). Olson and Barbier (20) hypothesized that the apparent enhancement was due to mechanical effects such as greater mixing and break up of gas bubbles as they enter an ultrasonic reactor. Increased mass transfer may also be the result of a diffusing ozone bubble oscillating or cavitating in the applied ultrasonic field. In this case, higher pressures in the ozone bubble force more ozone into solution. On the other hand, the apparent mass transfer effects may be due to the sonication of ozone reducing the aqueous ozone concentration below saturation allowing more ozone to absorbed from the gas-phase into solution per unit time. Finally, degassing may be a factor in sonolytic ozonation due to the high Henry's Law constant of ozone ($H = 1.08 \times 10^4$ $Pa \cdot m^3/mol$) (64), especially at low frequency. Figure 2.5 shows the various processes occurring upon the addition of ozone to an ultrasonic field.

Periodate

Periodic acid (H_5IO_6) or periodate (IO_4^-) is a well-known oxidant in organic chemistry (45,46,65). In most reactions it is a two-electron oxidant which is reduced to iodate (IO_3^-):

$$H_5IO_6 + H^+ + 2e^- = IO_3^- + 3\,H_2O \qquad E° = +1.6\ v \qquad (17)$$

As shown in Table 2.1, iodate also has a strong reduction potential ($E° = +1.2$ v) and is reduced to iodine (44). Periodate chemistry is complex; the molecule has three pK_a values, dehydrates and also forms dimers (46):

$$H_5IO_6 \Leftrightarrow H_4IO_6^- + H^+ \qquad pK_{a1} = 1.64 \qquad (18)$$

$$H_4IO_6^- \Leftrightarrow H_3IO_6^{2-} + H^+ \qquad pK_{a2} = 8.36 \qquad (19)$$

$$H_3IO_6^{2-} \Leftrightarrow H_2IO_6^{3-} + H^+ \qquad pK_{a3} = 14.98 \qquad (20)$$

$$H_4IO_6^- \Leftrightarrow IO_4^- + 2H_2O \qquad K_D = 40 \qquad (21)$$

$$2H_3IO_6^{2-} \Leftrightarrow H_2I_2O_{10}^{4-} + 2H_2O \qquad K_X = 141.1\ M^{-1} \qquad (22)$$

Periodate is selective and highly reactive with respect to the oxidation of 1,2-diols and 1,2-ketones. It is also very active with respect to the oxidation of a wide range of other organic compounds such as ketoacids, carbohydrates, carboxylic acids, sugars, amines, aldehydes, and aminoalcohols such as TEA. Dark reaction of periodate with glycols and related compounds involves the formation of a cyclic periodate complex (46).

Periodate reactions are known to become less selective with respect to specific functional groups with increasing temperature or by the addition of light (46). In order to enhance oxidation and to exploit the loss of substrate selectivity, the use of UV light with periodate was investigated. The photolysis of periodate and periodic acid has been studied over a wide range of pH and a large number of photochemical reactions involving periodate have been proposed (66-68). For example, the following mechanism for the photolysis of periodate has been suggested by Wagner and Strehlow (68):

$$IO_4^- + H^+ \xrightarrow{h\nu} IO_3\bullet + OH\bullet \qquad (23)$$

$$OH\bullet + IO_4^- \longrightarrow OH^- + IO_4\bullet \qquad (24)$$

$$2OH\bullet \longrightarrow H_2O_2 \qquad (25)$$

$$2IO_4 \bullet \longleftrightarrow I_2O_8 \quad (26)$$

$$I_2O_8 + H_2O \longrightarrow IO_3^- + IO_4^- + 2H^+ + O_2 \quad (27)$$

$$2IO_3 \bullet \longleftrightarrow I_2O_6 \quad (28)$$

$$I_2O_6 + H_2O \longrightarrow IO_4^- + IO_3^- + 2H^+ \quad (29)$$

$$IO_4^- \xrightarrow{h\nu} IO_3^- + O(3P) \quad (30)$$

$$O_2 + O \longrightarrow O_3 \quad (31)$$

$$O_3 + IO_3 \bullet \longrightarrow IO_4 \bullet + O_2 \quad (32)$$

The photolytic decomposition mechanism involves a number of highly reactive radical and non-radical intermediates such as IO_3•, •OH, IO_3^-, O_3, and IO_4•. Therefore, the photoassisted oxidation of organic substrates by periodate most likely occurs via free radical pathways. This mechanism indicates possible regeneration of IO_4^- through radical chain reactions. Studies of UV/TiO_2/O_2 systems with added IO_4^- show that oxidation of a wide variety of organic compounds occurs very rapidly when compared to UV/TiO_2/O_2 oxidation alone (50-52,69).

REFERENCES

1. Leighton, T. G. *The Acoustic Bubble*; Academic Press: London, 1994.

2. Roy, R. A. In *NATO Advanced Study Institute on Sonochemistry and Sonoluminescence*; Leavenworth, WA, 1997.

3. Mason, T. J.; Lorimer, J. P. *Sonochemistry: Theory, Applications and Uses of Ultrasound in Chemistry*; Ellis Horwood Ltd: Chichester, 1988.

4. Brennen, C. E. *Cavitation and Bubble Dynamics*; Oxford University Press: New York, 1995.

5. Hammitt, F. G. *Cavitation and Multiphase Flow Phenomena*; Mc Graw-Hill: New York, 1980.

6. Roy, R. A. In *NATO Advanced Study Institute on Sonochemistry and Sonoluminescence*; Leavenworth, WA, 1997.

7. Suslick, K. S. *Ultrasound: Its Chemical, Physical, and Biological Effects*; VCH Publishers, Inc.: New York, 1988.

8. Young, F. R. *Cavitation*; McGraw-Hill: London, 1989.

9. Minnaert, M., *Phil. Mag.*, **1933**, *16*, 235-248.

10. Drijvers, D.; De Baets, R.; De Visscher, A.; Van Langenhove, H., *Ultrasonics*

Sonochemistry, **1996**, *3*, S83-S90.

11. De Visscher, A.; Van Eenoo, P.; Drijvers, D.; Van Langenhove, H., *J. Phys. Chem.,* **1996**, *100*, 11636-11642.

12. Francony, A.; Pétrier, C., *Ultrasonics Sonochemistry,* **1996**, *3*, S77-S82.

13. Hart, E. J.; Henglein, A., *J. Phys. Chem.,* **1987**, *91*, 3654-3656.

14. Hart, E. J.; Fischer, C. H.; Henglein, A., *J. Phys. Chem.,* **1990**, *94*, 284-290.

15. Barbier, P. F.; Pétrier, C., *J. Adv. Oxid. Technol.,* **1996**, *1*, 154-159.

16. Hart, E. J.; Henglein, A., *J. Phys. Chem.,* **1986**, *90*, 3061-3061.

17. Hart, E. J.; Henglein, A., *J. Phys. Chem.,* **1985**, *89*, 4342-4347.

18. Höchemer, R. H. Ph. D. Thesis, California Institute of Technology, 1996.

19. Hua, I.; Hoffmann, M. R., *Environ. Sci. Technol.,* **1996**, *30*, 864-871.

20. Olson, T. M.; Barbier, P. F., *Wat. Res.,* **1994**, *28*, 1383-1391.

21. Berlan, J.; Trabelsi, F.; Delmas, H.; Wilhelm, A. M.; Petrignani, J. F., *Ultrasonics Sonochemistry,* **1994**, *1*, S97-S102.

22. Bhatnagar, A.; Cheung, H. M., *Environ. Sci. Technol.,* **1994**, *28*, 1481-1486.

23. Cost, M.; Mills, G.; Glisson, P.; Lakin, J., *Chemosphere,* **1993**, *27*, 1737-1743.

24. Gonze, E.; Gonthier, Y.; Boldo, P.; Bernis, A., *Canadian J. Chem. Engng.,* **1997**, *75*, 245-255.

25. Hua, I.; Höchemer, R. H.; Hoffmann, M. R., *Environ. Sci. Technol.,* **1995**, *29*, 2790-2796.

26. Hua, I.; Höchemer, R. H.; Hoffmann, M. R., *J. Phys. Chem.,* **1995**, *99*, 2335-2342.

27. Hua, I.; Hoffmann, M. R., *Environ. Sci. Technol.,* **1997**, *31*, 2237-2243.

28. Kontronarou, A.; Mills, G.; Hoffmann, M. R., *J. Phys. Chem.,* **1991**, *95*, 3630-3638.

29. Kontronarou, A.; Mills, G.; Hoffmann, M. R., *Environ. Sci. Technol.,* **1992**, *26*, 2420-2428.

30. Kontronarou, A.; Mills, G.; Hoffmann, M. R., *Environ. Sci. Technol.,* **1992**, *26*, 1460-1462.

31. Makino, K.; Mossoba, M. M.; Riesz, P., *J. Phys. Chem.,* **1983**, *87*, 1369-1377.

32. Nagata, Y.; Hirai, K.; Bandow, H.; Maeda, Y., *Environ. Sci. Technol.,* **1996**, *30*, 1133-1138.

33. Okouchi, S.; Nojima, O.; Arai, T., *Wat. Sci. Tech.,* **1992**, *26*, 2053-2056.

34. Pétrier, C.; Jeunet, A.; Luche, J.-L.; Reverdy, G., *J. Am. Chem. Soc.,* **1992**, *114*, 3148-3150.

35. Pétrier, C.; Lamy, M.-F.; Francony, A.; Benahcene, A.; David, B., *J. Phys. Chem.,* **1994**, *98*, 10514-10520.

36. Pétrier, C.; David, B.; Laguian, S., *Chemosphere,* **1996**, *32*, 1709-1718.

37. Serpone, N.; Terzian, R.; Hidaka, H.; Pelizzetti, E., *J. Phys. Chem.,* **1994**, *98*, 2634-2640.

38. Turai, L. L.; Rosario, F. d., *Appita,* **1982**, *35*, 407-411.

39. Prosperetti, A. In *NATO Advanced Study Institute on Sonochemistry and Sonophysics*; Leavenworth, WA, 1997.

40. Calvert, J. G.; Pitts, J. N. *Photochemistry*; John Wiley and Sons: New York, 1966.

41. Rabek, J. F. *Experimental Methods in Photochemistry and Photophysics, Part 2*; Wiley-Interscience: New York, 1982.

42. Hoffmann, M. R.; Martin, S. T.; Choi, W.; Bahneman, D. W., *Chem. Rev.,* **1995**, *95*, 69-96.

43. Legrini, O.; Oliveros, E.; Braun, A. M., *Chem. Rev.*, **1993**, *93*, 671-698.

44. Latimer, W. M. *Oxidation Potentials;* 2nd ed.; Prentice-Hall: Englewood Cliffs, 1952.

45. Buist, G. J. In *Comprehensive Chemical Kinetics*; C. H. Bamford and Tipper, C. F. H., Ed.; Elsevier: Amsterdam, 1972; Vol. 6; pp 435-492.

46. Dryhurst, G. *Periodate Oxiation of Diol and Other Functional Groups. Analytical and Structural Applications*; Pergamon Press: New York, 1970.

47. Masten, S. J.; Davies, S. H. R. In *Environmental Oxidants*; J. O. Nriagu and M. S. Simmons, Eds.; John Wiley & Sons: New York, 1994; pp 517-547.

48. Glaze, W. H.; Peyton, G. R., *Environ. Sci. Technol.*, **1982**, *16*, 454-458.

49. Gurol, M. D.; Vatistas, R., *Wat. Res.*, **1987**, *21*, 895-900.

50. Halmann, M., *J. Photochem. Photobiol. A: Chem.*, **1992**, *66*, 215-223.

51. Martin, S. T.; Lee, A. T.; Hoffmann, M. R., *Environ. Sci. Techol.*, **1995**, *29*, 2567.

52. Grätzel, C. K.; Jirousek, M.; Grätzel, M., *J. Mol. Catal.*, **1990**, *60*, 375-387.

53. Peyton, G. R.; Huang, F. Y.; Burleson, J. L.; Glaze, W. H., *Environ. Sci.*

Technol., **1982**, *16*, 448-453.

54. Peyton, G. R.; Glaze, W. H., *Environ. Sci. Technol.,* **1988**, *22*, 761-767.

55. Langlais, B.; Reckhow, D. A.; Brink, D. R. *Ozone in Water Treatment Application and Engineering*; AWWA Research Foundation and Lewis Publishers: Chelsea, 1991.

56. Glaze, W. H.; Kang, J. W.; Chapin, D. H., *Ozone Sci. & Engrg.,* **1987**, *9*, 335-352.

57. Chen, J. W., *Water,* **1972**, *69*, 61-70.

58. Dahi, E., *Wat. Res.,* **1976**, *10*, 677-684.

59. Sierka, R. A. "Mass Transfer and Reaction Rate Studies of Ozonated MUST Wastewaters in the Presence of Sound Waves," University of Arizona, 1976.

60. Sierka, R. A., *Ozone Sci. Engng.,* **1985**, *6*, 275-290.

61. Sierka, R. A.; Amy, G. L., *Ozone Sci. Engng.,* **1985**, *7*, 47-62.

62. Burleson, G. R.; Murray, T. M.; Pollard, M., *Appl. Micobiol.,* **1975**, *29*, 340-344.

63. Katzenelson, E.; Kletter, B.; Shuval, H. I., *Journal AWWA,* **1974**, *66*, 725-729.

64. Seinfeld, J. H. *Atmospheric Chemistry and Physics of Air Pollution*; Wiley-Interscience: New York, 1986.

65. Jackson, E. L. In *Organic Reactions*; R. Adams et al., Ed.; John Wiley & Sons: New York, 1944; Vol. 2; pp 341-375.

66. Kläning, U. K.; Sehested, K., *J. Chem. Soc., Faraday Trans. I,* **1978**, *74*, 2818-2838.

67. Kläning, U. K.; Sehested, K.; Wolff, T., *J. Chem. Soc., Faraday Trans. I,* **1981**, *77*, 1707-1718.

68. Wagner, I.; Strehlow, H., *Ber. Bunsenges. Phys. Chem.,* **1982**, *86*, 297-301.

69. Pelizzetti, E.; Carlin, V.; Minero, C., *New J. Chem.,* **1991**, *15*, 351-359.

Table 2.1 Reduction potentials of selected oxidants (44-46)

Redox half-reaction	E° (volts)
$H_2O_2 + 2\ H^+ + 2\ e^- = 2\ H_2O$	+1.77
$OH\bullet + H^+ + e^- = H_2O$	+2.80
$O_3 + 2\ H^+ + 2\ e^- = O_2 + H_2O$	+2.07
$HO_2\bullet + H^+ + e^- = H_2O_2$	+1.50
$HOI + H^+ + 2\ e^- = I^- + H_2O$	+0.99
$IO_3^- + 6\ H^+ + 5\ e^- = 1/2\ I_2 + 3\ H_2O$	+1.20
$H_5IO_6 + H^+ + 2\ e^- = IO_3^- + 3\ H_2O$	+1.60

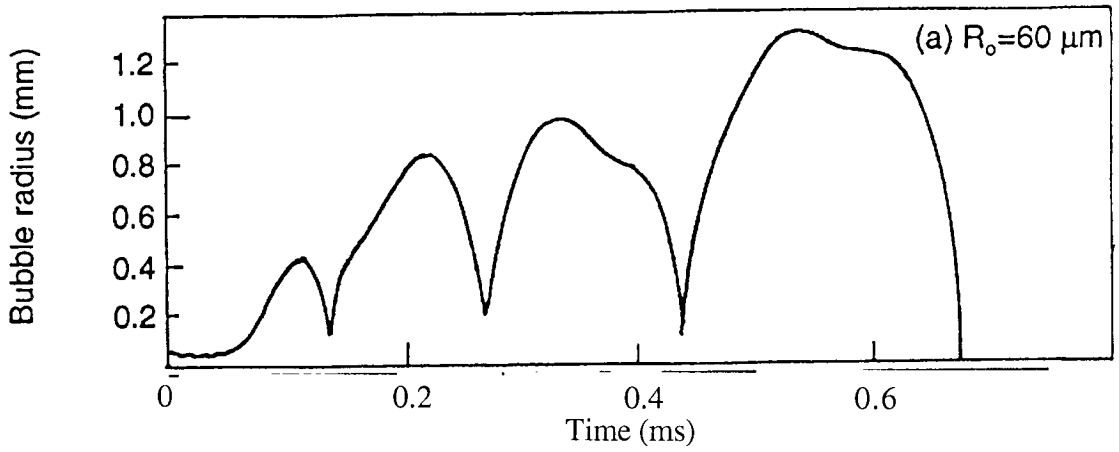

Figure 2.1: Bubble radius versus time predictions for a bubble of 60 μm initial size influenced by a 10 kHz sound field. (1)

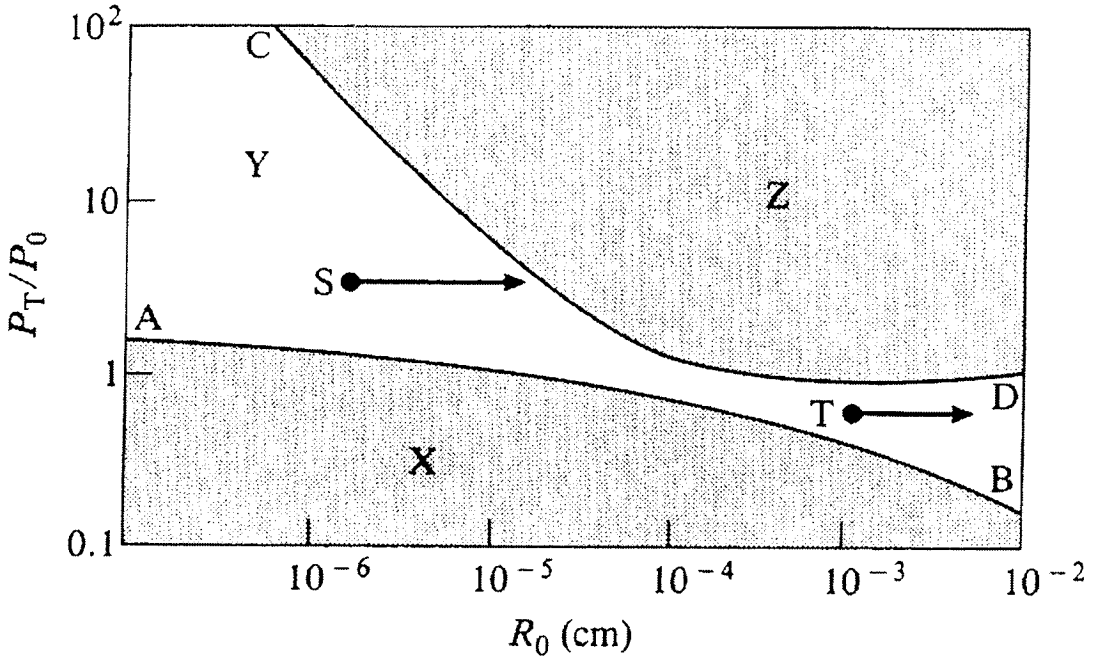

Figure 2.2: Cavitation bubble thresholds for rectified diffusion and transient cavitation for an air-saturated bubble at 20 kHz. Refer to text for meaning of regions and boundaries. (8)

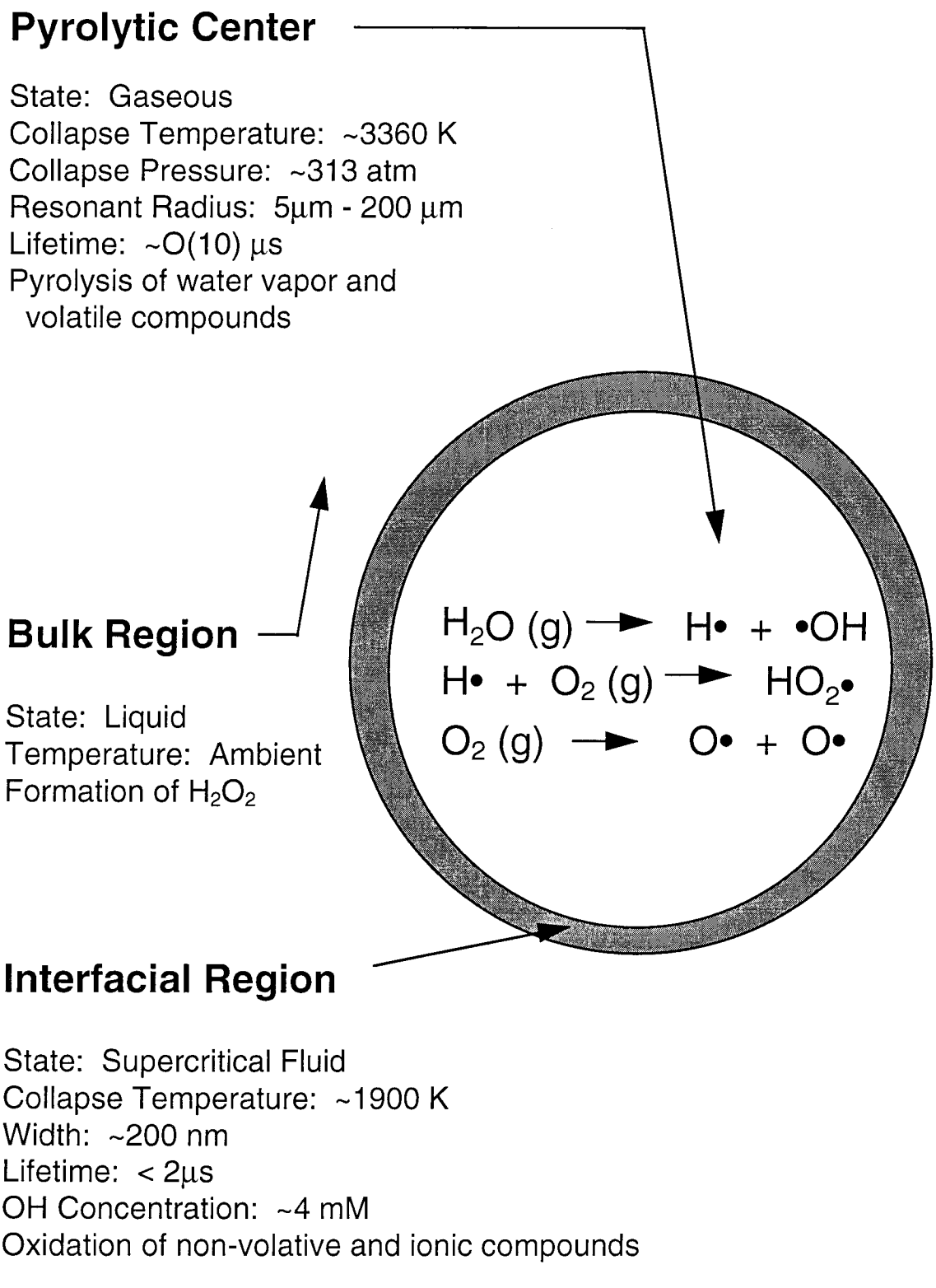

Figure 2.3: Reactive regions of a collapsing cavitation bubble.

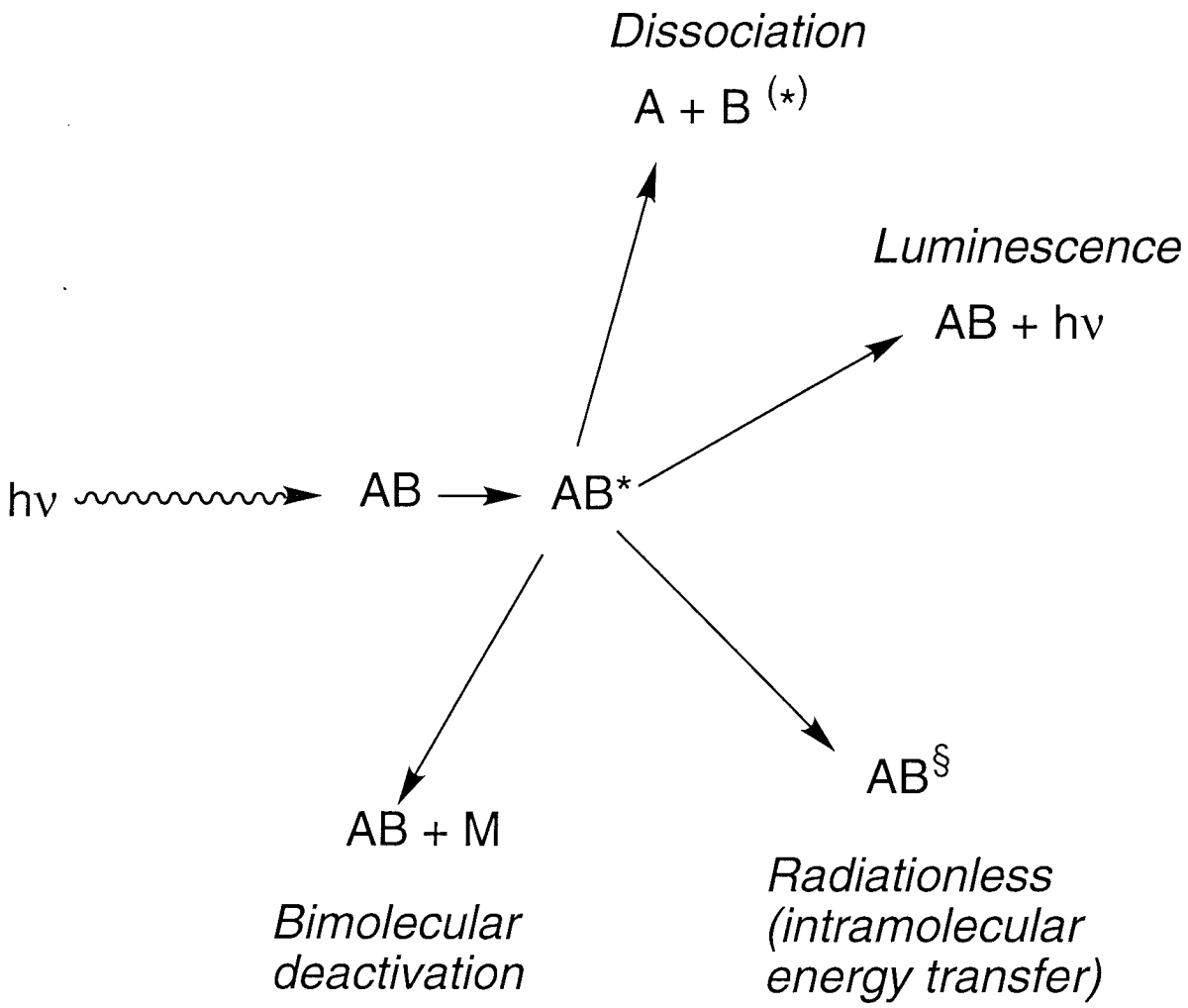

Figure 2.4: Dissipation mechanisms for a molecule excited by a photon.

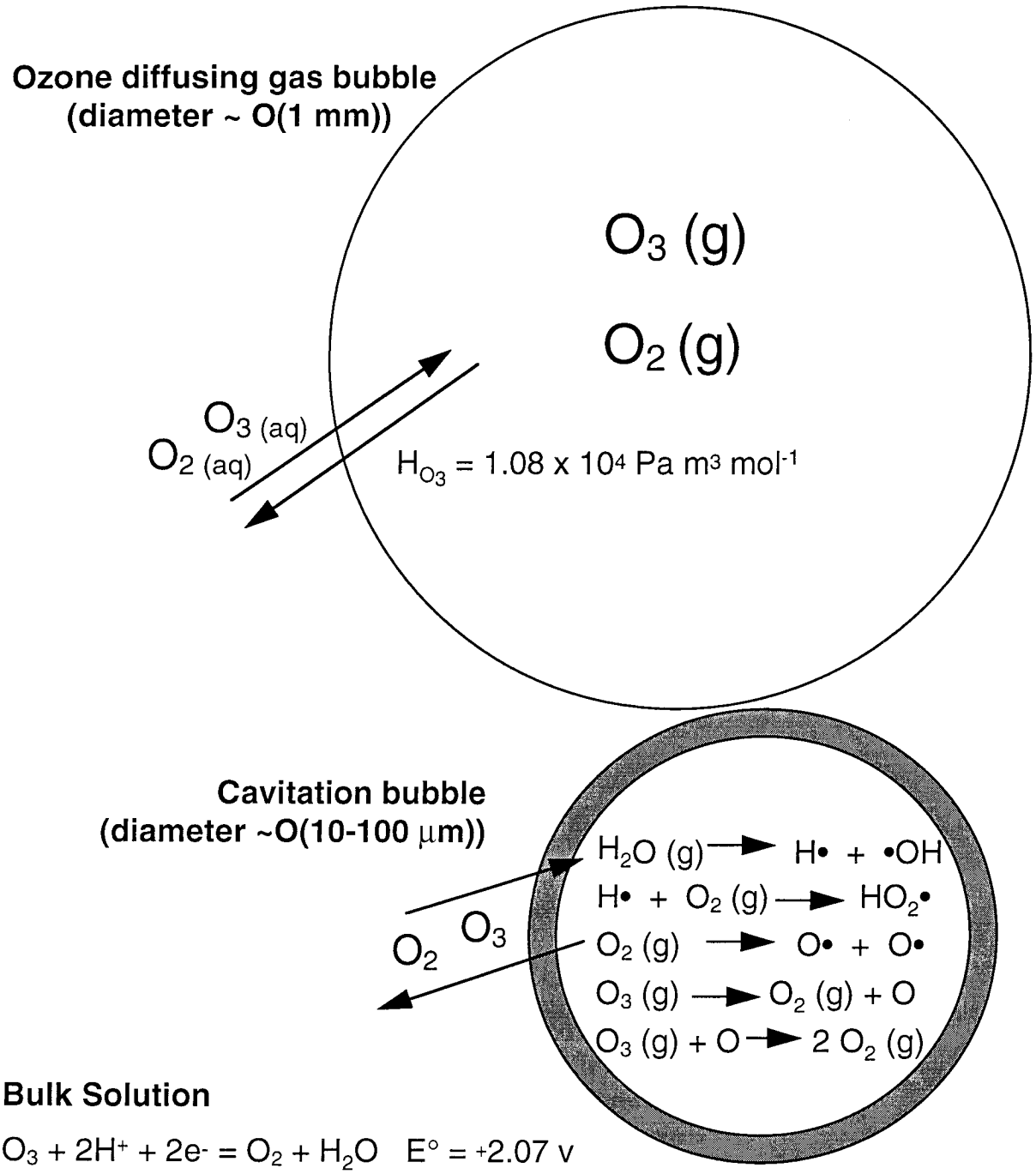

Bulk Solution

$O_3 + 2H^+ + 2e^- = O_2 + H_2O$ $E° = +2.07$ v

Under Acidic Conditions:

$O_3 \rightarrow O + O_2 \rightarrow O + H_2O \rightarrow 2\ OH$

Under Basic Conditions:

$O_3 + OH^- \rightarrow HO_2 + O_2^- \rightarrow OH$

Figure 2.5: Processes occurring with ozone bubbling through an ultrasonic reactor.

Chapter 3

Aromatic Compound Degradation in Water Using a Combination of Sonolysis and Ozonolysis

---

(Submitted to *Environmental Science and Technology*, July 1997)

ABSTRACT

Sonolysis, ozonolysis, and a combination of the two were used to facilitate the degradation of three known organic contaminants: nitrobenzene (NB), 4-nitrophenol (4-NP), and 4-chlorophenol (4-CP), in water. Experiments were performed at frequencies of 20 and 500 kHz. The observed rate constants for sonication at 500 kHz were larger by a factor of 10 than the corresponding rate constants measured at 20 kHz with the same power input into both systems. The first-order rate constants for oxidation by O_3, k_{O_3}, followed the trend of $k_{O_3,4\text{-}CP} > k_{O_3,4\text{-}NP} > k_{O_3,NB}$; k_{O_3} was greater than k_{US} in all cases. At 20 kHz there appeared to be an enhancement due to sonolytic ozonation while at 500 kHz an apparent retardation was seen. The catalytic effects of NB, 4-NP, and 4-CP degradation at 20 kHz increased with increasing Henry's Law constant, H ($Pa \cdot m^3/mol$), and k_{O_3} of the compounds, whereas the retardation at 500 kHz was correlated with increasing k_{O_3}. The correlation of apparent rate enhancement at 20 kHz and retardation at 500 kHz with k_{O_3} is consistent with a pathway involving the thermolytic destruction of ozone to form atomic oxygen. Atomic oxygen then reacts with water vapor in cavitation bubbles yielding gas phase hydroxyl radical. Enhancement in loss of total organic carbon (TOC) by sonolytic ozonation was considerable at both 20 and 500 kHz with all three compounds. Intermediate product formation was also observed.

Key Words: nitrobenzene, 4-nitrophenol, 4-chlorophenol, sonication, ozonation, degradation

INTRODUCTION

Ultrasonic irradiation of aqueous solutions has been shown to be effective for the in situ destruction of a variety of organic and inorganic contaminants (1-10). Ultrasonic irradiation produces cavitation bubbles which yield high temperatures and pressures upon their implosion (11,12). The center of a cavitation bubble contains water vapor, gas and volatile compounds. Destruction of organic compounds occur in the cavitation bubble itself or its interfacial sheath due to direct pyrolysis or hydroxylation which results from the gas-phase pyrolysis of H_2O. Reactions are also possible in the bulk aqueous phase by oxidation with hydrogen peroxide which has been observed to form in sonolytic systems. Sonication has been shown to be particularly effective with volatile and hydrophobic compounds since they can partition to the bubble or interfacial sheath rapidly (1,7).

A variety of advanced oxidation processes (AOPs) employing ozone at high pH, ozone combined with hydrogen peroxide, or ozone combined with ultraviolet irradiation have been explored. In these systems O_3 decomposes via a free radical chain reaction to generate hydroxyl radical (13-17). Even though ozone is a strong oxidant ($E^\circ = 2.07$ v), it is selective in terms of its reactions. For example, O_3 preferentially reacts with alkenes and sites with high electronic density. In contrast, hydroxyl radical is non-selective in its reactions allowing it to react with organic compounds either by H-atom abstraction, direct electron transfer, or insertion.

The coupling of ultrasonic irradiation with ozonation provides another possible AOP. In this case, OH• is generated from the decomposition of ozone. Ozone is decomposed thermolytically in the vapor phase of a cavitation bubble as follows (18,19):

$$O_3 \rightarrow O_2 + O(^3P) \qquad (1)$$

The initiation reaction yields atomic oxygen which reacts with water to form hydroxyl radical:

$$O(^3P) + H_2O \rightarrow 2\,OH\bullet \qquad (2)$$

The reaction sequence of eqs. 1 and 2 occurs in the vapor phase of the cavitation bubbles. The products then migrate to the interfacial sheath of the bubble where they are transferred into the aqueous phase. The combination of O_3 and ultrasound should be an effective oxidation system since 2 OH• molecules are formed per O_3 molecule consumed. Hydrogen peroxide accumulation in the aqueous phase provides an indirect measure of OH• production in the vapor phase and in the interfacial region. Previous studies have measured increased H_2O_2 production by sonolytic ozonation over sonolysis of oxygen (18,20). In addition, ultrasonic irradiation has been demonstrated to increase the mass transfer of ozone to solution, allowing more ozone to enter solution than in a non-irradiated system (21-23).

Previous studies of the combined process involving ultrasound and ozone have shown faster degradation rates for humic and fulvic acids, 4-nitrophenol, trinitrotoluene, and phenol than either system alone as well as very rapid decomposition of ozone due to an ultrasonic field (18-27). However, there have been no comprehensive studies demonstrating the importance of ozone decomposition and enhanced mass transfer mechanisms in enhancing degradation rates of substrates.

The primary objective of this study was to examine the degradation kinetics of three similar aromatic compounds, nitrobenzene (NB), 4-nitrophenol (4-NP), and 4-chlorophenol (4-CP), by ultrasound, by ozone, and by the combination of ultrasound and ozone. These compounds have a range of reaction rate constants with ozone as shown in Table 3.1 (28-32). As the reaction rates of the substrates with ozone increase we expect to see less enhancement due to the combined system if the thermal decomposition of ozone was the main process. On the other hand, if enhanced mass transfer due to sonication were

important, then few differences in the reaction rates should be seen. Experiments were performed at 20 kHz and 500 kHz to investigate the effects of ultrasonic frequency on reaction rates. The formation of intermediates and TOC degradation were also observed.

EXPERIMENTAL METHODS

Materials and Reagents

4-Nitrophenol (Aldrich, 99+%), 4-chlorophenol (Aldrich, 99+%), nitrobenzene (Aldrich, 99%), phosphoric acid (EM Science, 85%), sodium phosphate monobasic (Mallinkrodt), sodium hydroxide (Mallinkrodt), and sodium thiosulfate (Mallinkrodt) were used as received. All solutions were prepared with water purified by a Millipore Milli-Q UV Plus system (R = 18.2 MΩ-cm).

Sonochemical Experiments

The experimental setup consisted of a glass chamber reactor surrounded by a self-contained water jacket, a constant gas flow, and a source of ultrasound. The temperature of the solution was maintained constant by a 20° C water bath (Haake Co., model A81) flowing through the surrounding water jacket.

Oxygen gas was filtered through a Drierite and molecular sieve economy purifier (Alltech) and an activated charcoal hydrocarbon trap (Alltech) and flowed through an OREC Ozonator (Model O3V10-O) at 9 psig and 4.5 L min^{-1}. The gas flowed out of a coarse fritted-glass gas diffuser at 10 mL min^{-1}. The O_3 gas phase concentration was determined to be approximately 1.0% wt/wt by oxidation of indigo trisulfonic acid (33). No ozone was produced when voltage was not applied.

The sonication at 500 kHz was performed with an ultrasonic transducer (Undatim Ultrasonics) operating at 515 kHz and 100% power with a reaction volume of 640 ml, while the 20 kHz reactor was a direct immersion probe system (VCX-400 Vibracell, Sonic & Materials) operating at 50% power and a volume of 235 ml. The emitting area of the

transducers were 25.5 cm^2 and 1.20 cm^2 for the 500 kHz and 20 kHz systems, respectively. The electrical power outputs were determined by calorimetry, to be 48.3 W for the 500 kHz transducer and 56.1 W for the 20 kHz transducer. The 20 kHz probe was tuned in air and the titanium tip was polished prior to each sonication. Turbulence from the oxygen sparging was assumed to be sufficient for complete mixing in the 20 kHz reactor while a magnetic stirrer was used in the 500 kHz reactor.

Ozone decomposition is accelerated at high pH (34). To minimize the chain decomposition reactions of ozone with OH^-, all experiments were run at low pH. Initial solutions containing 100 μM of nitrobenzene, 4-nitrophenol or 4-chlorophenol were adjusted to a pH range of 2.3 to 2.5 using a 10 mM phosphate buffer consisting of a 3 to 1 ratio of H_3PO_4 to NaH_2PO_4. Measurements made before and after the experiments did not show a significant change in pH. To initiate a kinetic run, ultrasound and/or voltage from the ozonator was applied. Aliquots of 0.5 mL were collected at designated times. Samples were quenched with 0.1 mL of 70 mM thiosulfate to eliminate any residual ozone in solution. For 4-NP experiments 0.1 mL of 0.35 M NaOH was also added to adjust the pH to above 12 in order to have all of the 4-NP in the deprotonated form. All samples were filtered before analysis with 0.2 μm teflon syringe filters (Gelman). Experiments were performed in triplicate except for TOC experiments which were run once but analyzed in triplicate. Error bars on graphs represent experiment to experiment variation.

Analysis

In order to quantify 4-NP and its intermediate, 4-nitrocatechol (4-NC) a Hewlett Packard HP 8452a diode array spectrophotometer was used. The absorbance was measured at λ = 400 nm (ε = 17,909 M^{-1} cm^{-1} for 4-NP) and λ = 512 (ε = 12,500 M^{-1} cm^{-1} for 4-NC). Quantification of NB, 4-CP and their intermediates was done on a Hewlett-Packard Series II 1090 HPLC. A 5 mm, 100 x 2.1 mm ODS Hypersil column (Hewlett Packard) was used for the analysis of 4-CP and intermediates. With this column a gradient program was used with an eluent mixture consisting of an aqueous phosphate buffer

solution (pH = 3) and acetonitrile. For NB, a 3 mm 100 x 4 mm Hypersil BDS-C18 column (Hewlett Packard) was used. The eluent consisted of a 30:70 (water: acetonitrile) isocratic mixture. TOC analysis was performed on a Shimadzu 5000A total organic carbon analyzer operating in the non-purgable organic carbon (NPOC) mode.

RESULTS

Figure 3.1 shows the destruction of NB, 4-NP, and 4-CP by ultrasonic irradiation in the 20 kHz and 500 kHz reactors. The linearity in the first-order plot demonstrates that the degradation rate is first-order with respect to the primary substrates in both systems. Table 3.2 lists the first-order degradation rate constants by sonolysis (k_{US}). In the 20 kHz reactor, NB degrades the fastest and 4-NP the slowest but in the 500 kHz reactor 4-CP is the fastest while 4-NP is the most resistant to destruction by sonication. Lower frequency sonication results in a greater degree of vapor phase pyrolysis due to high temperatures achieved during bubble collapse conditions while higher frequencies favor OH• production (35). Our results are consistent with these observations since NB has the highest Henry's Law constant and reacts considerably faster in the 20 kHz system than 4-CP or 4-NP. In contrast, in the 500 kHz system, 4-CP reacts most rapidly due to its fast reaction rate with OH• and its high K_{OW} which suggests a greater partitioning to the bubble interface due to its higher hydrophobicity.

In order to compare degradation rate constants obtained in the 500 kHz reactor with constants for the 20 kHz reactor, the rate constants at 500 kHz are normalized to values at the 20 kHz rate by the respective power inputs per volume as follows:

$$k_{norm,\ 500} = k_{obs,\ 500} \frac{V_{500}}{P_{500}} \frac{P_{20}}{V_{20}} \qquad (3)$$

where $k_{norm,\ 500}$ is the normalized rate constant at 500 kHz, $k_{obs,\ 500}$ is the observed rate constant at 500 kHz, V is the volume of solution in the reaction chamber at 20 or 500 kHz, and P is the input power at 20 or 500 kHz as measured by calorimetry. The P/V ratio is a factor of 3.2 greater for the 20 kHz probe than for the 500 kHz reactor as shown in Table 3.3. However, the normalized rate constants are between 12 and 38 times greater at 500 kHz than at 20 kHz. Therefore, to destroy NB, 4-NP, or 4-CP considerably more energy is needed at 20 kHz than at 500 kHz. This is consistent with previous studies of the effects of frequency on reaction rates (3,36-38).

The reaction of ozone with these compounds also followed a pseudo first-order degradation rate law for the loss of substrate over 4 half-lives. As expected from the known overall second-order reaction rate constants of O_3 with NB, 4-NP and 4-CP (see Table 3.1), NB reacts the slowest and 4-CP the fastest. These results are shown in Figure 3.2 and Table 3.2. An O_3 gas flow rate of 10 mL min^{-1} was used with both reactors. Since the volume and geometries are different, the reported reaction rates in the 20 and 500 kHz reactors are not equal. Correcting these rates for the volume (V_{500}/V_{20} = 2.7) brings the values to within approximately 20%. The discrepancy is due to the different geometries of the reactors.

Figure 3.3 represents the loss of NB, 4-NP, and 4-CP by sonication in an oxygen/ozone (99/1 w/w) system. The combination of ultrasound with ozone also follows apparent pseudo first-order kinetics. As observed in the ozonation of the compounds, degradation is greater at 20 kHz. Since the reaction rate constant ratio of ozone for each compound, $k_{O_3,\ 20}/k_{O_3,\ 500}$, is merely a function of physical parameters when performed in the 20 kHz or 500 kHz reactors, it can be used as a basis for comparison. If the effect of sonication coupled with ozonation was the same in both systems we would expect a similar increase in the amount degradation to that seen with ozonation alone. However, the difference of the k_{20}/k_{500} ratios in the ozone and combination experiments shows an increase of 23%, 43%, and 55% for 4-NP, 4-CP, and NB, respectively. This indicates

that the combination of sonolysis and ozonolysis is enhanced at 20 kHz compared to 500 kHz, although the degradation rates for sonication with oxygen are considerably less in the 20 kHz system. A similar effect is seen by normalizing the degradation rate constant at 500 kHz to 20 kHz with eq. 3. Table 3.3 shows that $k_{norm,500}$ is slightly less than k_{20} for the combined system indicating that less ultrasonic energy with the same O_3 input is required at low frequency for the same degree of degradation in the combined system. This is in contrast to sonication with O_2 where the 500 kHz reactor was ultrasonically more efficient.

As shown in Figures 3.4 and 3.5, ozonolysis is observed to be slower than sonolysis combined with ozonolysis and sonolysis is slowest for all the compounds at both frequencies. At 20 kHz, degradation of compounds in an ultrasonic field is considerably slower than reactions with ozone or ultrasound combined with ozone. However, at 500 kHz all three types of experiments for each compound were within a factor of 2.

Intermediates indentified in these systems are listed in Table 3.4. NB degradation products at 20 and 500 kHz are shown in Figure 3.6. During a 3.5 hour sonolysis experiment at 20 kHz, intermediates were produced throughout the run, while in the 500 kHz reactor, the intermediate concentrations grew then began to degrade. The 20 kHz sonolysis experiments showed intermediate concentrations up to 10 μM. In general, the concentration of the intermediate species increased initially and then decreased after reaching a peak concentration. The rate of disappearance was slower than the rate of accumulation. Typical concentrations observed reached levels of <1 μM to 4 μM. In all cases the intermediates peaked earlier with sonolytic ozonation than with sonication or ozonation alone. Earlier intermediate peak formation with sonolytic ozonation indicates the more rapid degradation of the parent compound than with the separate systems. The NB intermediates, 4-NP and 3-NP, in the combined system, had higher peak concentrations than the separate processes. More significant accumulation of 4-NP in the combined system demonstrates that 4-NP is less reactive by sonolytic ozonation than NB, as shown in Figure 3.3.

Initial first-order degradation rate constants for the loss of TOC associated with NB, 4-NP, and 4-CP are given in Table 3.5. The rate constant, $k_{obs\ TOC}$, is approximately 0.1 of k_{obs} of the parent compound. This is expected since the degradation products will contribute to the TOC until the carbon species are oxidized to CO_2. Similar to what was observed with the destruction of the parent compounds, sonication with O_2 yielded the slowest reaction rate with the TOC. Although ozonation showed rapid initial destruction over the first 3 hours, the rates decreased as intermediates resistant to oxidation by ozone were formed. Degradation rates of TOC by sonolytic ozonation were faster than sonication or ozonation alone and followed first-order kinetics. Intermediates which are refactory to destruction by ozone are destroyed by OH formed from sonolytic decomposition of ozone. The compounds were mineralized to CO_2 in 3 hours with the 20 kHz probe, and 6 hours in the 500 kHz reactor. Normalizing the 500 kHz first-order rate constants for loss of TOC by US/O_3 ($k_{norm\ TOC\ NB} = 0.011\ min^{-1}$, $k_{norm\ TOC\ 4\text{-}NP} = 0.016\ min^{-1}$, $k_{norm\ TOC\ 4\text{-}CP} = 0.024\ min^{-1}$) and comparing to the 20 kHz system, the 500 kHz system appears to be ultrasonically more efficient for sonolytic ozonation with 4-NP and 4-CP for TOC destruction. The TOC associated with NB is more efficiently degraded at the lower frequency by sonolytic ozonation. This is most likely due to its higher Henry's Law constant, resulting in greater vapor-phase partitioning.

DISCUSSION

In order to evaluate the amount of enhancement upon combining sonolysis with ozonolysis, the overall rate of substrate disappearance can be represented by a linear combination of contributing terms similar to that proposed by Peyton *et al.* for O_3 combined with ultraviolet irradiation (17):

$$-\frac{dC}{dt} = k_{US}\,C + k_{O_3}\,C + k_{US/O_3}\,C \qquad (4)$$

where k_{US}, k_{O_3}, and k_{US/O_3} are, respectively, the first-order degradation rate constants for sonolysis, ozonolysis, and the residual kinetic effect upon combining the two systems. Gas stripping of compounds was not expected to be significant in this system over the time period of degradation. Eq. 4 can be expressed as:

$$-\frac{dC}{dt} = k_{total}\,C = \sum_{i} k_i\,C \qquad (5)$$

where k_{total} is the sum of constants for the contributing processes. Values of k_{US} and k_{O_3} were determined from separate experiments involving only sonication or ozonation. The $k_{US}C$ term combines all pyrolysis and OH radical reactions with the substrates observed in the plain sonication experiments. The term, $k_{O_3}C$ includes both direct O_3 reactions and radical reactions from O_3 autodecomposition that occur in the non-irradiated experiments. For there to be an enhanced effect of combining the systems over the individual components, k_{US/O_3} must be positive, otherwise there would be no benefit upon combining ultrasound with ozone. Table 3.2 lists the rate constants for all three substrates in both reactors as well as the model k values required for the case of no antagonism or synergism in the system (*i.e.* $k = k_{US} + k_{O_3}$).

Figures 3.4 and 3.5 show the first-order plots for substrate degradation in both the 20 kHz and 500 kHz reactors, respectively. At 20 kHz the model consistently predicts rates slower than those observed. Rate constants are 114%, 54%, and 65% higher for NB, 4-NP, and 4-CP, respectively, for the combined system than for the linear combination of separate experiments. However, in the 500 kHz system the model consistently over predicts the degradation rates by 13%, 22%, and 34% for NB, 4-NP, and 4-CP,

respectively. Therefore, at 20 kHz synergism is observed while at 500 kHz antagonism is seen.

Initial first-order rate constants for TOC loss corresponding to NB, 4-NP, or 4-CP solutions as well as the linear combination of k_{US} and k_{O_3} are tabulated in Table 3.5. The model underpredicted the rate constant at both frequencies for the mineralization of the compounds. At 20 kHz the enhancements were 411%, 213%, and 302% for NB, 4-NP, and 4-CP, respectively. The enhancements were not as significant at 500 kHz, but followed the same general trend of NB (137%) > 4-CP (64%), > 4-NP (35%).

Sonication of O_3 affects the O_3 concentration in solution and hence the amount of O_3 available to react directly with the substrate. Enhanced mass transfer of O_3 is a process that has been observed in ultrasonic fields (21-23). This enhancement should increase k_{O_3}. Enhanced mass transfer may be due to the growth and collapse of the cavitation bubble forcing ozone into solution, due to the turbulence caused in the ultrasonic field, which is greater at 20 kHz, or due to a phenomena called acoustic streaming which creates a force in the direction away from the transducer. The 500 kHz transducer causes a horizontal pressure, and the 20 kHz probe points downward, therefore acoustic streaming in the 20 kHz probe will act against the buoyancy force of the bubble allowing for longer contact times of ozone with solution. However, the sonication of ozone, which has been observed to cause an extremely rapid destruction of ozone (18), decreases k_{O_3} due to less ozone available in solution. Reactions of ozone with NB, 4-NP, and 4-CP are second-order reactions overall and first-order in [O_3] and [substrate], and thus k_{O_3} is coupled with the aqueous ozone concentration. In addition, sonication produces OH•, HO_2•, and H_2O_2 in water (38-40). OH•, O_2^- and HO_2^-, are involved in the autodecomposition of O_3 (15,41). This in turn causes k_{O_3} to be reduced. Degassing is another mechanism that can occur in an ultrasonic system. k_{O_3} is reduced when degassing occurs.

Reduction in the magnitude of k_{US} will result from O_3 reacting with OH• formed during the sonolytic cleavage of water vapor:

$$O_3 + OH\bullet \rightarrow HO_2\bullet + O_2 \qquad (6)$$

This reaction will occur in both the gas phase and in the aqueous phase and will result in less OH• available for direct reaction with the substrates. However, O_3 combined with ultrasound is not expected to alter the partitioning of the substrate to the cavitation bubble interface. The gas inside the bubble in the combined system is composed of 99% O_2 and 1% O_3 whereas the gas in the sonolysis system in the absence of O_3 is 100% O_2. The maximum collapse temperature in the bubble varies with the polytropic index of the gas, K (12):

$$T_{max} = T_0\{(K-1)\frac{P_m}{P}\} \qquad (7)$$

where T_{max} is the bubble temperature at collapse, T_0 is the temperature of the bulk solution, P is the pressure in the bubble at its maximum size, P_m is the pressure in solution at the time of transient bubble collapse, and $K = C_p/C_v$. $K_{O_2} = 1.4$ and $K_{O_3} = 1.2$ (42) therefore, adding 1% O_3 to the oxygen stream will change the effective K slightly, reducing the bubble collapse temperature by less than a percent. This will have little effect on the direct pyrolysis of both water and substrate occurring in the bubble.

Other factors altering the reactivity of the combined system include the reaction of O_3 with atomic oxygen in the vapor phase of the bubbles as follows (18):

$$O_3 + O\bullet \rightarrow 2\,O_2 \qquad (8)$$

The flowrate of O_3 entering the reactor may also be a factor in the alteration of the degradation rates in the combined US/O_3 system. The flowrate used was the same for both systems, even though the reactor volume was a factor of 2.7 larger for the 500 kHz

chamber. A larger flowrate in the 500 kHz reactor should increase the reaction rate constant for ozonation, and perhaps also the degree of enhancement for sonolytic ozonation.

The above description of possible processes occurring in the combined US/O_3 system demonstrates the added complexities with US/O_3 over the individual systems. As shown in Figure 3.5, the combination of the individual terms, $k_{US} + k_{O_3}$, is greater than k_{total} for the sonolytic ozonation of the substrates at 500 kHz. Since it is unlikely an individual substrate is formed, a modified version of eq 4 describes the combined system better:

$$-\frac{dC}{dt} = k'_{US}\,C + k'_{O_3}\,C + k_{US/O_3}\,C \qquad (11)$$

where k'_{US} and k'_{O_3} are the altered rate constants for sonolysis and ozonolysis in the combined system. These processes still occur in the combined system but not at the same rates as in the individual systems. As in eq. 4, k_{US/O_3} is the residual kinetic effect due to the combination of processes, which may be due to effects such as enhanced mass transfer and additional OH• formation. For substrate removal in the 500 kHz chamber, the following relation holds:

$$k_{US} + k_{O_3} > k'_{US} + k'_{O_3} + k_{US/O_3} \qquad (12)$$

The US/O_3 rate constants, k'_{US} and/or k'_{O_3} are smaller than k_{US} and k_{O_3} from the separate sonolysis and ozonolysis experiments at 500 kHz. If the term, k_{US/O_3} exists at 500 kHz it does not compensate for the reductions in k'_{US} and/or k'_{O_3} in the combined system compared to the individual systems. In the 20 kHz reactor and for TOC destruction in both reactors, the opposite condition exists:

$$k_{US} + k_{O_3} < k'_{US} + k'_{O_3} + k_{US/O_3} \quad (13)$$

k_{US/O_3} is larger than the amount of reduction in k'_{US} and/or k'_{O_3} in relation to the separate ultrasound and ozone systems. It is even possible that k'_{O_3} is larger than in the individual experiments. However, it is impossible to determine the values of k'_{US}, k'_{O_3}, and k_{US/O_3} from the experiments performed.

As seen in Table 3.3, even though the 500 kHz reactor requires less ultrasonic energy per molecule degraded than the 20 kHz reactor system for sonolytic degradation of NB, 4-NP, and 4-CP, there appear to be no catalytic effects in combining sonication with O_3. Antagonism increases with increasing k_{O_3}. Although the 500 kHz system does not give benefits over ozonation or sonication with oxygen for the destruction of the parent compounds, the antagonism does follow the trend we expect for thermolytic ozone destruction in a cavitation bubble. The negative factors affecting the observed rate constants appear to be greater than the effects of enhanced mass transfer and increased radical production occurring in the combined system. At 20 kHz even though NB has the slowest reaction rate with O_3 and highest Henry's Law constant, H, the degradation rate of NB is enhanced substantially more than those for 4-NP and 4-CP. At 20 kHz, the rate of enhancement follows the apparent trend in Henry's Law constants. In spite of the complexity of the combined treatment system, it appears that OH radical formation from O_3 decomposition is the main mechanism for sonolytic ozonation.

ACKNOWLEDGMENTS

Financial support provided by Defense Advanced Research Projects Agency (DARPA), the Office of Naval Research (ONR), and the Electric Power Research Institute (EPRI) is gratefully acknowledged.

REFERENCES

1. Hua, I.; Hoffmann, M. R., *Environ. Sci. Technol.,* **1996**, *30*, 864-871.

2. Cost, M.; Mills, G.; Glisson, P.; Lakin, J., *Chemosphere,* **1993**, *27*, 1737-1743.

3. Drijvers, D.; Baets, R. D.; Visscher, A. D.; Langenhove, H. V., *Ultrasonics Sonochemistry,* **1996**, *3*, S83-S90.

4. Hua, I.; Höchemer, R. H.; Hoffmann, M. R., *J. Phys. Chem.,* **1995**, *99*, 2335-2342.

5. Hua, I.; Höchemer, R. H.; Hoffmann, M. R., *Environ. Sci. Technol.,* **1995**, *29*, 2790-2796.

6. Kontronarou, A.; Mills, G.; Hoffmann, M. R., *J. Phys. Chem.,* **1991**, *95*, 3630-3638.

7. Kontronarou, A.; Mills, G.; Hoffmann, M. R., *Environ. Sci. Technol.,* **1992**, *26*, 2420-2428.

8. Kontronarou, A.; Mills, G.; Hoffmann, M. R., *Environ. Sci. Technol.,* **1992**, *26*, 1460-1462.

9. Serpone, N.; Terzian, R.; Hidaka, H.; Pelizzetti, E., *J. Phys. Chem.,* **1994**, *98*, 2634-2640.

10. Turai, L. L.; Rosario, F. d., *Appita,* **1982**, *35*, 407-411.

11. Leighton, T. G. *The Acoustic Bubble*; Academic Press: London, 1994.

12. Mason, T. J.; Lorimer, J. P. *Sonochemistry: Theory, Applications and Uses of Ultrasound in Chemistry*; Ellis Horwood Ltd: Chichester, 1988.

13. Glaze, W. H.; Kang, J. W.; Chapin, D. H., *Ozone Sci. Eng.,* **1987**, *9*, 335-352.

14. Gurol, M. D.; Vatistas, R., *Wat. Res.,* **1987**, *21*, 895-900.

15. Langlais, B.; Reckhow, D. A.; Brink, D. R. *Ozone in Water Treatment Application and Engineering*; AWWA Research Foundation and Lewis Publishers: Chelsea, 1991.

16. Masten, S. J.; Davies, S. H. R. In Environmental Oxidants,J. O. Nriagu and M. S. Simmons; John Wiley & Sons: New York, 1994; pp 517-547.

17. Peyton, G. R.; Huang, F. Y.; Burleson, J. L.; Glaze, W. H., *Environ. Sci. Technol.,* **1982**, *16*, 448-453.

18. Hart, E. J.; Henglein, A., *J. Phys. Chem.,* **1986**, *90*, 3061-3061.

19. Hart, E. J.; Henglein, A., *J. Phys. Chem.,* **1985**, *89*, 4342-4347.

20. Barbier, P. F.; Pétier, C. In *The First International Conference on Advanced Oxidation Technologies for Water and Air Remediation*; London, Ontario, Canada,

1994; pp. 94-96.

21. Olson, T. M.; Barbier, P. F., *Wat. Res.*, **1994**, *28*, 1383-1391.

22. Sierka, R. A. "Mass Transfer and Reaction Rate Studies of Ozonated MUST Wastewaters in the Presence of Sound Waves," University of Arizona, 1976.

23. Dahi, E., *Wat. Res.*, **1976**, *10*, 677-684.

24. Sierka, R. A., *Ozone Sci. Engng.*, **1985**, *6*, 275-290.

25. Sierka, R. A.; Amy, G. L., *Ozone Sci. Engng.*, **1985**, *7*, 47-62.

26. Burleson, G. R.; Murray, T. M.; Pollard, M., *Appl. Micobiol.*, **1975**, *29*, 340-344.

27. Chen, J. W., *Water,* **1972**, *69*, 61-70.

28. Buxton, G. V.; Greenstock, C. L.; Helman, W. P.; Ross, A. B., *J. Phys. Chem. Ref. Data,* **1988**, *17*, 513-817.

29. Hoigné, J.; Bader, H., *Wat. Res.*, **1983**, *17*, 173-183.

30. Hoigné, J.; Bader, H., *Wat. Res.*, **1983**, *17*, 185-194.

31. Mackay, D.; Shiu, W. Y.; Ma, K. C. *Illustrated Handbook of Physical-Chemical Properties and Environmental Fate for Organic Chemicals*; Lewis Publishers: Boca

Raton, 1995; Vol. IV Oxygen, Nitrogen and Sulfur Containing Compounds.

32. Seinfeld, J. H. *Atmospheric Chemistry and Physics of Air Pollution*; Wiley-Interscience: New York, 1986.

33. Bader, H.; Hoigné, J., *Wat. Res.*, **1981**, *15*, 449-456.

34. Sehested, K.; Corfitzen, H.; Holcman, J.; Fischer, C. H.; Hart, E. J., *Environ. Sci. Technol.*, **1991**, *25*, 1589-1596.

35. Pétrier, C.; Jeunet, A.; Luche, J.-L.; Reverdy, G., *J. Am. Chem. Soc.*, **1992**, *114*, 3148-350.

36. Francony, A.; Pétrier, C., *Ultrasonics Sonochemistry*, **1996**, *3*, S77-S82.

37. Höchemer, R. H., *Ph. D. Thesis*, California Institute of Technology, 1996.

38. Hua, I., *Ph. D. Thesis*, California Institute of Technology, 1996.

39. Makino, K.; Mossoba, M. M.; Riesz, P., *J. Phys. Chem.*, **1983**, *87*, 1369-1377.

40. Riesz, P.; Kondo, T.; Krishna, C. M., *Ultrasonics*, **1990**, *28*, 295-303.

41. Staehelin, J.; Hoigné, J., *Environ. Sci. Technol.*, **1982**, *16*, 676-681.

42. Perry, R. H.; Green, D. *Perry's Chemical Engineers' Handbook*; Mc Graw-Hill: New York, 1984.

Table 3.1: Selected properties and rate constants of compounds.

Compound	pK_a *	H* ($Pa \cdot m^3/mol$)	log K_{OW}*	k_{O_3} (29, 30) (M^{-1} sec^{-1})	k_{OH} (28) (M^{-1} sec^{-1})
ozone	-	1.08×10^4	-	-	1.1×10^8
nitrobenzene	-	1.3	1.83	0.09	3.9×10^9
4-nitrophenol	7.14	4.21×10^{-5}	1.2	<50	3.8×10^9
4-chlorophenol	9.38	0.0567	2.16	600	7.6×10^9

* Values from (31) except for ozone which is from (32).

Table 3.2: Pseudo first-order rate constants for degradation of NB, 4-CP, and 4-NP under various conditions.

Experiment	$k_{20\ kHz}$ (min^{-1})	$k_{500\ kHz}$ (min^{-1})
Nitrobenzene		
Sonication w/O_2: k_{US}	3.2×10^{-3}	1.2×10^{-2}
Ozonation: k_{O_3}	3.8×10^{-2}	1.7×10^{-2}
Sonication w/O_3: k_{total}	8.9×10^{-2}	2.6×10^{-2}
Model prediction: $k = k_{US} + k_{O_3}$	4.1×10^{-2}	3.0×10^{-2}
4-Nitrophenol		
Sonication w/O_2: k_{US}	1.8×10^{-3}	1.2×10^{-2}
Ozonation: k_{O_3}	4.9×10^{-2}	1.8×10^{-2}
Sonication w/O_3: k_{total}	7.8×10^{-2}	2.3×10^{-2}
Model prediction: $k = k_{US} + k_{O_3}$	5.1×10^{-2}	3.0×10^{-2}
4-Chlorophenol		
Sonication w/O_2: k_{US}	1.7×10^{-3}	2.1×10^{-2}
Ozonation: k_{O_3}	6.0×10^{-2}	2.6×10^{-2}
Sonication w/O_3: k_{total}	1.0×10^{-1}	3.1×10^{-2}
Model prediction: $k = k_{US} + k_{O_3}$	6.2×10^{-2}	4.7×10^{-2}

Table 3.3: Power per volume ratio and pseudo first-order rate constants of degradation normalized to 20 kHz for sonication in an oxygen or ozone saturated solution.

	Sonication w/O_2		Sonication w/O_3	
	20 kHz	500 kHz	20 kHz	500 kHz
P/Vol (W/mL)	2.4×10^{-1}	7.5×10^{-2}	2.4×10^{-1}	7.5×10^{-2}
$k_{Nitrobenzene}(min^{-1})$	3.2×10^{-3}	4.0×10^{-2}	8.9×10^{-2}	8.3×10^{-2}
$k_{4\text{-}Nitrophenol}$ (min^{-1})	1.8×10^{-3}	3.7×10^{-2}	7.8×10^{-2}	7.4×10^{-2}
$k_{4\text{-}Chlorophenol}$ (min^{-1})	1.7×10^{-3}	6.6×10^{-2}	1.0×10^{-1}	9.9×10^{-2}

Table 3.4: Aromatic intermediates observed in the degradation of NB, 4-NP, and 4-CP at 20 and 500 kHz by sonolysis, ozonolysis and the combination.

Experiment	20 kHz*	500 kHz*
Nitrobenzene		
Sonication w/O_2	4-NP (1.3), 3-NP (2.8), 4-NC (7.8)	4-NP (0.9), 3-NP (2.1), 2-NP(3.2), 4-NC (3.8)
Ozonation	4-NP (1.2), 3-NP (0.3)	4-NP (1.3), 3-NP (1.1), 2-NP (2.1), 4-NP (0.3)
Sonication w/O_3	4-NP (2.9), 3-NP (2.1), 4-NC (1.0)	4-NP (2.2), 3-NP (2.3), 2-NP (1.9), 4-NC (2.9)
4-Nitrophenol		
Sonication w/O_2	4-NC (3.0)	4-NC (7.6)
Ozonation	4-NC (1.2)	none detected
Sonication w/O_3	4-NC (1.2)	none detected
4-Chlorophenol		
Sonication w/O_2	4-CC (10.3)	4-CC (13.7)
Ozonation	none detected	4-CC (16.4)
Sonication w/O_3	none detected	none detected

Values in parenthesis represent maximum μM concentrations observed during an experiment.

* Abbreviations: 4-NP, 4-nitrophenol; 3-NP, 3-nitrophenol; 2-NP, 2-nitrophenol; 4-NC, 4-nitrocatechol; and 4-CC, 4-chlorocatechol.

Table 3.5: Pseudo first-order rate constants for degradation of TOC associated with NB, 4-CP, and 4-NP under specified conditions.

Experiment	$k_{20\ kHz}$ (min^{-1})	$k_{500\ kHz}$ (min^{-1})
Nitrobenzene		
Sonication w/O_2: k_{US}	3.2×10^{-4}	3.5×10^{-4}
Ozonation: k_{O_3}	2.2×10^{-3}	1.1×10^{-3}
Sonication w/O_3: k_{total}	1.3×10^{-2}	3.4×10^{-3}
Model prediction: $k = k_{US} + k_{O_3}$	2.5×10^{-3}	1.5×10^{-3}
4-Nitrophenol		
Sonication w/O_2: k_{US}	$\sim 0 \times 10^{-3}$	1.1×10^{-3}
Ozonation: k_{O_3}	3.4×10^{-3}	2.7×10^{-3}
Sonication w/O_3: k_{total}	1.1×10^{-2}	5.0×10^{-3}
Model prediction: $k = k_{US} + k_{O_3}$	3.4×10^{-3}	3.7×10^{-3}
4-Chlorophenol		
Sonication w/O_2: k_{US}	$\sim 0 \times 10^{-3}$	1.4×10^{-3}
Ozonation: k_{O_3}	4.6×10^{-3}	3.3×10^{-3}
Sonication w/O_3: k_{total}	1.9×10^{-2}	7.7×10^{-3}
Model prediction: $k = k_{US} + k_{O_3}$	4.6×10^{-3}	4.7×10^{-3}

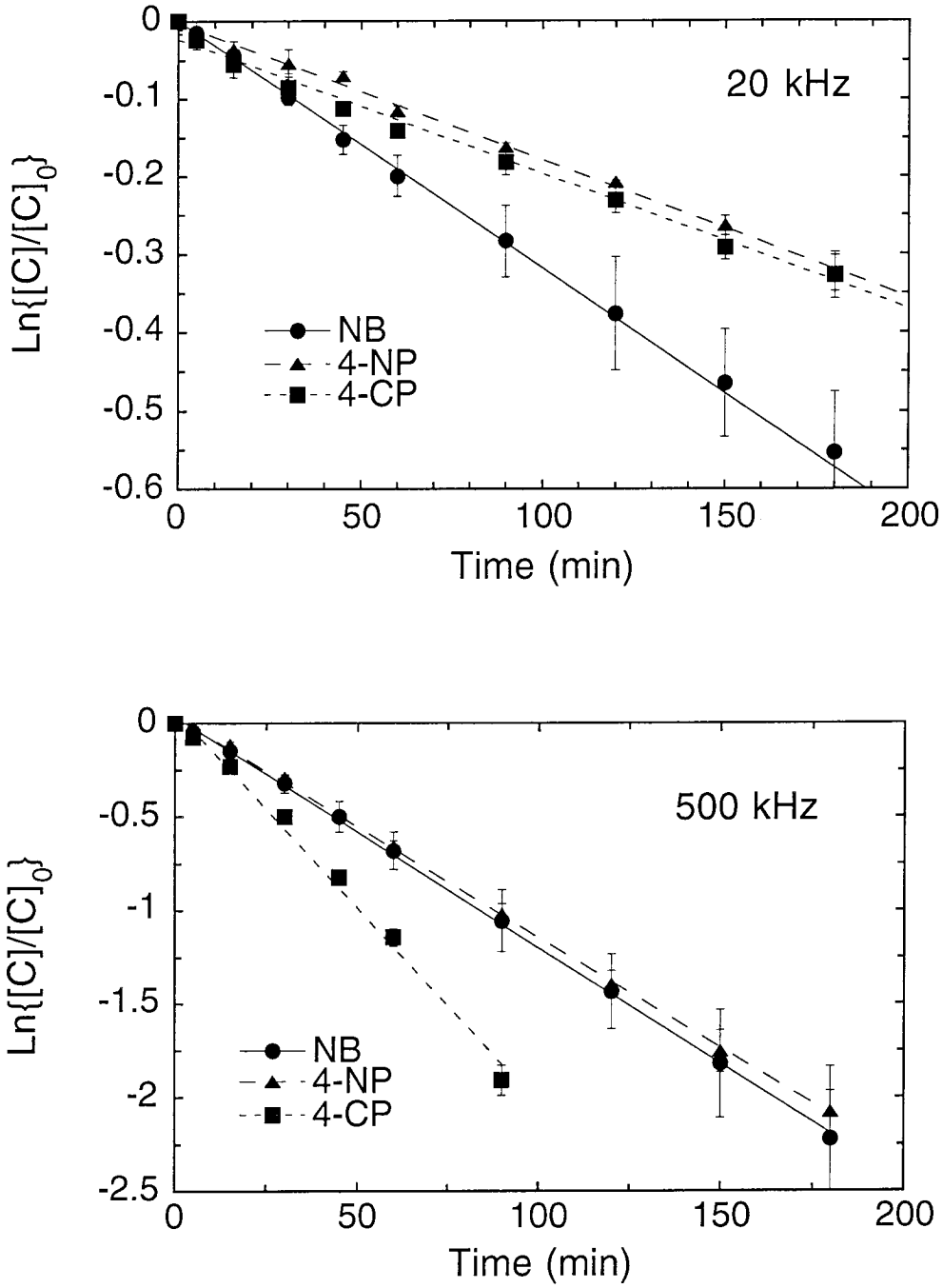

Figure 3.1: Sonolytic degradation of NB, 4-NP, and 4-CP at 20 kHz and 500 kHz. O_2 gas flowrate = 10 mL min^{-1}, pH = 2.4 ± 0.2, T= 293 K, initial concentration of substrate = 100 μM, power = 56.1 W at 20 kHz and 48.3 W at 500 kHz.

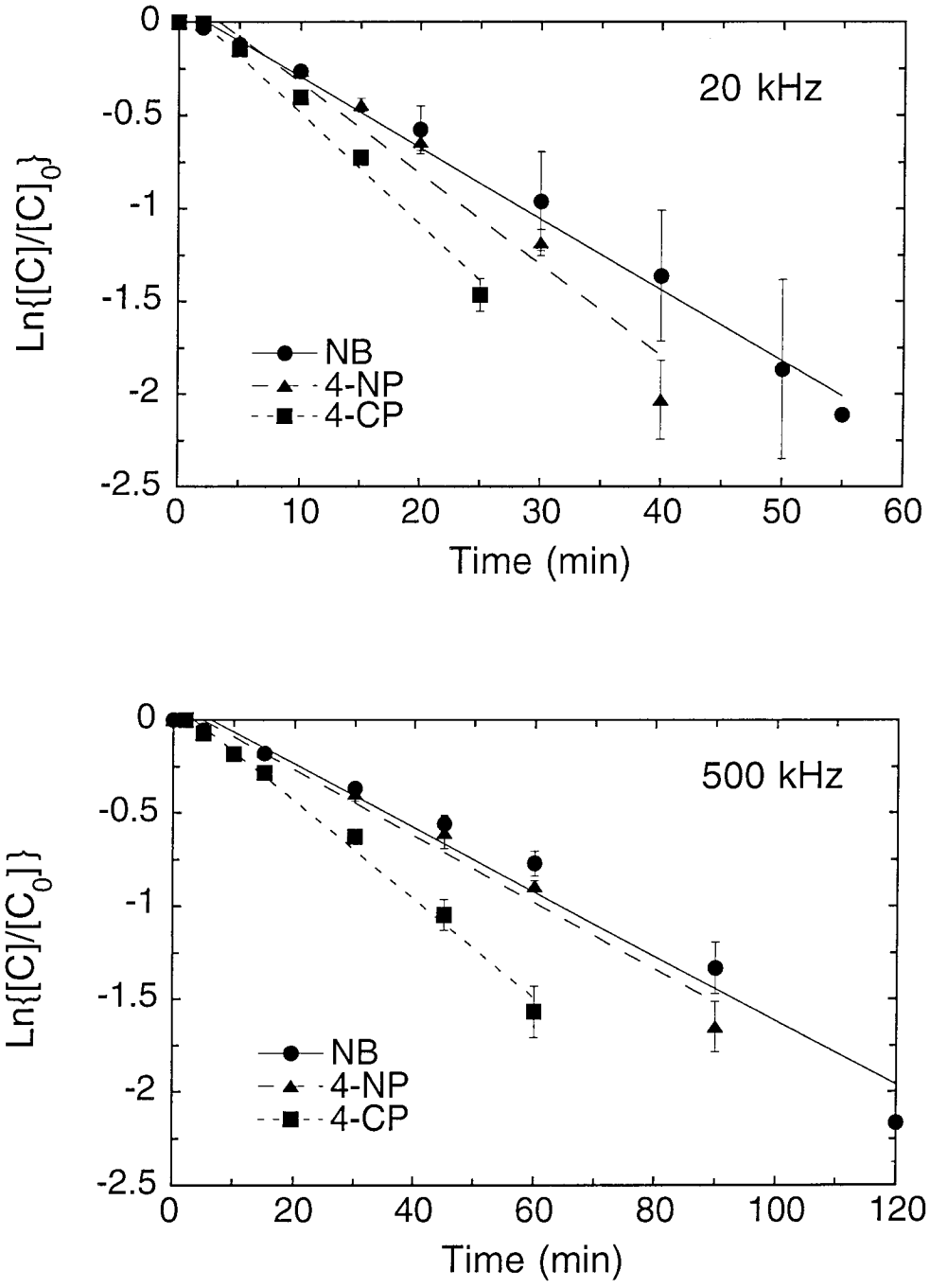

Figure 3.2: Ozonation of NB, 4-NP, and 4-CP in the 20 kHz and 500 kHz reactors. O_3 gas flowrate = 10 mL min^{-1}, pH = 2.4 ± 0.1, T= 293 K, initial concentration of substrate = 100 μM.

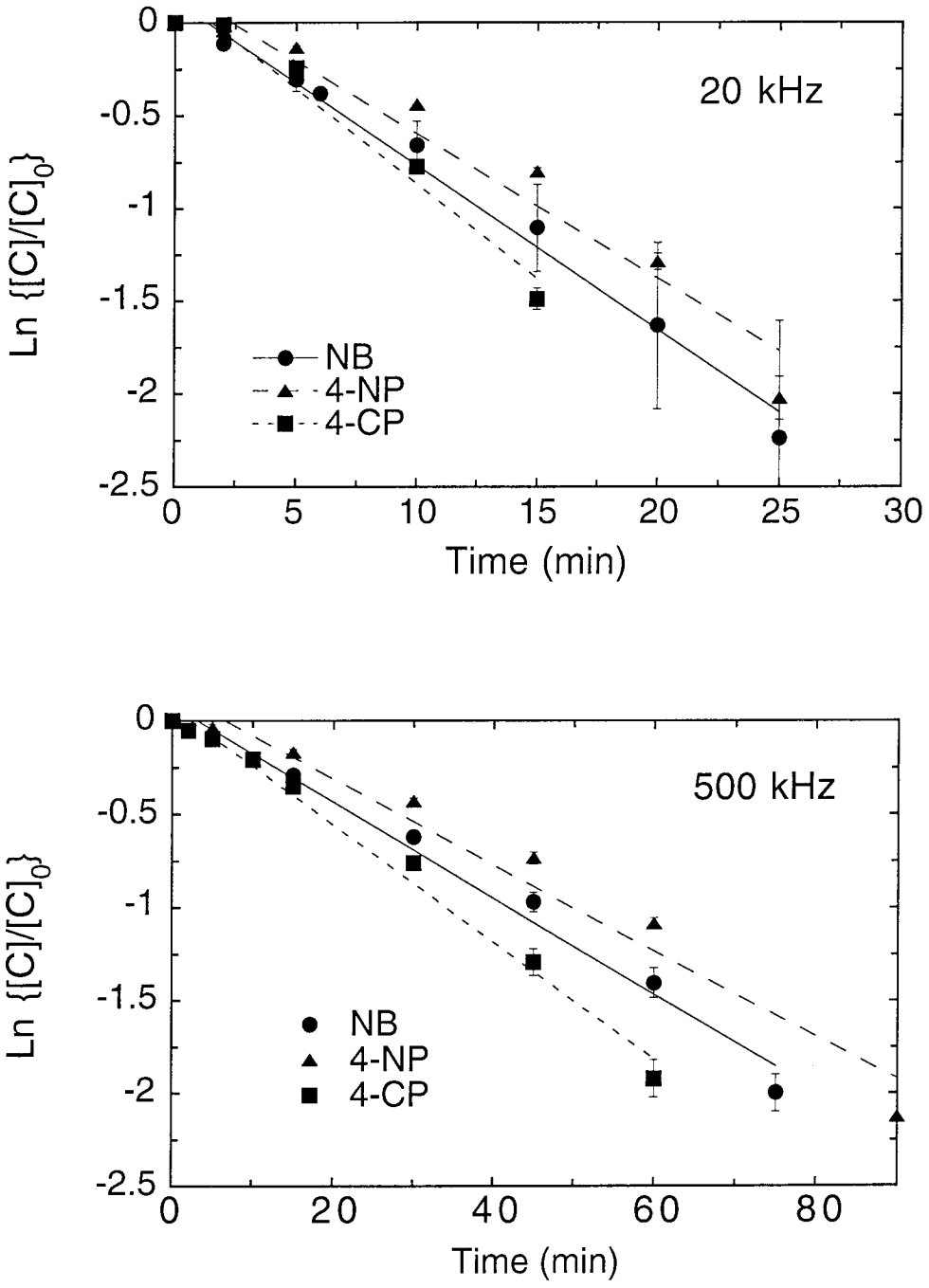

Figure 3.3: Sonolytic ozonation of NB, 4-NP, and 4-CP at 20 kHz and 500 kHz. O_3 gas flowrate = 10 mL min^{-1}, pH = 2.4 ± 0.2, T= 293 K, initial concentration of substrate = 100 μM, power = 56.1 W at 20 kHz and 48.3 W at 500 kHz.

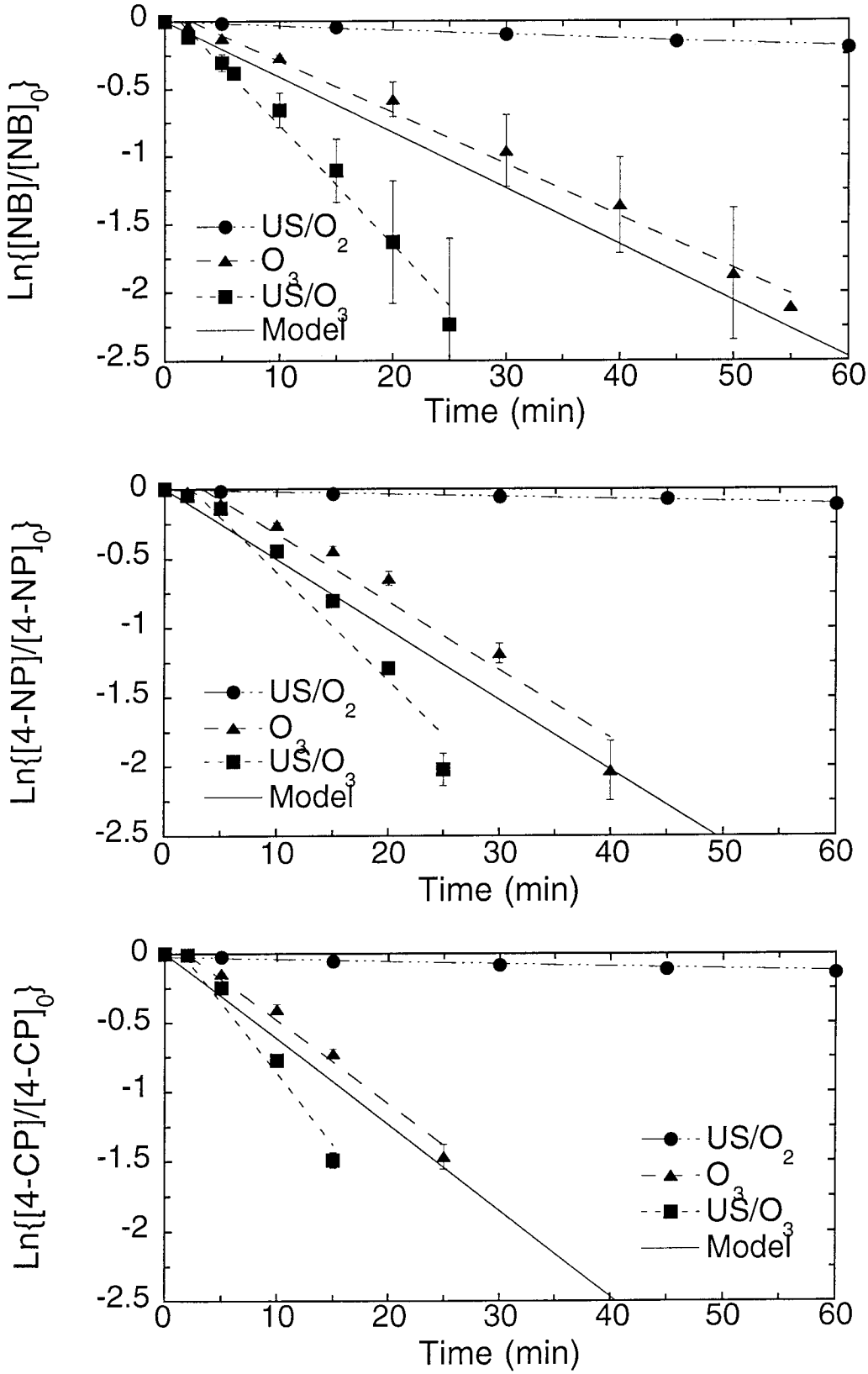

Figure 3.4: First-order degradation of NB, 4-NP, and 4-CP due to sonication with O_2 ozonation, and sonolytic ozonation in the 20 kHz reactor. O_3 gas flowrate = 10 mL min^{-1}, pH = 2.4 ± 0.2, T= 293 K, initial concentration of substrate = 100 μM, power = 56.1 W.

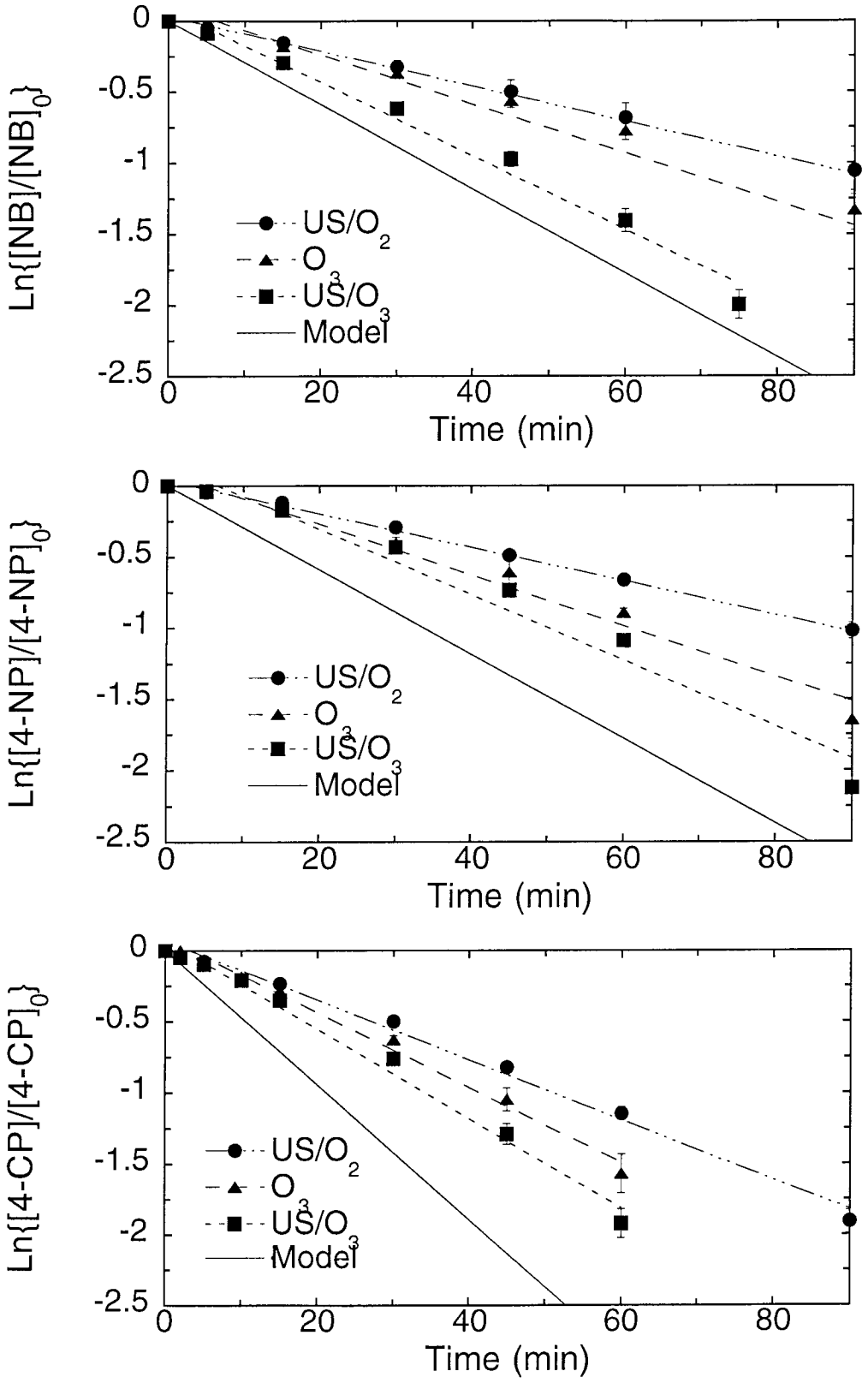

Figure 3.5: First-order degradation of NB, 4-NP, and 4-CP due to sonication with O_2, ozonation, and sonolytic ozonation in the 500 kHz reactor. O_3 gas flowrate = 10 mL min^{-1}, pH = 2.4 ± 0.2, T= 293 K, initial concentration of substrate = 100 μM, power = 48.3 W.

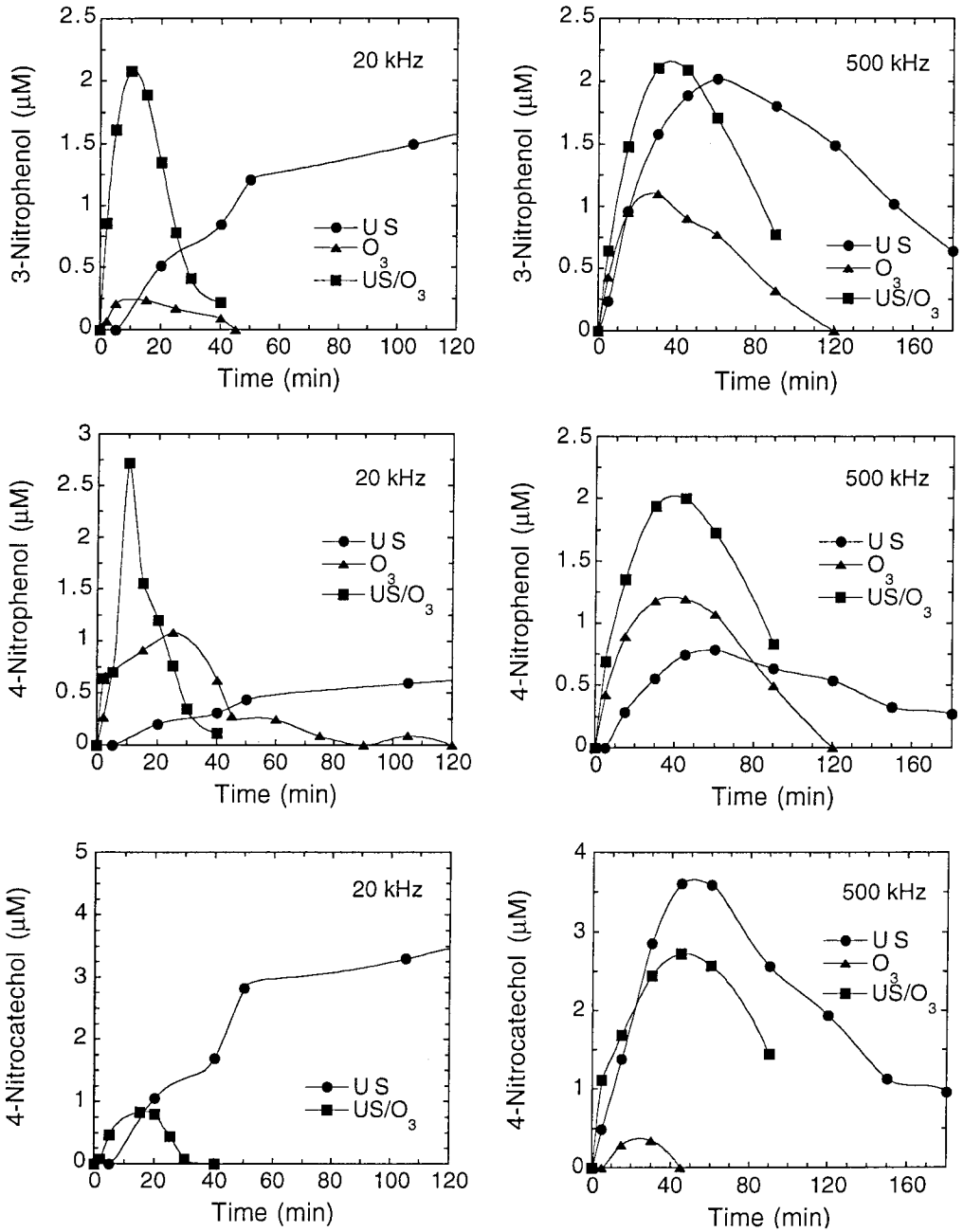

Figure 3.6: Formation of NB degradation products by sonication with O_2, ozonation, and sonolytic ozonation at 20 and 500 kHz. O_3 gas flowrate = 10 mL min^{-1}, pH = 2.4 ± 0.2, T= 293 K, $[NB]_0$ = 100 μM, power = 56.1 W at 20 kHz and 48.3 W at 500 kHz.

Chapter 4

The Sonolytic Decomposition of Ozone in Aqueous Solution: Mass Transfer Effects

(Submitted to *Journal of Physical Chemistry A,* September 1997)

ABSTRACT

The sonolytic degradation of ozone (O_3) was investigated in both closed and open continuous-flow systems in order to examine effects of mass transfer on chemical reactivity in the presence of ultrasound. Degradation of O_3 followed apparent first-order kinetics at both 20 and 500 kHz in all the systems. At 500 kHz, the destruction of O_3 was accelerated by a factor of 3 at the same power density. Degassing was observed at 20 kHz due to the effects of rectified diffusion and larger resonant radii of the cavitation bubbles than at 500 kHz. Mass transfer effects due to ultrasound as measured by the transfer coefficent, $k_L a_2$, were observed at both frequencies. At 20 kHz, an increase in mass transfer rates may be attributed to turbulence induced by acoustic streaming. However, the main process of mass transfer in the presence of ultrasonic waves appears to be due to the sonolytic degradation of O_3 creating a larger driving force for gaseous O_3 to dissolve into solution. First-order rate constants for cyclohexene degradation during sonolytic ozonation were $k_{US/O_3,20} = 0.204\ min^{-1}$ at 20 kHz and $k_{US/O_3,500} = 0.065\ min^{-1}$ at 500 kHz, respectively. In comparison, the sum of the rate constants for sonications and ozonations ($k_{US,20} + k_{O_3,20} = 0.191\ min^{-1}$, $k_{US,500} + k_{O_3,500} = 0.069\ min^{-1}$) agreed within experimental error to the combined process at both frequencies. From these results and comparing the large diameter of an O_3 diffusing gas bubble to the size of an active cavitation bubble, it appears that diffusing gas bubbles containing O_3 are not directly influenced by ultrasonic fields.

INTRODUCTION

A number of advanced oxidation processes (AOPs) using ozone have been developed to destroy a variety of chemical contaminants in water. These processes including ozonation at high pH, ozonation combined with hydrogen peroxide, and ozonation combined with ultraviolet irradiation are based on the in-situ decomposition of ozone to form hydroxy radical leading to the initiation of a free-radical chain reaction.[1-7]

Ozonation combined with ultrasonic irradiation (sonolysis) is a similar, although less developed AOP. Ultrasonic irradiation has been investigated for the destruction of aqueous organic and inorganic pollutants.[8-22] Sound waves just above the audible range produce cavitation bubbles. Upon collapse of these bubbles, high temperatures and pressures are generated inside the bubble. The chemical destruction of compounds has been demonstrated to occur inside either imploding bubbles, or in the supercritical interfacial sheaths surrounding the bubbles either by direct pyrolysis or by hydroxylation resulting from the gas phase pyrolysis of H_2O. The addition of ozone into sonolytic systems has been demonstrated to increase the net transformation rates of a wide range of chmeical species.[23-31]

The thermal decomposition of ozone in collapsing cavitation bubbles appears to be the main mechanism for the enhanced destruction of chemical contaminants.[23] Ozone decomposes into oxygen and atomic oxygen as follows:

$$O_3 \xrightarrow{M} O_2 + O(^3P), \qquad (1)$$

atomic oxygen then reacts with H_2O vapor to form hydroxyl radical: [32,33]

$$O(^3P) + H_2O \longrightarrow 2\ OH\bullet \qquad (2)$$

Also, previous studies have reported increased mass transfer coefficents, $k_L a$, of ozone diffusing into solution in the presence of ultrasound.[26,29,31] k_L is the mass transfer velocity (cm/s) and a is the specific interfacial area for mass transfer (cm^2/cm^3). Olson and Barbier [31] hypothesized that the apparent enhancement was due to mechanical effects such as greater mixing and break up of gas bubbles as they enter an ultrasonic reactor. Increased mass transfer may also be the result of a diffusing ozone bubble oscillating or cavitating in the applied ultrasonic field. In this case, higher pressures in the ozone bubble force more ozone into solution. On the other hand, the apparent mass transfer effects may be due to the sonication of ozone reducing the aqueous ozone concentration below saturation allowing more ozone to enter solution.

Ultrasonic degassing has many commercial applications. For example, the ultrasonic treatment of liquids is currently used in industry to degas carbonated drinks, photographic solutions, and other liquids such as molten metals, electroplating solutions, and beer. Equipment in the 20 to 40 kHz range is typically used.[17,18,34,35] Degassing may be a factor in sonolytic ozonation due to the high Henry's Law constant of ozone ($H = 1.08 \times 10^4$ $Pa \cdot m^3/mol$),[36] especially at low frequency.

The primary objective of this study was to explore the various mass transfer mechanisms occuring during sonolytic ozonation. By investigating the decomposition of ozone in a continuously-stirred tank reactor (CSTR) mode under conditions closed to the atmosphere, open to the atmosphere, and open to the atmosphere with ozone gas bubbling, mass transfer coefficients were determined. The role of degassing in the sonolytic ozonation system was also investigated. Cyclohexene degradation experiments were used to determine the interactions of a diffusing ozone bubble with an ultrasonic field. Two ultrasonic frequencies, 20 and 500 kHz, were employed for all experiments.

EXPERIMENTAL METHODS

Materials and Reagents

Cyclohexene (Aldrich, 99+%) and perchloric acid (Mallinckrodt, 70%) were used as received. All solutions were prepared with water purified by a Millipore Milli-Q UV Plus system (R = 18.2 MΩ-cm).

Ozone Experiments

The experimental setup, shown in Figure 4.1, consisted of a 2 L water-jacketed glass reactor to continually saturate solutions with ozone, a water-jacketed glass reactor for sonication reactions capable of operating either open or closed to the atmosphere, a source of ultrasound, a Masterflex peristalic pump (Cole-Parmer) to pump aqueous solutions between the reactors, and a diode array spectrophotometer (Hewlett Packard, model 8452A). The temperature of the solution was maintained constant at 20° C (Haake, Model A81 Temperature Regulator) by using water jackets on both reactors. Tubing in contact with gaseous or aqueous ozone was Teflon except at connections and in the pump where Viton was used.

Oxygen gas was filtered through Drierite and a molecular sieve (Alltech), and through an activated-charcoal hydrocarbon trap (Alltech) before introduction to an OREC ozonator (Model O3V10-O) at 0.6 atm and 4.5 L min^{-1}. The O_2/O_3 gas mixture entered the reactors at a flowrate of 4 L min^{-1}. During open system operation with gas bubbling, 100 mL min^{-1} flowed out of a fritted-glass gas diffuser into the sonication reactor. In open and closed experiments, the 100 mL min^{-1} flow was vented during sonication. The O_3 gas phase concentrations were determined by oxidation of indigo trisulfonic acid as described by Bader and Hoigné.[37]

The sonications at 500 kHz were performed with an ultrasonic transducer (Undatim Ultrasonics) operating at 515 kHz with a reaction volume of 475 mL. The 20 kHz reactor was a direct immersion probe system (VCX-400 Vibracell, Sonic & Materials) with a volume of 235 mL. The total volume of the circulating solution was 2 L for the 500 kHz reactor and 1.5 L for the 20 kHz probe. The emitting areas of the transducers were 25.5

cm^2 and 1.20 cm^2 for the 500 kHz and 20 kHz systems, respectively. The electrical power outputs were measured by calorimetry. The 20 kHz probe was tuned in air and the titanium tip was polished prior to each sonication. Turbulence from the oxygen sparging was assumed to be sufficient for complete mixing in the 20 kHz reactor while a magnetic stirrer was used in the 500 kHz reactor.

Ozone decomposition is accelerated at high pH.[38] To minimize the chain decomposition reactions of ozone with OH^-, all experiments were run at pH 2. Ultrapure water was adjusted to pH 2 with concentrated $HClO_4$ at a net ionic strength of 0.01 M. Measurements made before and after the experiments did not show a significant change in the pH. The aqueous solution was continually pumped at 95 mL min^{-1} from the saturated ozone reservior to the ultrasonic reactor, through the spectrophotometer, and back to the saturated ozone reservior. Since the aqueous flowrate was much smaller than the volume of the reservior, the reservior maintained a constant aqueous ozone concentration throughout the experiment. Aqueous ozone concentrations were measured spectrophotometrically at λ = 260 nm (ε = 3292 M^{-1} cm^{-1}) [39]. Particles and bubbles generated from sonication were not observed to interfere with absorbance measurements. During initiation of an experiment, ozone was bubbled into both reactors with the solution circulating. Once a steady-state ozone saturation was obtained, ultrasound was applied until a second steady-state ozone concentration was achieved.

Sonications were performed either closed to the atmosphere, open to the atmosphere, or open to the atmosphere with gas bubbling. Saturated aqueous-phase concentrations of ozone were determined and acheived for all ozone gas concentrations used. All ozone decomposition experiments were performed in triplicate. Error bars on graphs represent experiment to experiment variation.

Cyclohexene Oxidation

The sonolytic oxidation of cyclohexene was studied under batch reactor conditions in both ultrasonic reactors. Initial solutions containing 2.5 mM of cyclohexene were

adjusted to pH 2 with $HClO_4$. Measurements made before and after the experiments did not show a significant change in pH. To initiate a kinetic run, oxygen bubbling, ultrasound, and/or voltage from the ozonator was applied. In the 20 kHz reactor, 20 mL min^{-1} of gas were bubbled through the solution while 40 mL min^{-1} of gas were bubbled through the 500 kHz chamber.

Sample aliquots of 2.0 mL were collected at designated times and transferred to vials without a free headspace. Due to the rapid reaction rate of ozone with cyclohexene, residual ozone was below detection. All samples were filtered before analysis with 0.2 μm Teflon syringe filters (Gelman). Quantification of cyclohexene was achieved with a Hewlett-Packard gas chromatograph (HP 5890 series II, GC) with a mass-selective detector (HP 5989A-MSD). A 0.32 mm x 25 m FFAP chromatographic column (Hewlett Packard) was used for GC separation.

RESULTS

In order to observe the effects of mass transfer enhancement and degassing of ozone due to sonication, experiments were performed with the ultrasonic reactor closed to the atmosphere (closed), open to the atmosphere (open) to observe degassing, and open to the atmosphere with gas bubbling (sparged) to observe enhanced mass transfer of ozone to solution. The three different systems will be referred to as closed, open, and sparged, respectively. The sonication reactor system was treated as a continuously-stirred tank reactor (CSTR). By solving the corresponding mass balance equations for the three different systems, reaction rate constants and mass transfer coefficients were determined for each scenario. The general mass balance equation for the CSTR reactor is given as:

$$\frac{dM}{dt} = \frac{dC(t)}{dt} V = qC_S - qC(t) - rV \qquad (3)$$

where C(t) is the ozone concentration (μM) in the ultrasonic reactor, V is the sonicated volume (L) in the ultrasonic reactor, C_S is the ozone concentration (μM) in the saturated ozone reservior, q is the volumetric flowrate (L min^{-1}) of aqueous ozone between reactors, and r is the combined first-order reaction rate (μM min^{-1}) for all ozone loss mechanisms due to ultrasound. In the case of the closed system, the mass balance equation becomes:

$$\frac{dC(t)}{dt} = \frac{q}{V}[C_S - C(t)] - kC(t) \qquad (4)$$

where k is the first-order reaction rate coefficient (min^{-1}) for the degradation of ozone by sonication. The open system has an additional loss term due to the sonolytically induced degassing of ozone, $k_L a_1$ (min^{-1}), shown by:

$$\frac{dC(t)}{dt} = \frac{q}{V}[C_S - C(t)] - [k + k_L a_1]\, C(t) \qquad (5)$$

The sparged system has another mass-transfer term resulting from ozone diffusing from a gas bubble in the presence of ultrasound, $k_L a_2$ (min^{-1}). The sparged system is represented as:

$$\frac{dC(t)}{dt} = \frac{q}{V}[C_S - C(t)] - [k + k_L a_1]\, C(t) + k_L a_2[C_S - C(t)] \qquad (6)$$

Combining terms in the three cases we obtain a generalized equation of the following form:

$$\frac{dC(t)}{dt} = -AC(t) + BC_S \qquad (7)$$

where in the closed, open, and sparged systems, respectively, A and B are:

$$A = k + \frac{q}{V} \qquad B = \frac{q}{V} \qquad \text{(Closed)} \qquad (8)$$

$$A = k + \frac{q}{V} + k_L a_1 \qquad B = \frac{q}{V} \qquad \text{(Open)} \qquad (9)$$

$$A = k + \frac{q}{V} + k_L a_1 + k_L a_2 \qquad B = \frac{q}{V} + k_L a_2 \qquad \text{(Sparged)} \qquad (10)$$

Integrating with initial conditions: $t = 0$, $C = C_S$, and applying the boundary conditions: $t = \infty$, $C = C_\infty$, we obtain:

$$C(t) - C_\infty = (C_S - C_\infty)\, e^{-At} \qquad (11)$$

where

$$C_\infty = \frac{BC_S}{A} \qquad (12)$$

k, $k_L a_1$, and $k_L a_2$ are obtained as follows:

$$k = (A - B)_{closed} \qquad (13)$$

$$k_L a_{1\ open} = (A - B)_{open} - (A - B)_{closed} \qquad (14)$$

$$k_L a_{1\ Sparged} = (A - B)_{sparged} - (A - B)_{closed} \qquad (15)$$

$$k_L a_2 = B_{sparged} - B_{open} \qquad (16)$$

Figure 4.2 shows results from the decomposition of ozone with the 500 kHz sonication reactor in the closed system configuration at a power density of 96 W L^{-1} and 2% w/w ozone in the gas phase. Sonication was initiated at 5 min. The first-order plot in Figure 4.2b demonstrates the first-order kinetics over four half-lives. Open and sparged system experiments at 500 kHz as well as experiments at 20 kHz were also found to be first-order. Four different aqueous ozone concentrations corresponding to ozone gas concentrations were used. As shown in Table 4.1, first-order degradation rate constants in the 500 kHz reactor at a power density of 96 W L^{-1} demonstrate first-order kinetics both as a function of time and concentration. In the 20 kHz reactor, at a power density of 263 W L^{-1}, the first-order degradation rate constant increases slightly as a function of increasing concentration. This is opposite to the trend observed by De Visscher *et al.* [21] and not nearly as significant. They observed a 3-fold increase in k with decreasing the initial concentration by a factor of 3. Our 20 kHz results show a 20% increase in k upon increasing the initial concentration by a factor of 1.75.

The effect of ultrasonic power on O_3 decomposition and ultrasonically enhanced mass transfer was investigated at 20 kHz and 500 kHz with 1.3% w/w O_3 in the gas stream. Figure 4.3 shows a linear dependence of the first-order degradation rate constant on power density (power input/volume sonicated) at both frequencies. The slope of k is 2.6 times steeper in the 500 kHz reactor than with the 20 kHz probe. In both systems with no power applied the degradation of O_3 was negligible. The rate equation for the degradation of O_3 by sonolysis at constant pH, T, and μ is:

$$-\frac{d[O_3]}{dt} = [O_3]\,\gamma P \qquad (17)$$

where $[O_3]$ is the O_3 concentration in solution, γ is the slope of the curves in Figure 4.3 (3.3×10^{-3} and 8.5×10^{-3} L min^{-1} W^{-1} at 20 and 500 kHz, respectively), and P is the power density. Therefore, with the same amount of power input per volume sonicated, O_3

is destroyed energetically more efficiently at 500 kHz. In contrast, Barbier and Pétrier observed a more rapid sonochemical degradation of O_3 at 20 kHz.[27] At an equivalent power density, we observed a considerably larger first-order degradation rate constant at 500 kHz (0.85 min^{-1} for this study compared to 0.17 min^{-1}) but at 20 kHz the first-order degradation rate constant was similar to that reported by Barbier and Pétrier (0.33 min^{-1} for this study compared to 0.29 min^{-1}). A variety of reasons could account for the differences between the studies including: the reactor geometries, the volume of solution sonciated, the area of radiating surface, and the experimental setup (CSTR without headspace vs. batch with recirculating headspace).

The mass transfer coefficient of ozone entering solution by bubbling during sonication, k_La_2, also follows a linear trend as seen in Figure 4.3. k_La_2 increases more rapidly by a factor of 1.5 with power density at 500 kHz than at 20 kHz. However, by extrapolating to 0 power density, k_La_2 is still significant at both frequencies. The 20 kHz probe had k_La_2 values approximately 4 times greater than the 500 kHz reactor over the power density range studied.

In Table 4.2 the dependence of the ozone mass transfer coefficient for degassing during sonication, k_La_1, on power density is shown. The results are shown for k_La_1 in the open system and in the sparged system. The open system experiments show evidence of degassing with the 20 kHz probe. The mass transfer coefficient appears to be largest at a moderate power and approximately a factor of 3 smaller at both lower and higher power densities. However, k_La_1 is considerably smaller in the sparged system and within experimental error of $k_La_1 = 0$ min^{-1} indicating that degassing is not occuring when O_3 is bubbled during sonolysis. In the 500 kHz reactor degassing is not observed. All of the values are within the error limits of $k_La_1 = 0$ min^{-1} for these experiments.

The effect of increasing the O_2/O_3 gas flowrate in the ultrasonic reactor from 0 to 150 mL min^{-1} was observed in the 20 and 500 kHz system. Increasing the flowrate corresponds to a larger net surface area for mass transfer of O_3 to solution. As shown in

Figure 4.4, $k_L a_2$ increases linearly with flowrate in the 500 kHz reactor. With the 20 kHz probe, $k_L a_2$ rises rapidly and reaches an apparent saturation value. The increase in $k_L a_2$ is a stronger function of flowrate in the 20 kHz system than in the 500 kHz reactor, however the power input is not the same in these reactors.

In addition, the variation of the mass transfer coefficient due to sonication, $k_L a_2$, was examined with different sized glass-frit diffusers ranging from a glass tube to a coarse fritted diffuser. The pore size diameter of the coarse and extra coarse frit are 40 - 60 μm and 170 - 220 μm, respectively, while the diameter of the opening on the tube without a diffuser frit is approximately 1 mm. Changing the frit size but using the same flowrate of gaseous O_3, altered the effective bubble size and the interfacial surface area for ozone diffusing into solution. The largest frit size corresponded to the smallest surface area (*i.e.*, no frit) and the smallest frit size, coarse, yields the largest interfacial surface area. Figure 4.5 illustrates that the decrease in frit size corresponds to an increase in $k_L a_2$ in the 500 kHz reactor. As observed with the increase of the O_3 gas flowrate, in the 20 kHz system, $k_L a_2$ initially increased then reached an apparent saturation value.

Loss of 2.5 mM cyclohexene by oxygen bubbling, sonication with O_2, ozonation, and sonolytic ozonation was observed in the 20 and 500 kHz reactors. Figures 4.6 and 4.7 show the results of degradation with the 20 kHz probe and 500 kHz reactor, respectively. Loss by these processes followed pseudo first-order kinetics as shown by the linearity of the curves in Fig. 4.6 and 4.7. The non-zero intercept is due to the initiation period for cavitation nuclei formation. The Henry's Law constant, H, is large for cyclohexene (H = 4568 Pa m^3 mol^{-1}) [40], therefore loss by O_2 bubbling is due to volatilization not oxidation. The gas flowrate per volume of solution was the same in both reactors yet volatilization was larger in the 20 kHz reactor ($k_{O_2,20} = 0.074$ min^{-1}, $k_{O_2,500} = 0.030$ min^{-1}). Different geometries of the reactors account for the larger volatilization rates with the 20 kHz probe. The 20 kHz reactor is taller and has a larger opening to the atmosphere allowing longer contact times of the diffusing bubbles with the solution and more surface area exposed to

the atmosphere than with the 500 kHz system. Since gas bubbling occurred in all experiments, the rate constant for loss due to volatilization (k_{O_2}) was subtracted from other rate constants. In Table 4.3 the corrected k values for each process at both frequencies are listed. In each system, degradation by sonication combined with ozonation is fastest followed by separate experiments of sonication and ozonation. In order to compare the sonolytic degradation rate constant obtained in the 500 kHz reactor to that in the 20 kHz reactor, the rate constant at 500 kHz is normalized to the 20 kHz rate by:

$$k_{norm,500} = k_{obs,500} \frac{P_{20}}{P_{500}} \qquad (18)$$

where P_{20} = 263 W L^{-1} and P_{500} = 96 W L^{-1} at 20 kHz and 500 kHz, respectively. $k_{norm,500}$ = 0.137 min^{-1} compared to k_{20} = 0.134 min^{-1}. These values differ by 2% which demonstrates that for the degradation of cyclohexene, 20 kHz frequency is as energetically efficient as the 500 kHz frequency. This is in contrast to previous studies finding more rapid degradation of 2,4,6-trinitrotoluene, phenol, carbon tetrachloride and trichloroethylene at 500 kHz compared to 20 kHz.[15,19,20,30]

DISCUSSION

Degassing was observed only in the 20 kHz reactor. This is consistent with frequencies used for degassing solutions in industry.[34] However, the highest rate of degassing occurred with a moderate power setting. Also, when adding ozone into the sonication reactor in the presence of ultrasound, the degassing effect was minimized considerably. One possible mechanism for degassing involves rectified diffusion and bubble coalescence[35]. Rectified diffusion causes a bubble to grow more during rarefaction cycles than during compression cycles. Bubbles typically grow from a bubble nucleus above the Blake threshold (*e.g.*, radius = 10^{-9} to 10^{-6} m) to a value near their resonant

radius (*e.g.*, radius = 163 μm at 20 kHz) where they cavitate. However, bubbles smaller than resonant size cluster at pressure antinodes as a result of Bjerkenes forces. Here the bubbles coalesce, and if they are large enough they will be removed by buoyancy forces.[35] The resonant radius of a bubble in O_2 saturated water at 20 kHz is 163 μm and 6.5 μm at 515 kHz.[35] Therefore, at 20 kHz since the resonant radius is larger, the bubbles will be larger when they cluster at the anitnodes and coalesce. This will result in a larger amount of degassing at the lower frequency. Degassing also depends on the acoustic amplitude and size of the bubble before it undergoes rectified diffusion. These dependencies may result in the maximal $k_L a_1$ at a moderate power. Lower degassing rates in the system with gas sparging may actually be a lower degradation rate constant, k, due to diffusing bubbles cushioning cavitation.

Using different flowrates of O_3 gas and different gas diffuser-frits gives insight into the mechanical mixing effects of the ultrasound at both frequencies. If mechanical effects were not important we would expect to see a linear increase in the flowrate due to a linear increase in the gas-liquid surface area for O_3 dissolving into solution. This was observed at 500 kHz, however at 20 kHz $k_L a_2$ increases rapidly until it reaches an apparent maximum at higher flowrates. The non-linear effect is due to the turbulence present at a larger degree in the 20 kHz reactor. Decreasing the frit size of the diffuser shows similar results. An open tube diffuser should yield the smallest gas-liquid interfacial area whereas a coarse frit should result in the greatest interfacial area for the same gas flowrate. At 500 kHz there is an increase in $k_L a_2$ with increasing gas-liquid surface area but at 20 kHz an extra coarse frit has the same $k_L a_2$ as the coarse frit. In these experiments, the 20 kHz probe was operating at 62 W, with a radiating area of 1.2 cm^2. However, the 500 kHz transducer has an radiating area of 25.5 cm^2 and was operating at a power of 24 W. Acoustic streaming is caused by an energy gradient in the direction of propagation of the acoustic wave. The energy gradient corresponds to a force which when acting on a liquid causes the liquid to accelerate. The larger acoustic intensity (power input/surface area of

emitter) at 20 kHz causes a larger force and hence a larger acceleration of the liquid. This should result in more turbulence at 20 kHz. Therefore, a smaller gaseous flowrate or a larger frit size will yield similar amounts of mass transfer if there is considerable acoustic streaming. Since this is a mechanical effect, it is dependent on the reactor configuration. Turbulence would be reduced in a larger reactor with the same probe.

As shown in Figure 4.3, k_La_2 is linear with increasing power density. However, extrapolating to 0 power, k_La_2 is non-zero with both the 20 and 500 kHz frequencies. Enhanced mass transfer, k_La_2, is present in both systems but there was no evidence of mechanical effects causing this at 500 kHz. As a result of these artifacts it seems that k_La_2 is due to sonolytic degradation of ozone. Reducing the aqueous O_3 concentration below the saturation value allows more O_3 to diffuse into solution. Figure 4.3 shows that O_3 is degraded faster with increasing power at both frequencies. However, the dependency on power is stronger for k than it is for k_La_2 as is expected if sonolytic degradation of O_3 is causing enhanced mass transfer. This is due to faster degradation of aqueous O_3 by sonication than resaturation by diffusing gas bubbles. The discrepancy between the k and k_La_2 is larger at 500 kHz than at 20 kHz, which again shows the effect of acoustic streaming at 20 kHz.

To investigate the effect ultrasound had on an O_3 gas bubble diffusing into solution, cyclohexene degradation by sonication, ozonation, and sonolytic ozonation was performed. Cyclohexene reacts very rapidly with both O_3 ($k = 3.9 \times 10^6\ M^{-1}\ s^{-1}$) [41] and OH• ($k = 8.8 \times 10^9\ M^{-1}\ s^{-1}$) [42]. Because of its rapid reaction rate with O_3 it will react at the gas-liquid interface and no O_3 will be present in solution. Therefore, if an O_3 gas bubble is influenced by ultrasound either by the diffusing gas bubbles breaking up, by turbulence, or by O_3 being pumped into solution by the propagating ultrasound wave, a difference should be seen in the first-order degradation rate constant by sonolytic ozonation over the sum of the rate constants by sonication and ozonation. Adding the independently-obtained rate constants for sonication and ozonation ($k_{US} + k_{O_3} = 0.191\ min^{-1}$) at 20 kHz and comparing

it to the combined process of sonolytic ozonation ($k_{US/O_3} = 0.204\ min^{-1}$), the difference is only 6%. Similarly at 500 kHz, $k_{US} + k_{O_3} = 0.069\ min^{-1}$ and $k_{US/O_3} = 0.065\ min^{-1}$ and the difference is again 6%. Since the combined system has a slightly larger rate constant at 20 kHz than the linear combination of separate processes, some mechanical effects of ultrasound are apparent. However, these apparent effects are within the range of experimental error. Also, a diffusing O_3 bubble is on the order of 1000 μm in diameter but the resonant radii at which the bubble will be maximally perturbed by ultrasonic waves are 163 μm and 6.5 μm at 20 and 515 kHz, respectively. Hence, an O_3 bubble diffusing into solution is not influenced to a significant extent by ultrasound. O_3 first dissolves into solution and then re-diffuses into a gaseous cavitation bubble where it will undergo thermolytic decomposition.

CONCLUSIONS

The sonolytic degradation of O_3 is rapid with 90% degradation occurring in less than 5 minutes. Degradation of O_3 at 500 kHz appears to be energetically more efficient than at 20 kHz over the range of power densities employed.

Degassing was present only in the low frequency reactor. Rectified diffusion occurs at both frequencies, but the resonant radii of bubbles at 20 kHz are much larger and thus allows cavitation nuclei to grow larger before cavitational collapse. These larger bubbles will be more easily removed by buoyancy.

Mechanical effects of ultrasonic waves as shown by non-linear increases in $k_L a_2$ with flowrate and with a decreased frit size of the gas sparger appear to influence the mass transfer of O_3 to solution in the 20 kHz system. This effect is due to higher power intensities in the 20 kHz reactor resulting in greater acoustic streaming forces. Turbulence due to acoustic streaming will depend, in part, on the reactor dimensions; it may not be present in larger volume systems. However, ultrasonically enhanced mass transfer is

mainly a function of sonolytically degrading O_3 and thus lowering the aqueous $[O_3]$ below saturation values which allows more O_3 to dissolve into solution as a function of time.

Experiments focused on the degradation of cyclohexene demonstrate that a diffusing gas bubble much larger than the resonant radius for a given ultraonic frequency used is not influenced by ultrasound. The overall process of sonolytic ozonolysis involves initial dissolution of O_3 into solution; the dissolved O_3 then diffuses into a growing cavitation bubble where it is thermolytically decomposed. These observations have interesting implications in reactor design. For example, gaseous O_3 does not need to be added directly in the presence of ultrasound to gain beneficial effects of the combined process.

ACKNOWLEDGMENT: The authors wish to thank Ralf Höchemer for valuable discussions and insight. Financial supported provided by Defense Advanced Research Projects Agency (DARPA), the Office of Naval Research (ONR), and the Electric Power Research Institute (EPRI) is gratefully acknowledged.

REFERENCES

(1) Glaze, W. H.; Kang, J. W.; Chapin, D. H., *Ozone Sci. Eng.,* **1987**, *9*, 335-352.

(2) Bellamy, W. D.; Hickman, G. T.; Mueller, P. A.; Ziemba, N., *J. Water Pollut. Control Fed.,* **1991**, *63*, 120-128.

(3) Gurol, M. D.; Vatistas, R., *Wat. Res.,* **1987**, *21*, 895-900.

(4) Langlais, B.; Reckhow, D. A.; Brink, D. R. *Ozone in Water Treatment Application and Engineering*; AWWA Research Foundation and Lewis Publishers: Chelsea, 1991.

(5) Legrini, O.; Oliveros, E.; Braun, A. M., *Chem. Rev.,* **1993**, *93*, 671-698.

(6) Masten, S. J.; Davies, S. H. R. In *Environmental Oxidants*; J. O. Nriagu and M. S. Simmons, Eds.; John Wiley & Sons: New York, 1994; pp 517-547.

(7) Peyton, G. R.; Huang, F. Y.; Burleson, J. L.; Glaze, W. H., *Environ. Sci. Technol.,* **1982**, *16*, 448-453.

(8) Hua, I.; Höchemer, R. H.; Hoffmann, M. R., *J. Phys. Chem.,* **1995**, *99*, 2335-2342.

(9) Hua, I.; Höchemer, R. H.; Hoffmann, M. R., *Environ. Sci. Technol.,* **1995**, *29*, 2790-2796.

(10) Hua, I.; Hoffmann, M. R., *Environ. Sci. Technol.,* **1996**, *30*, 864-871.

(11) Kontronarou, A.; Mills, G.; Hoffmann, M. R., *J. Phys. Chem.*, **1991**, *95*, 3630-3638.

(12) Kontronarou, A.; Mills, G.; Hoffmann, M. R., *Environ. Sci. Technol.*, **1992**, *26*, 2420-2428.

(13) Kontronarou, A.; Mills, G.; Hoffmann, M. R., *Environ. Sci. Technol.*, **1992**, *26*, 1460-1462.

(14) Makino, K.; Mossoba, M. M.; Riesz, P., *J. Phys. Chem.*, **1983**, *87*, 1369-1377.

(15) Pétrier, C.; Lamy, M.-F.; Francony, A.; Benahcene, A.; David, B., *J. Phys. Chem.*, **1994**, *98*, 10514-10520.

(16) Serpone, N.; Terzian, R.; Hidaka, H.; Pelizzetti, E., *J. Phys. Chem.*, **1994**, *98*, 2634-2640.

(17) Suslick, K. S. *Ultrasound: Its Chemical, Physical, and Biological Effects*; VCH Publishers, Inc.: New York, 1988.

(18) Mason, T. J.; Lorimer, J. P. *Sonochemistry: Theory, Applications and Uses of Ultrasound in Chemistry*; Ellis Horwood Ltd: Chichester, 1988.

(19) Francony, A.; Pétrier, C., *Ultrasonics Sonochemistry*, **1996**, *3*, S77-S82.

(20) Drijvers, D.; Baets, R. D.; Visscher, A. D.; Langenhove, H. V., *Ultrasonics Sonochemistry,* **1996**, *3*, S83-S90.

(21) De Visscher, A.; Van Eenoo, P.; Drijvers, D.; Van Langenhove, H., *J. Phys. Chem.,* **1996**, *100*, 11636-11642.

(22) Cost, M.; Mills, G.; Glisson, P.; Lakin, J., *Chemosphere,* **1993**, *27*, 1737-1743.

(23) Weavers, L. K.; Ling, F. H.; Hoffmann, M. R., *Environ. Sci. Technol.,* **submitted**.

(24) Sierka, R. A.; Amy, G. L., *Ozone Sci. Engng.,* **1985**, *7*, 47-62.

(25) Sierka, R. A., *Ozone Sci. Engng.,* **1985**, *6*, 275-290.

(26) Sierka, R. A. "Mass Transfer and Reaction Rate Studies of Ozonated MUST Wastewaters in the Presence of Sound Waves," University of Arizona, 1976.

(27) Barbier, P. F.; Pétrier, C., *J. Adv. Oxid. Technol.,* **1996**, *1*, 154-159.

(28) Chen, J. W., *Water,* **1972**, *69*, 61-70.

(29) Dahi, E., *Wat. Res.,* **1976**, *10*, 677-684.

(30) Höchemer, R. H. Ph. D. Thesis, California Institute of Technology, 1996.

(31) Olson, T. M.; Barbier, P. F., *Wat. Res.,* **1994**, *28*, 1383-1391.

(32) Hart, E. J.; Henglein, A., *J. Phys. Chem.*, **1986**, *90*, 3061-3061.

(33) Hart, E. J.; Henglein, A., *J. Phys. Chem.*, **1985**, *89*, 4342-4347.

(34) Brown, B.; Goodman, J. E. *High-Intensity Ultrasonics*; D. Van Nostrand: Princeton, 1965.

(35) Leighton, T. G. *The Acoustic Bubble*; Academic Press: London, 1994.

(36) Seinfeld, J. H. *Atmospheric Chemistry and Physics of Air Pollution*; Wiley-Interscience: New York, 1986.

(37) Bader, H.; Hoigné, J., *Wat. Res.*, **1981**, *15*, 449-456.

(38) Sehested, K.; Corfitzen, H.; Holcman, J.; Fischer, C. H.; Hart, E. J., *Environ. Sci. Technol.*, **1991**, *25*, 1589-1596.

(39) Hart, E. J.; Sehested, K.; Holcman, J., *Anal. Chem.*, **1983**, *55*, 46-49.

(40) Mackay, D.; Shiu, W. Y.; Ma, K. C. *Illustrated Handbood of Physical-Chemical Properties and Environmental Fate for Organic Chemicals*; Lewis Publishers: Boca Raton, 1991; Vol. III Volatile Organic Chemicals.

(41) Kuo, C. H. "Reactions of Dissolved Pollutants with Ozone in Aqueous Solutions," Mississippi State University, 1984.

(42) Buxton, G. V.; Greenstock, C. L.; Helman, W. P.; Ross, A. B., *J. Phys. Chem. Ref. Data,* **1988**, *17*, 513-817.

Table 4.1: First-order reaction rate constants for the sonochemical degradation of ozone at 20 kHz and 500 kHz.

Gas Concentration (%)	Initial Aqueous Conc. (μM)	k_{20} (min^{-1})	k_{500} (min^{-1})
0.66	85 ± 5	-	0.62 ± 0.09
0.98	140 ± 4	0.67 ± 0.10	0.62 ± 0.17
1.3	200 ± 4	0.77 ± 0.04	0.69 ± 0.18
2.0	245 ± 3	0.84 ± 0.07	0.66 ± 0.08

Table 4.2: Mass transfer coefficients of ozone loss due to degassing in the presence of ultrasound.

Ultrasonic frequency (kHz)	Power Density ($W\ L^{-1}$)	$k_L a_l$ (open) (min^{-1})	$k_L a_l$ (sparged) (min^{-1})
20	71.1	0.12 ± 0.02	0.03 ± 0.04
20	263.0	0.42 ± 0.05	0.16 ± 0.25
20	431.9	0.17 ± 0.22	0.08 ± 0.24
500	14.5	0.005 ± 0.004	-0.004 ± 0.004
500	33.7	-0.029 ± 0.046	-0.063 ± 0.050
500	50.3	0.011 ± 0.044	0.003 ± 0.054
500	96.0	0.04 ± 0.21	-0.084 ± 0.22

Table 4.3: Corrected first-order degradation rate constants for the loss of cyclohexene under various conditions.

Experiment	k_{20} (min^{-1})	k_{500} (min^{-1})
Sonication w/O_2	0.134	0.050
Ozonation	0.057	0.019
Sonication w/O_3	0.204	0.065

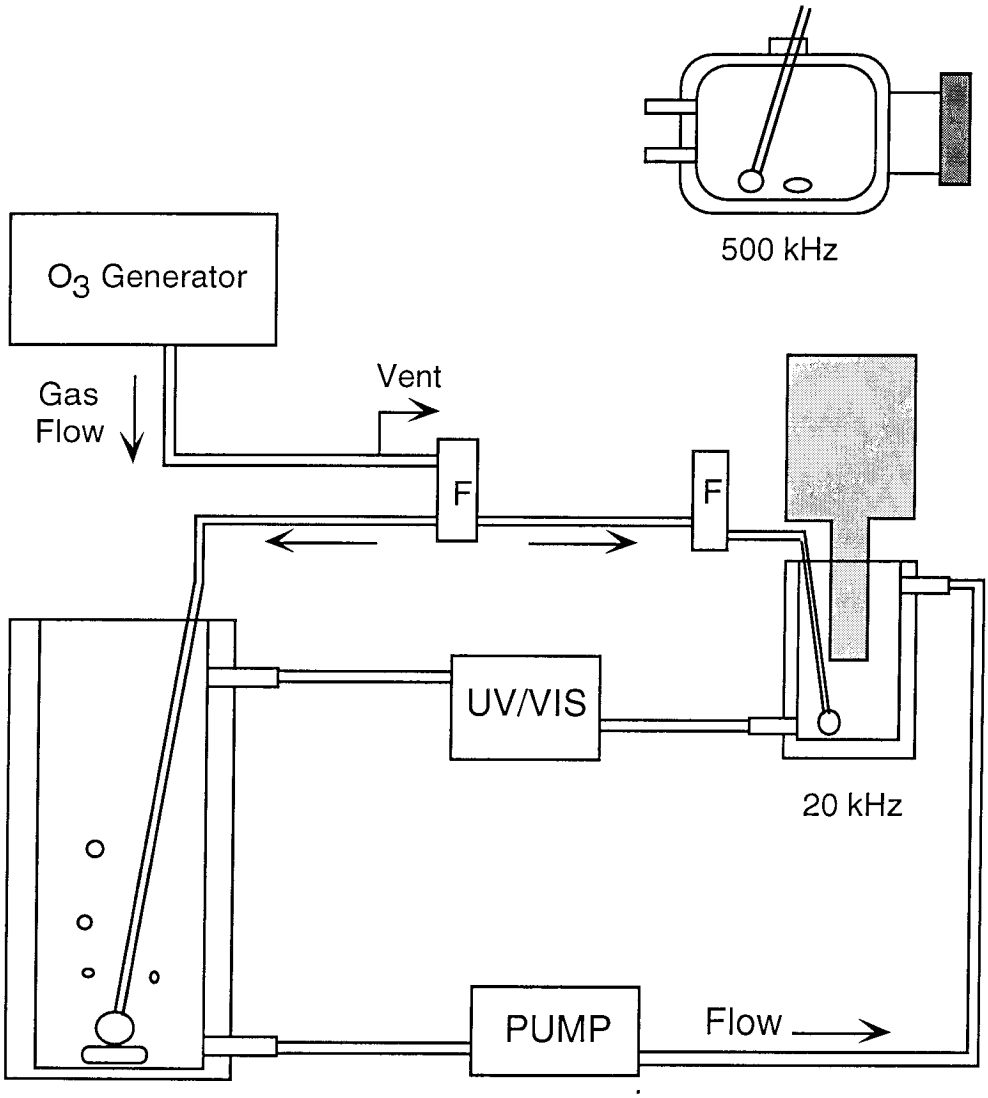

Figure 4.1: Schematic diagram of the reactor systems. 20 kHz = 235 mL volume 20 kHz probe reactor, 500 kHz = 475 mL volume 515 kHz reactor, F = gas flowmeter.

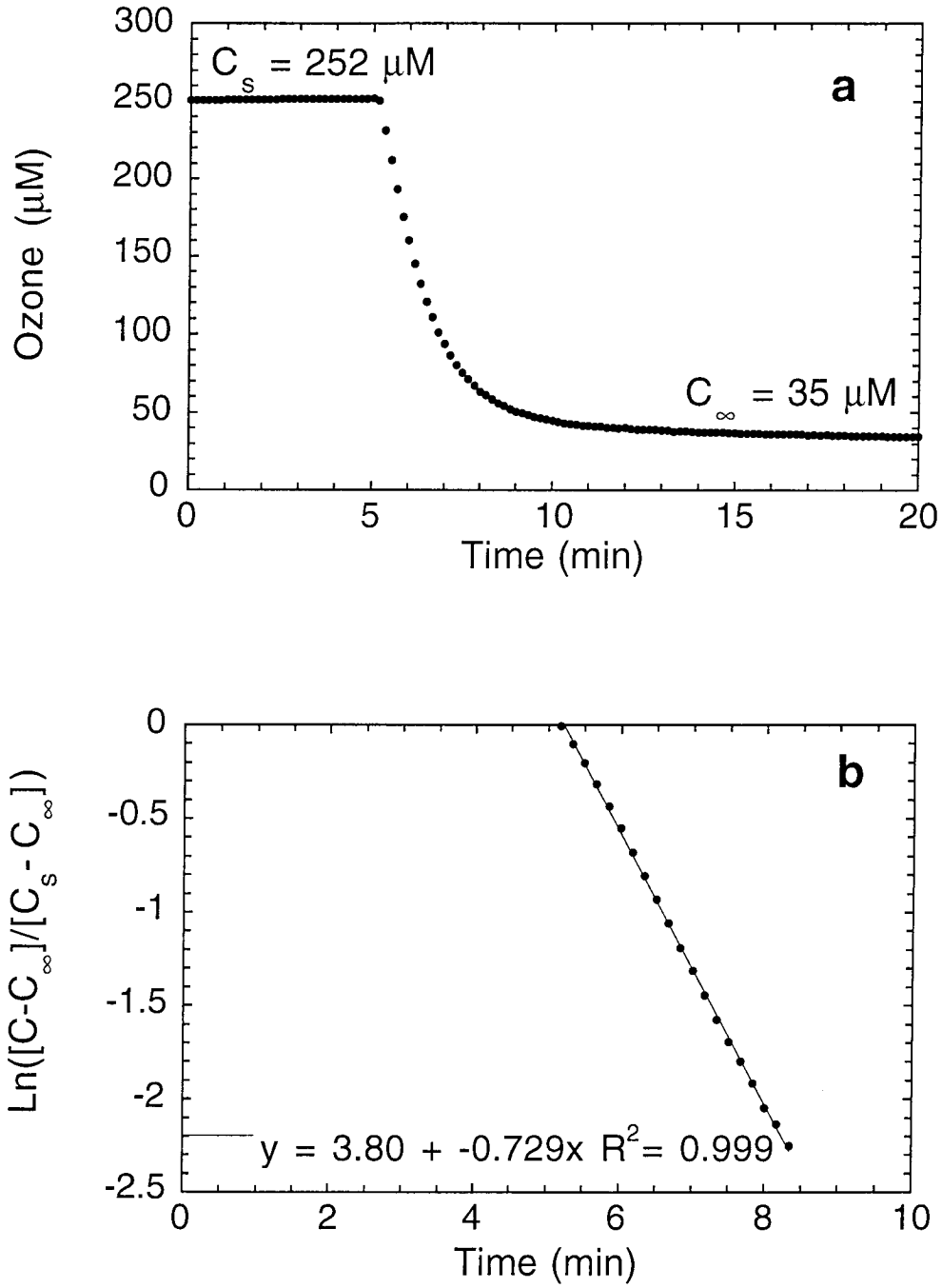

Figure 4.2: (a) Ozone decomposition in the 500 kHz sonication reactor in closed system configuration. (b) First-order degradation of O_3 in 500 kHz reactor. Power density = 96 W L^{-1}, 2% w/w O_3 in O_2 gas, pH = 2.

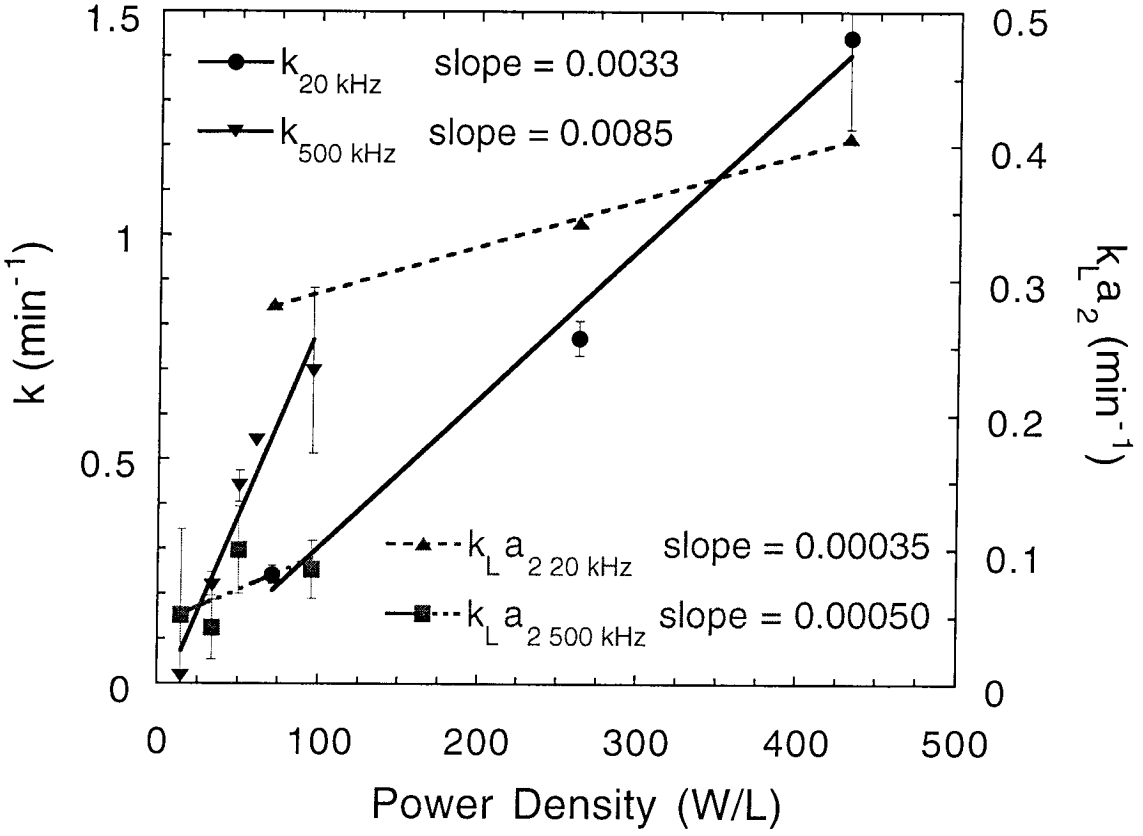

Figure 4.3: First-order degradation rate coefficient, k, and mass transfer coefficient, k_La_2, due to sonication vs. power density at 20 and 500 kHz. Gas flowrate = 100 mL min^{-1}, pH = 2, 1.3% w/w O_3 in O_2 gas.

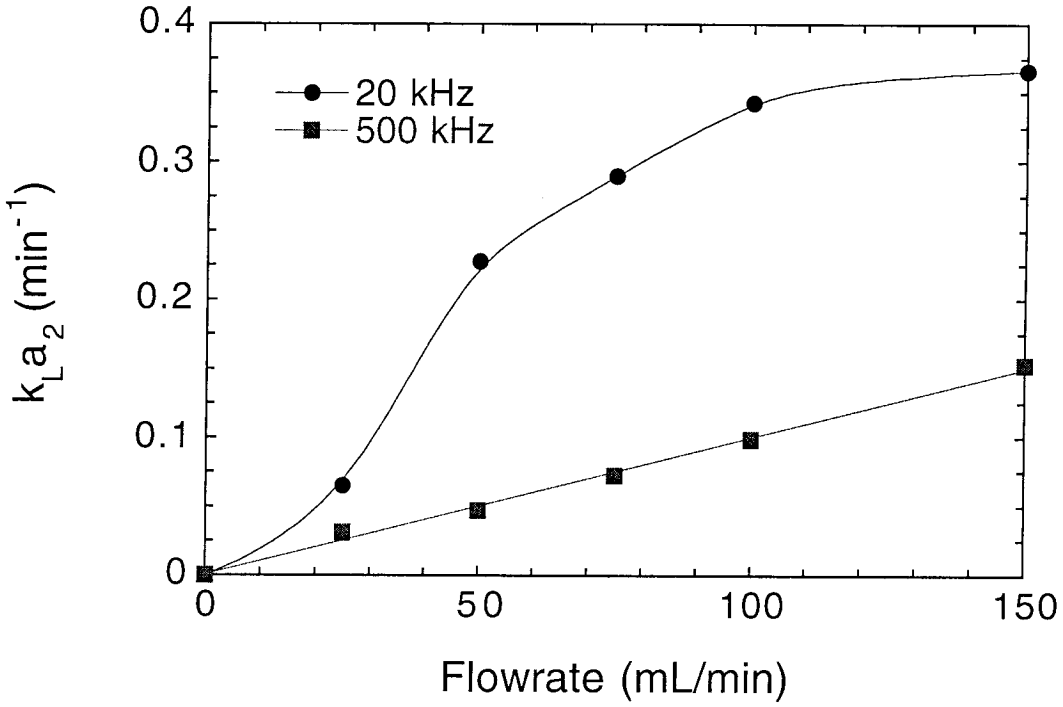

Figure 4.4: Mass transfer coefficient, $k_L a_2$, vs. gas flowrate at 20 and 500 kHz. 1.3% w/w O_3 in O_2 gas, pH = 2, power density = 50.3 W L^{-1} at 500 kHz and 263 W L^{-1} at 20 kHz.

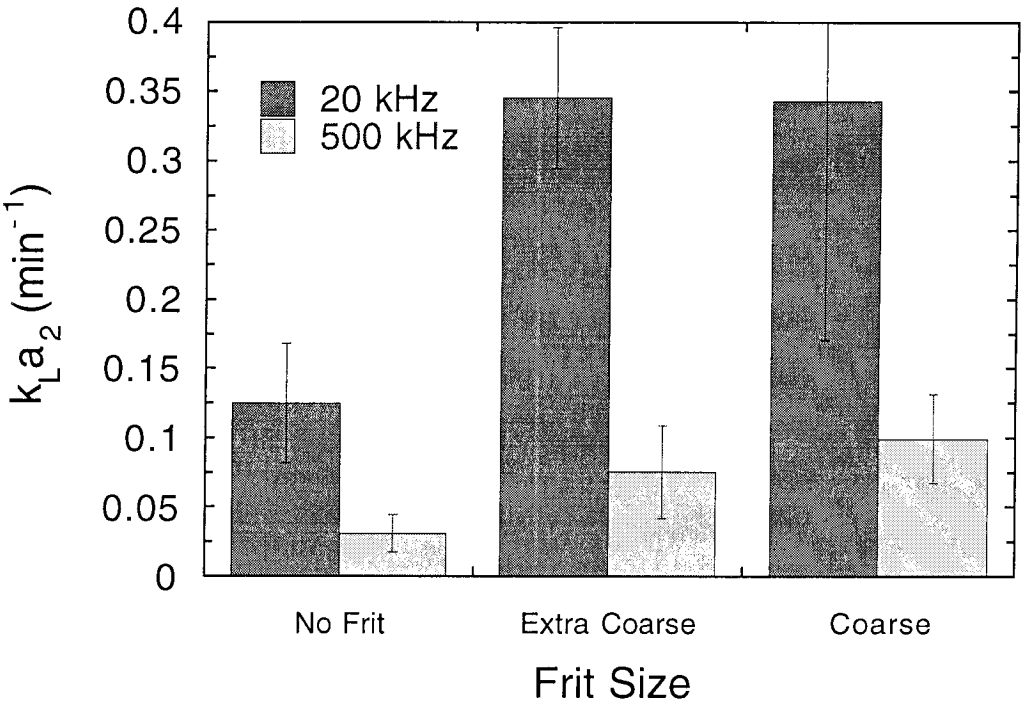

Figure 4.5: Mass transfer coefficient, $k_L a_2$, vs. diffuser frit size at 20 and 500 kHz. 1.3% w/w O_3 in O_2 gas, pH = 2, power density = 50.3 W L^{-1} at 500 kHz and 263 W L^{-1} at 20 kHz. Pore diameters of frits: extra coarse = 170 - 220 μm, coarse = 40 - 60 μm, no frit = 1 - 1.5 mm opening.

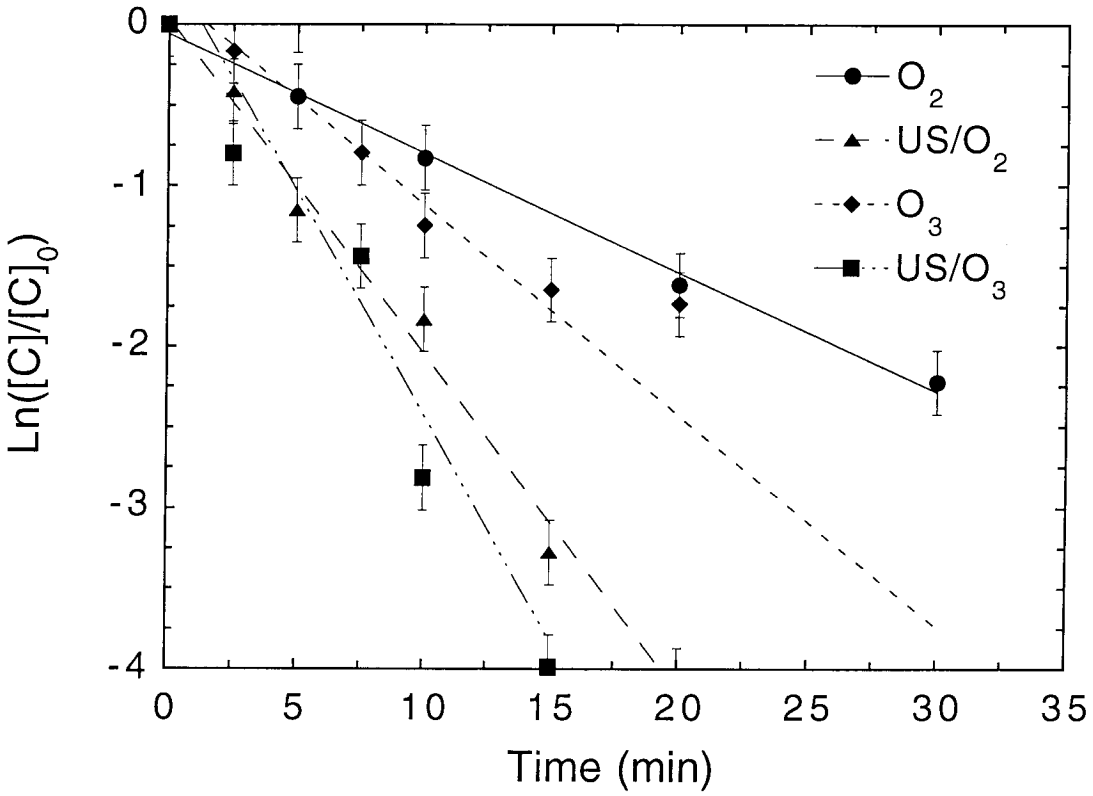

Figure 4.6: First-order degradation of cyclohexene due to oxygen bubbling, sonication with oxygen, ozonation, and sonolytic ozonation in the 20 kHz reactor. O_3 gas flowrate = 20 mL min^{-1}, pH = 2, initial concentration of substrate = 2.5 mM, power density = 263 W L^{-1}.

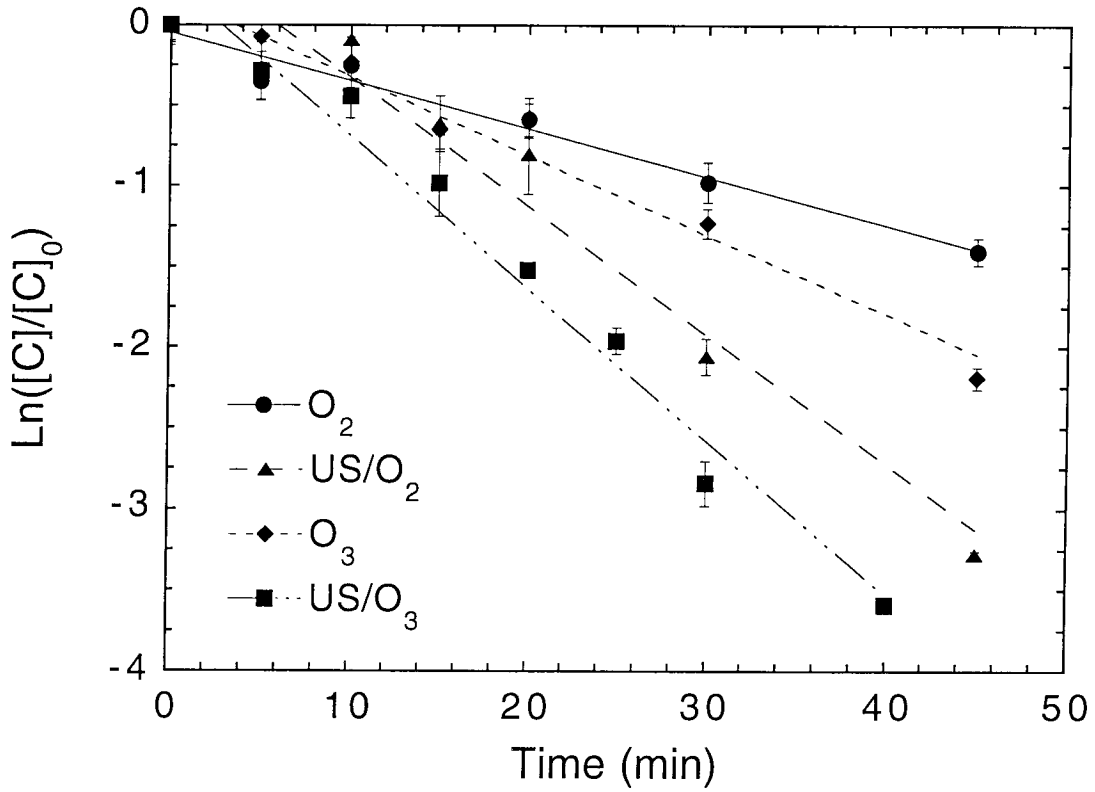

Figure 4.7: First-order degradation of cyclohexene due to oxygen bubbling, sonication with oxygen, ozonation, and sonolytic ozonation in the 500 kHz reactor. O_3 gas flowrate = 40 mL min^{-1}, pH = 2, initial concentration of substrate = 2.5 mM, power density = 96 W L^{-1}.

Chapter 5

Kinetics and Mechanism of Pentachlorophenol Degradation by Sonication, Ozonation, and Sonolytic Ozonation

(Submitted to *Environmental Science and Technology*, November 1997)

ABSTRACT

Degradation of 20 and 60 μM pentachlorophenol (PCP) was investigated under sonication, ozonation, and the combination of sonication and ozonation at a frequency of 20 and 500 kHz. At 20 kHz, sonication under oxygen in a probe reactor resulted in a normalized observed first-order rate constant for 60 μM PCP of 0.021 min^{-1} compared to 0.080 min^{-1} for the 20 kHz Tube Resonator, and 0.35 min^{-1} for the 500 kHz Orthoreactor. The addition of ozone during sonication did not affect the first-order degradation constant of PCP at 20 μM or 60 μM compared to the linear combination of separate sonication and ozonation experiments. Enhancement in the reduction of total organic carbon (TOC) of 33% and 57% in a 20 kHz Tube Resonator and 500 kHz Orthoreactor, respectively, was observed for sonolytic ozonation compared to the separate sonication and ozonation experiments. Observed byproducts of sonication include: tetrachloro-o-benzoquinone (o-chloranil), tetrachlorocatechol (TCC), oxalate, chloride, and hypochlorous acid (HOCl). Aromatic intermediates were not detected for ozonation or sonolytic ozonation, however, oxalate was observed to form at lower concentrations by sonolysis combined with ozonolysis than by sonolysis or ozonolysis separately.

INTRODUCTION

Pentachlorophenol (PCP) has been used extensively throughout the world as a wood preservative and general biocide (1). PCP residues are widespread in the environment. In fact, PCP was detected in 80% of urine specimens in an EPA study. While PCP is an EPA priority pollutant and a suspected carcinogen, the formation of polychlorodibenzodioxins (PCDDs) and polychlorodibenzofurans (PCDFs), which are considerably more toxic than PCP, result from the pyrolysis and combustion of PCP liquid solutions and PCP impregnated wood (2).

Ultrasonic irradiation of aqueous solutions has been shown to be effective for the in situ destruction of a variety of organic and inorganic contaminants (3-12). Ultrasonic irradiation produces cavitation bubbles which yield high temperatures and pressures upon their implosion (13). Destruction of organic compounds occur in the cavitation bubble itself or its interfacial sheath due to direct pyrolysis or hydroxylation which results from the gas-phase pyrolysis of H_2O. Reactions are also possible in the bulk aqueous phase by oxidation with hydrogen peroxide which has been observed to form in sonolytic systems. Sonication has been shown to be particularly effective with volatile and hydrophobic compounds since they can partition to the bubble or interfacial sheath rapidly (6). Selected physical properties and relevant rate constants of PCP for sonication are shown in Table 5.1 (14-16).

Ozone in a collapsing cavitation bubble results in the thermolytic decomposition of ozone and subsequent OH• formation as follows (17,18):

$$O_3 \rightarrow O_2 + O(^3P) \qquad (1)$$

$$O(^3P) + H_2O \rightarrow 2\,OH\bullet \qquad (2)$$

These initiation reactions occur in the gas phase and products migrate to the interfacial sheath of the bubble where they react in the aqueous phase. Even for compounds that react quickly with O_3 such as PCP, the combination of O_3 and ultrasound could be more effective since 2 OH• molecules are formed per O_3 molecule consumed. Hydrogen peroxide production, which is enhanced during the sonolysis of water reflects increased OH• concentrations in the gas phase and the interfacial region (17,19). Also, ultrasonic irradiation has been demonstrated to increase the mass transfer of ozone to solution, allowing more ozone to enter solution than in a non-irradiated system (20-22).

The sonolytic degradation of PCP has been performed previously at both 20 and 500 kHz (23-25). Investigators have observed decomposition of PCP and subsequent formation of Cl^-, CO, and CO_2 (23). Pétrier et al. found more rapid destruction at 500 kHz than 20 kHz and hypothesized an OH• reaction pathway (24). Gonze et al. used PCP to probe key geometric parameters of reactor design such as volumetric power input (25). However, byproduct formation and the mechanism of degradation have not been explored.

The primary objective of this study was to investigate the degradation of PCP in different reactor systems and to determine kinetics and the mechanism of degradation. In addition, ozone gas was added to the system to determine its effect. The formation of intermediates were observed and degradation of total organic carbon (TOC) associated with PCP was followed.

EXPERIMENTAL METHODS

Materials and Reagents

Pentachlorophenol (Sigma), octachlorodibenzodioxin (Chem Service), tetrachlorohydroquinone (Kodak), tetrachloro-p-benzoquinone (Sigma), tetrachlorocatechol (Aldrich), tetrachloro-o-benzoquinone (Sigma), sodium chloride (Baker), oxalic acid (Mallinkrodt), sodium phosphate monobasic (Mallinkrodt), sodium phosphate dibasic

(Baker), phosphoric acid (EM Science, 85%), sodium hydroxide (Mallinkrodt), and sodium thiosulfate (Mallinkrodt) were used as received. All solutions were prepared with water purified by a Millipore Milli-Q UV Plus system (R = 18.2 MΩ-cm).

Sonochemical Reactors

The experimental setup consisted of a reactor surrounded by a self-contained water jacket, a constant gas flow, and a source of ultrasound. The temperature of the solution was maintained constant at approximately 30° C with a recirculating water bath (Haake Co., model A81) flowing through the surrounding water jacket. Selected experiments were conducted at 50° C.

Three different reaction systems were used for the destruction of PCP. Sonication experiments at 500 kHz were performed with an Orthoreactor ultrasonic transducer (Undatim Ultrasonics) operating at 515 kHz and 100% power. Two 20 kHz reactors were used: a direct immersion probe system (Sonifier cell disruptor 200, Branson) operating at 70% power, and a Tube Resonator (Telesonics, model SG-22-2000S) emitting ultrasound radially over its shaft and operating at the lowest power setting. The electrical power outputs were determined by calorimetry. Characteristics of the different systems are tabulated in Table 5.2. Turbulence from the oxygen sparging was assumed to be sufficient for complete mixing in the 20 kHz reactor while a magnetic stirrer was used in the 500 kHz reactor.

Oxygen gas was filtered through a Drierite and molecular sieve economy purifier (Alltech) and an activated charcoal hydrocarbon trap (Alltech) and flowed through an OREC Ozonator (Model O3V10-O) at 0.3 atm and 3 L min^{-1}. The gas flowed into the reactors through a coarse fritted-glass gas diffuser. The O_3 gas phase concentration was determined to be approximately 0.7% wt/wt by oxidation of indigo trisulfonic acid (26). No ozone was produced when voltage was not applied.

Initial solutions containing either 20 μM or 60 μM of PCP were adjusted to pH 7.3 using 5 mM phosphate buffer. Measurements made before and after the experiments did

not show a significant change in pH. To initiate a kinetic run, ultrasound and/or voltage from the ozonator was applied. Aliquots were collected at designated times and quenched with 100 mM thiosulfate to eliminate any residual ozone in solution. All samples were filtered before analysis with 0.2 μm Teflon syringe filters (Gelman).

Analysis

A Hewlett Packard Series II 1090 HPLC was used to quantify PCP and aromatic intermediates. A 5 mm, 100 x 2.1 mm ODS Hypersil column (Hewlett Packard) with an eluent gradient of aqueous phosphate buffer solution (pH = 3) and methanol was used for analysis. Chloride and organic ions were detected by ion chromatography with electrical conductivity detection (Bio-LC, Dionex). An AS-11 column (Dionex) with NaOH and methanol as the mobile phase was used. TOC analysis was performed on a Shimadzu 5000A total organic carbon analyzer operating in the non-purgable organic carbon (NPOC) mode. The possible formation of dioxins were observed with a Hewlett-Packard gas chromatograph (HP 5890 series II, GC) with a mass-selective detector (HP 5989A-MSD). A 0.25 mm x 30 m HP-1 chromatographic column (Hewlett Packard) was used for GC separation. Samples of 4 mL were extracted into 1 mL of toluene to enhance detection.

RESULTS

As shown in Figures 5.1 and 5.2, sonolysis of PCP under O_2 initially followed first-order kinetics according to the following rate equation:

$$-\frac{d[PCP]}{dt} = k_{obs}[PCP] \qquad (3)$$

However, pseudo first-order rate constants summarized in Table 5.3 demonstrate that at both 20 kHz and 500 kHz a lower initial concentration of PCP resulted in more rapid destruction.

The effect of temperature was explored in the 20 kHz Tube Resonator. Degradation of 60 μM PCP is slightly faster at 30°C than at 50°C ($k_{T=30°C}$ = 0.016 compared to $k_{T=50°C}$ = 0.014 min^{-1}) but within experimental error. Both increased and decreased first-order reaction rate constants have been observed with increased temperature (27-29). A lower k with increased temperature is attributed to increased water vapor in collapsing cavitation bubbles resulting in cushioning of the collapse. An increased k with temperature can be attributed to increasing the vapor pressure of the substrate and hence the concentration of the substrate in the bubble. Since PCP is deprotonated at pH 7 and will not volatilize, it is plausible that no effect in k with temperature was observed.

Pseudo first-order rate constants for the degradation of 20 and 60 μM PCP by sonication, ozonation, and sonolytic ozonation are shown in Table 5.4. Degradation by ozonolysis was rapid due to its fast second-order reaction rate with O_3 as shown in Table 5.1. Ozone was continually bubbled into the reactor, thus PCP loss followed pseudo first-order kinetics. Although the gas flow rate was proportional to the volume of solution in both reactors, the geometries were different causing a higher k in the 20 kHz Tube Resonator. Sonolytic ozonation of PCP also followed a pseudo first-order rate law. Loss of PCP by sonolysis combined with ozonolysis was faster with $[PCP]_0$ = 20 μM than $[PCP]_0$ = 60 μM in both reactors. Errors are larger with $[PCP]_0$ = 20 μM due to the detection limit of the analysis equipment, and the shorter time frame for sampling.

The decrease in TOC for $[PCP]_0$ = 60 μM is shown in Table 5.5. The degradation of TOC initially followed pseudo first-order kinetics. The loss of TOC by sonication alone had a half-life of decay of 250 and 195 min in the 20 kHz Tube Resonator and 500 kHz Orthoreactor, respectively. Loss of TOC by ozonation and sonication combined with

ozonation were much more rapid. The half-lives were 20 and 14 min at 20 kHz and 76 and 35 min at 500 kHz for ozonation and sonolytic ozonation, respectively.

Sonication of PCP in the 20 kHz Tube Resonator and 500 kHz Orthoreactor is shown in Figures 5.3 and 5.4. Aromatic intermediates, tetrachloro-o-benzoquinone (o-chloranil), and tetrachlorocatechol (TCC) were formed and destroyed. Chloride was recovered after 3-1/2 hours. Recovery of $Cl^-/5$ of greater than 60 μM reflects the slight non-linearity of the standard curve at high concentrations. Organic acids such as succinic, maleic, formic, acetic, glycolic, and fumaric acid were not detected. However, oxalic acid was formed. Other intermediates were detected by ion chromatography, however they were formed and destroyed over the 4 hour sonication in both reactors. The formation of octachlorodibenzodioxin as an intermediate as followed with GC-MS did not occur.

In addition, intermediates were followed for ozonation and sonication combined with ozonation. Aromatic intermediates which were formed during sonication alone were not detected. As shown in Figure 5.5, there was a rapid release of Cl^- during sonolytic ozonation and ozonation, and a gradual release with sonication. HOCl was formed during sonication and during sonication in the presence of O_3 experiments. However, only small amounts were formed during ozonolysis. The mass balance of chlorine shifted from Cl^- during sonication combined with ozonation to yield more HOCl after the release of Cl^- at both 20 and 500 kHz. In addition, the formation of oxalate was observed as shown in Figure 5.6.

DISCUSSION

The effect of concentration on the sonochemical degradation rate of substrates has been observed previously (8,9,12,22,30,31). For hydrophobic volatile compounds an elaborate model was developed which took into account the higher specific heat of organic compounds (120 J mol^{-1} K^{-1}) compared to water vapor (36 J mol^{-1} K^{-1}) and air (30 J mol^{-1}

K^{-1}). As the specific heat is increased in the vapor, the temperature rise upon collapse is decreased, thus smaller rate constants are observed at higher concentrations due to lower temperatures reached for pyrolysis reactions (30). In addition, decrease in the first-order rate constant with concentration was observed for destruction of p-nitrophenol (8). Loss of p-nitrophenol was assumed to decay by parallel zero- and first-order rates corresponding to OH• attack and liquid phase pyrolysis. An increase with concentration in the zero-order degradation rate for the destruction of phenolate and hydrogen sulfide have been reported (9,12). For H_2S, this was attributed to competition kinetics for scavenging OH• radicals by S(-II) and OH• (9). Decomposition of O_3 was observed to increase slightly with concentration but follow first-order kinetics (22).

PCP is hydrophobic in the deprotonated form with a deprotonated octanol-water partition coefficient, log K_{ip}, of 2.68 (32). Therefore, it is expected to accumulate at the gas-liquid interface although it will not volatilize and enter the cavitation bubble. Lower frequency cavitation is expected to produce fewer but more violent bubble collapses than higher frequency cavitation (33). However, larger H_2O_2 generation at high frequency is attributed to more acoustics cycles per time. Therefore, it is assumed that a lower frequency maybe favorable if higher temperatures are preferred over the generation of free radicals (33). An increase of 40% in the rate constant with a decrease in the concentration was observed at 500 kHz, but at 20 kHz the increase was 50%. This indicates that parallel pathways are occurring by pyrolysis and OH radical attack yielding the following overall rate expression:

$$-\frac{d[PCP]}{dt} = k_{pyr}[PCP] + k_{OH}[PCP][OH] \qquad (4)$$

At the interface, [OH] production is constant and [OH] is assumed to be larger than [PCP] at the concentration range studied, therefore, the overall rate is:

$$-\frac{d[PCP]}{dt} = k_{pyr}[PCP] + k'_{OH}[PCP] \quad (5)$$

Depending on the steady-state [OH], the pyrolysis pathway may be more effective at low concentrations. At higher concentrations of [PCP], as shown for gas phase pyrolysis reactions (30), the pyrolysis rate is decreased. We expect this to occur with PCP in the interfacial region as well, due to the reduced surface tension of the bubble and injection of liquid droplets into the gas phase during the collapse of a bubble cloud. A larger reduction in k_{obs} at 20 kHz compared to 500 kHz indicates that k'_{OH} is influenced less by [PCP] than k_{pyr}. This apparent change in the pathway with concentration has been observed with p-nitrophenol (8).

To compare the degradation rate constants of the different reactor systems, the pseudo first-order rate constants were normalized to the degradation rate constant of the 20 kHz probe by:

$$k_{norm} = k_{obs} \frac{1}{\text{PowerDensity}_{reactor}} \text{Power Density}_{20kHz\ probe} \quad (6)$$

where k_{norm} is the normalized rate constant under specified conditions, k_{obs} is the observed rate constant in the reactor under specified conditions, and power density is the power input per volume of solution sonicated as measured by calorimetry. Normalized rate constants indicate the energy input per volume of solution degraded. Values in Table 5.3 demonstrate that the 20 kHz probe reactor has the slowest normalized degradation rate constant. k_{norm} is a factor of 3.4 greater in the 20 kHz Tube Resonator than in the 20 kHz probe. Similarly, k_{norm} in the 500 kHz reactor is a factor of 4.4 greater than in the 20 kHz Tube Resonator. The Tube Resonator has similar power intensity and power density compared to the 500 kHz system whereas the 20 kHz probe utilizes considerably more energy per volume and the area of input is much smaller. For PCP destruction, Pétrier and

co-workers observed an enhancement factor of 4.8 at 500 kHz over 20 kHz (24) which is similar to the enhancement seen comparing the Tube Resonator to the 500 kHz Orthoreactor. The reactors used in Pétrier et al. experiments (12) have the same area for emitting ultrasound as well as the same power density. In addition, other studies of the frequency effect with organic compounds have observed enhancement at 500 kHz over 20 kHz (4,12,34-36). The significant difference between the probe and Tube Resonator demonstrate the large effect of power intensity. Hua and Höchemer have also demonstrated the effect of intensity (37).

PCP reacts very rapidly with both O_3 and OH• as shown in Table 5.1. Because of its rapid reaction rate with O_3, it will react at the gas-liquid interface and small amounts of O_3 will be present in solution. Therefore, unless sonication influences an O_3 gas bubble either by the diffusing gas bubbles breaking up, by turbulence, or by O_3 being pumped into solution by the propagating ultrasound wave, a difference should not be observed in the first-order degradation rate constant by sonolytic ozonation over the sum of the rate constants by sonication and ozonation. Adding the independently-obtained rate constants for sonication and ozonation in the 20 kHz Tube Resonator and comparing it to the combined process of sonolytic ozonation, the difference is within experimental error, but the combined process appears more rapid at both concentrations. Similarly at 500 kHz, the difference is within experimental error but slower than the separate processes at both concentrations. Since the combined system has a slightly larger rate constant at 20 kHz than the linear combination of separate processes, some mechanical effects of ultrasound are apparent. These results are consistent with the concept that O_3 first dissolves into solution and then re-diffuses into a gaseous cavitation bubble where it will undergo thermolytic decomposition (22).

On the other hand, the loss of TOC associated with PCP is more rapid than the linear combination of separate experiments at both frequencies. Enhancement of the combined process over the separate processes is 33% and 57% at 20 and 500 kHz,

respectively. In the degradation of PCP, intermediates such as oxalate do not react with O_3, therefore the decomposition of O_3 into reactive radicals is beneficial for the oxidization of byproducts during PCP destruction. In a previous study, the degradation of nitrobenzene, 4-chlorophenol, and 4-nitrophenol, showed greater enhancements in the 20 kHz probe reactor than the 500 kHz reactor (36). The difference could be the result of the different 20 kHz reactor system in this study. Ozone diffusing gas bubbles in the 20 kHz Tube Resonator coalesced under the influence of ultrasound. This reduced the surface area to volume ratio and thus the amount of O_3 diffusing into solution. The lower power intensity in the 20 kHz Tube Resonator compared to the 20 kHz probe could also account for differences seen in the two studies.

The formation of o-chloranil and TCC is due to OH• attack on the aromatic ring. OH• reacts with the ring by either e- abstraction or OH• addition as follows (14):

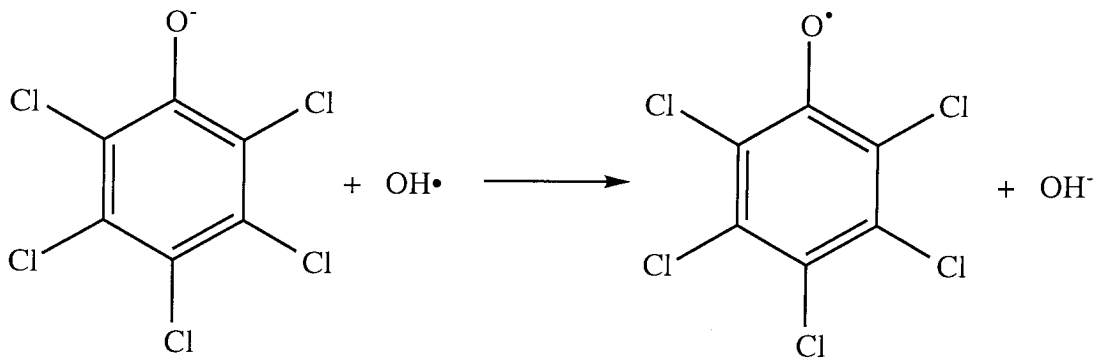

(7)

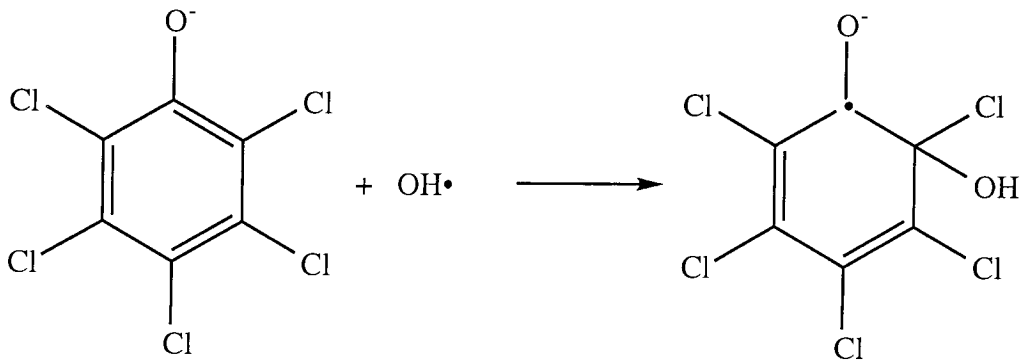

(8)

At temperatures greater than 400 K, OH• reacts with phenols and aromatics mainly by H-atom abstraction (38). However, based on the products observed the overall reaction appears to proceed via OH• addition. Furthermore, OH• addition is expected to occur at the ortho and para positions due to resonance stabilization provided by the phenoxyl substituent, but the ortho position will be favored based on statistical considerations. O-chloranil and the semiquinone radical is then formed by oxidation:

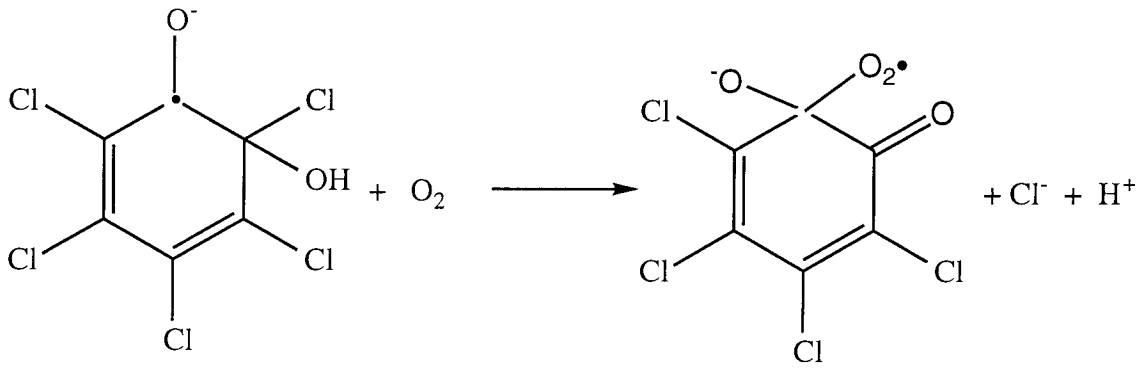

(9)

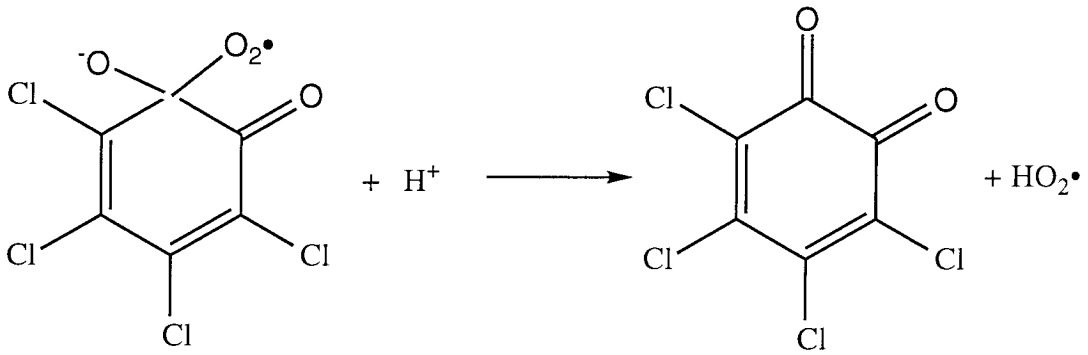

(10)

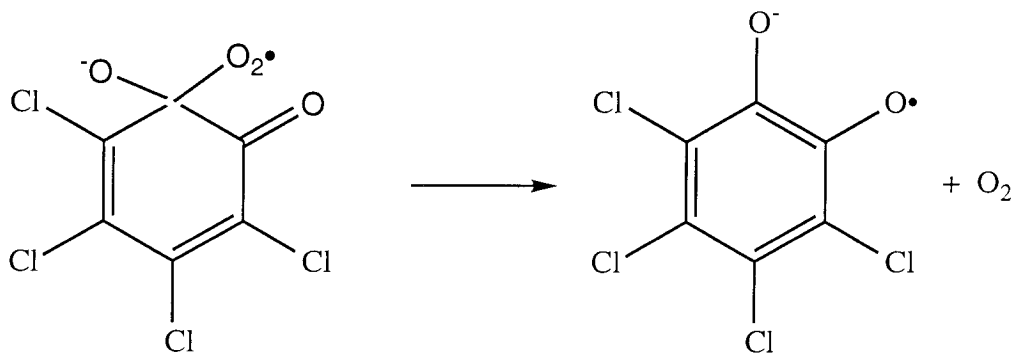

(11)

The semiquinone radical disproportionates to form o-chloranil and TCC. Intermediates in the para position were not detected, possibly due to their expected formation in smaller quantities. Aromatic ring opening is expected to occur by decomposition of o-chloranil yielding organic acids such as oxalate and chlorinated organic acids. In the sonochemical experiments, formation and loss of peaks by ion chromatography not associated with non-chlorinated organic acids occurred as o-chloranil was decreased and Cl^- was increased and provides evidence that these peaks are chlorinated organic acids.

Pyrolysis products have been observed in sonolysis (3,44), however octachlorodibenzodioxin (OCDD), a known product of PCP combustion was not detected. Although they were not detected, pyrolysis byproducts such as OCDD may have been formed. The sonication of ethylbenzene produced a wide range of pyrolysis products which were detected only by sophisticated extraction techniques (3). The apparent absence of pyrolysis products could also indicate that an OH• pathway as indicated is predominate over liquid-phase pyrolysis.

As discussed in previous investigations, since chlorophenols are derivatives of phenol, degradation of chlorophenols by O_3 are expected to follow similar pathways to those of phenol (39-42). The reaction mechanism of O_3 directly with PCP is expected to occur by electrophillic addition of O_3 at the ortho and para positions of the aromatic ring similar to the oxidation of phenol (40). The oxidation will initially form TCC and TCHQ which is oxidized to o-chloranil and p-chloranil. In the oxidation of phenol, further oxidation ruptures the aromatic ring resulting in formation of oxalic acid. A similar, pathway is expected with PCP. At alkaline pH, aqueous decomposition of O_3 occurs and is known to produce OH• (43) which will react with PCP as shown in eqns 7-11.

Comparing the combined sonolysis and ozonolysis experiments to the separate sonolysis and ozonolysis experiments, less oxalate was formed by sonolytic ozonation at both frequencies. At 500 kHz, ozonation produced 7 times the [oxalate] compared to

sonolytic ozonation. The difference at 20 kHz was less significant with a factor of 1.5 more formed by ozonation than by sonolytic ozonation. At pH values above 5, H_2O_2 accelerates the decomposition of O_3 resulting in bulk phase OH• formation as follows (45):

$$H_2O_2 \longleftrightarrow HO_2^- + H+ \qquad pK_a = 11.6 \qquad (12)$$

$$O_3 + HO_2^- \longrightarrow OH\bullet + O_2\bullet^- + O_2 \qquad (13)$$

H_2O_2 is a known byproduct of sonolysis and the rate of H_2O_2 formation at 500 kHz has been shown to be a factor of 6.2 greater than that at 20 kHz (24). Therefore, less oxalate at 500 kHz is a result of HO_2^- reacting with O_3 and subsequent OH• formation.

At both frequencies, the combined sonolysis and ozonolysis experiments liberated Cl^- rapidly, Cl^- formation leveled off, then decreased slightly. HOCl was formed after Cl^- was released indicating that Cl^- is oxidized rather than HOCl formation from Cl•. The reaction of O_3 with Cl^- is a very slow process (46), thus very little HOCl is formed in ozonation reactions. A plausible oxidation reaction of Cl^- to HOCl is as follows (47-49):

$$Cl^- + OH\bullet \longrightarrow ClOH^- \qquad (14)$$

$$ClOH^- + H+ \longrightarrow Cl\bullet + H_2O \qquad (15)$$

$$Cl\bullet + Cl^- \longrightarrow Cl_2\bullet^- \qquad (16)$$

$$Cl_2\bullet^- + OH\bullet \longrightarrow HOCl \qquad (17)$$

HOCl is used as a disinfectant in water and wastewater treatment plants, and is highly oxidizing. HOCl forms after most of the TOC is lost by sonolytic ozonation. Therefore, the formation of HOCl provides in situ disinfection.

ACKNOWLEDGMENT

The authors wish to thank Anne Johansen and Peter Green for help with analysis of intermediates. Financial support provided by Defense Advanced Research Projects Agency (DARPA), Office of Naval Research (ONR), and Electrical Power Research Institute (EPRI) is gratefully acknowledged.

REFERENCES

1. Crosby, D. G., *Pure & Appl. Chem.,* **1981**, *53*, 1051-1080.

2. Narang, A. S.; Swami, K.; Narang, R. S.; Eadon, G. A., *Chemosphere,* **1991**, *22*, 1029-1043.

3. De Visscher, A.; Van Langenhove, H.; Van Eenoo, P., *Ultrasonics Sonochemistry,* **1997**, *4*, 145-151.

4. Drijvers, D.; De Baets, R.; De Visscher, A.; Van Langenhove, H., *Ultrasonics Sonochemistry,* **1996**, *3*, S83-S90.

5. Francony, A.; Pétrier, C., *Ultrasonics Sonochemistry,* **1996**, *3*, S77-S82.

6. Hua, I.; Hoffmann, M. R., *Environ. Sci. Technol.,* **1996**, *30*, 864-871.

7. Hua, I.; Höchemer, R. H.; Hoffmann, M. R., *J. Phys. Chem.,* **1995**, *99*, 2335-2342.

8. Kontronarou, A.; Mills, G.; Hoffmann, M. R., *J. Phys. Chem.,* **1991**, *95*, 3630-3638.

9. Kontronarou, A.; Mills, G.; Hoffmann, M. R., *Environ. Sci. Technol.,* **1992**, *26*, 2420-2428.

10. Kontronarou, A.; Mills, G.; Hoffmann, M. R., *Environ. Sci. Technol.,* **1992**, *26*,

1460-1462.

11. Okouchi, S.; Nojima, O.; Arai, T., *Wat. Sci. Tech.,* **1992**, *26*, 2053-2056.

12. Pétrier, C.; Lamy, M.-F.; Francony, A.; Benahcene, A.; David, B., *J. Phys. Chem.,* **1994**, *98*, 10514-10520.

13. Leighton, T. G. *The Acoustic Bubble*; Academic Press: London, 1994.

14. Terzian, R.; Serpone, N.; Barton Draper, R.; Fox, M. A.; Pelizzetti, E., *Langmuir,* **1991**, *7*, 3081-3089.

15. Mackay, D.; Shiu, W. Y.; Ma, K. C. *Illustrated Handbook of Physical-Chemical Properties and Environmental Fate for Organic Chemicals*; Lewis Publishers: Boca Raton, 1995; Vol. IV Oxygen, Nitrogen and Sulfur Containing Compounds.

16. Hoigné, J.; Bader, H., *Wat. Res.,* **1983**, *17*, 185-194.

17. Hart, E. J.; Henglein, A., *J. Phys. Chem.,* **1986**, *90*, 3061-3061.

18. Hart, E. J.; Henglein, A., *J. Phys. Chem.,* **1985**, *89*, 4342-4347.

19. Barbier, P. F.; Pétrier, C., *J. Adv. Oxid. Technol.,* **1996**, *1*, 154-159.

20. Dahi, E., *Wat. Res.,* **1976**, *10*, 677-684.

21. Olson, T. M.; Barbier, P. F., *Wat. Res.,* **1994**, *28*, 1383-1391.

22. Weavers, L. K.; Hoffmann, M. R., *J. Phys. Chem. A,* **submitted**.

23. Pétrier, C.; Micolle, M.; Merlin, G.; Luche, J. L.; Reverdy, G., *Environ. Sci. Technol.,* **1992**, *26*, 1639-1642.

24. Pétrier, C.; David, B.; Laguian, S., *Chemosphere,* **1996**, *32*, 1709-1718.

25. Gonze, E.; Gonthier, Y.; Boldo, P.; Bernis, A., *Canadian J. Chem. Engng.,* **1997**, *75*, 245-255.

26. Bader, H.; Hoigné, J., *Wat. Res.,* **1981**, *15*, 449-456.

27. Mason, T. J.; Lorimer, J. P. *Sonochemistry: Theory, Applications and Uses of Ultrasound in Chemistry*; Ellis Horwood Ltd: Chichester, 1988.

28. Olson, T. M.; Kolodziej, D. D.; Gonlzalez, A. C. In *Environmental Applications of Advanced Oxidation Technologies*; Electric Power Research Institute: San Francisco, 1996; pp. 7-49-7-58.

29. Rassokhin, D. N.; Kovalev, G. V.; Bugaenko, L. T., *J. Am. Chem. Soc.,* **1995**, *117*, 344-347.

30. De Visscher, A.; Van Eenoo, P.; Drijvers, D.; Van Langenhove, H., *J. Phys. Chem.,* **1996**, *100*, 11636-11642.

31. Serpone, N.; Terzian, R.; Hidaka, H.; Pelizzetti, E., *J. Phys. Chem.,* **1994**, *98*,

2634-2640.

32. Jafvert, C. T.; Westall, J. C.; Grieder, E.; Schwarzenbach, R. P., *Environ. Sci. Technol.,* **1990**, *24*, 1795-1803.

33. Crum, L. A., *Ultrasonics Sonochemistry,* **1995**, *2*, S147-152.

34. Hua, I.; Hoffmann, M. R., *Environ. Sci. Technol.,* **1997**, *31*, 2237-2243.

35. Höchemer, R. H. Ph. D. Thesis, California Institute of Technology, 1996.

36. Weavers, L. K.; Ling, F. H.; Hoffmann, M. R., *Environ. Sci. Technol.,* **submitted**.

37. Hua, I.; Höchemer, R. H.; Hoffmann, M. R., *Environ. Sci. Technol.,* **1995**, *29*, 2790-2796.

38. He, Y. Z.; Mallard, W. G.; Tsang, W., *J. Phys. Chem.,* **1988**, *92*, 2196-2201.

39. Singer, P. C.; Gurol, M. D., *Water Res.,* **1983**, *17*, 1163-1171.

40. Kuo, C. H.; Huang, C. H., *J. Haz. Mat.,* **1995**, *41*, 31-45.

41. Gould, J. P.; Weber, W. J., *J. Water Pollut. Contr. Fed.,* **1976**, *48*, 47-60.

42. Eisenhauer, H. R., *J. Water Pollut. Contr. Fed.,* **1968**, *40*, 1887-1899.

43. Langlais, B.; Reckhow, D. A.; Brink, D. R. *Ozone in Water Treatment Application and Engineering*; AWWA Research Foundation and Lewis Publishers: Chelsea, 1991.

44. Hart, E. J.; Fischer, C. H.; Henglein, A., *J. Phys. Chem.,* **1990**, *94*, 284-290.

45. Staehelin, J.; Hoigné, J., *Environ. Sci. Technol.,* **1982**, *16*, 676-681.

46. Hoigné, J.; Bader, H., *Water Res.,* **1985**, *19*, 993-1004.

47. Jayson, G. G.; Parsons, B. J., *J. Chem. Soc. Faraday Trans. I,* **1973**, *69*, 1597-1607.

48. Kläning, U. K.; Wolff, T., *Ber. Bunsenges. Phys. Chem.,* **1985**, *89*, 243-245.

49. Wagner, I.; Karthäuser, J.; Strehlow, H., *Ber. Bunsenges. Phys. Chem.,* **1986**, *90*, 861-867.

Table 5.1: Selected physical properties and rate constants of PCP.

Property	Value (15)
pK_a	4.71
log K_{ow}	5.09
Henry's constant (Pa m^3 mol^{-1})	0.079
k_{OH} (M^{-1} s^{-1})	3.7×10^{9} ‡
k_{O_3} (M^{-1} s^{-1})	$>3 \times 10^{5}$ *

‡ measured at pH 8 (14)
* measured at pH 2 (16)

Table 5.2: Reactor characteristics.

Reactor	Freq. (kHz)	Reaction Volume (mL)	Emitting Area (cm^2)	Calorimetric Power (W)	Power Intensity ($W\ cm^{-2}$)	Power Density ($W\ L^{-1}$)	Gas Flowrate ($mL\ min^{-1}$)
Ortho-reactor	515	640	25.5	48.3	1.89	75.5	30
Tube Resonator	20	1750	376	466	1.24	266	82
Probe	20	50	1.20	66.5	55.8	1340	50

Table 5.3: Pseudo first-order rate constants of PCP degradation normalized to the 20 kHz probe for sonication in an oxygen saturated solution.

Experiment	$[PCP]_0$ (μM)	k (min^{-1})	k_{norm} (min^{-1})
20 kHz Probe	60	0.021	0.021
20 kHz Tube Res.	60	0.016	0.080
20 kHz Tube Res. T=50°C	60	0.014	0.071
20 kHz Tube Res.	20	0.024	0.10
500 kHz Orthoreactor	60	0.020	0.35
500 kHz Orthoreactor	20	0.028	0.49

Table 5.4: Pseudo first-order rate constants for degradation of PCP under various conditions.

Experiment	$k_{20\ \mu M}$ (min^{-1})	$k_{60\ \mu M}$ (min^{-1})
20 kHz Tube Resonator		
Sonication w/O_2: k_{US}	0.0238 ± 0.001	0.0158 ±0.001
Ozonation: k_{O_3}	0.571 ± 0.09	0.451 ± 0.03
Sonication w/O_3: k_{US/O_3}	0.687 ± 0.07	0.529 ± 0.09
$k = k_{US} + k_{O_3}$	0.595 ± 0.071	0.467 ± 0.031
500 kHz Orthoreactor		
Sonication w/O_2: k_{US}	0.0277 ± 0.001	0.020 ± 0.001
Ozonation: k_{O_3}	0.337 ± 0.07	0.311 ± 0.03
Sonication w/O_3: k_{US/O_3}	0.304 ± 0.09	0.260 ± 0.09
$k = k_{US} + k_{O_3}$	0.365 ± 0.071	0.331 ± 0.031

Table 5.5: Pseudo first-order rate constants for degradation of TOC associated with $[PCP]_0$ = 60 μM

Experiment	$k_{20\ kHz}$ (min^{-1})	k_{500kHz} (min^{-1})
Sonication w/O_2: k_{US}	0.00275	0.00354
Ozonation: k_{O_3}	0.0344	0.00897
Sonication w/O_3: k_{US/O_3}	0.0493	0.0196
$k = k_{US} + k_{O_3}$	0.0371	0.0125

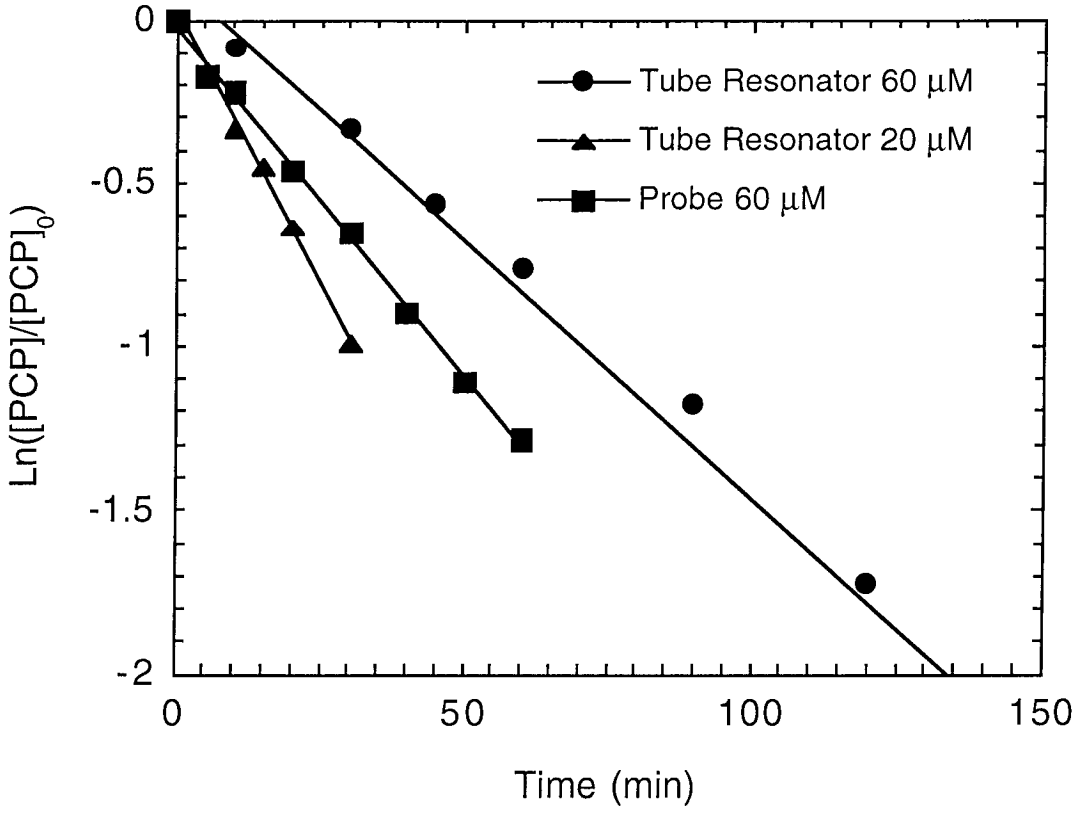

Figure 5.1: First-order plot of [PCP] degradation by sonication at 20 kHz.

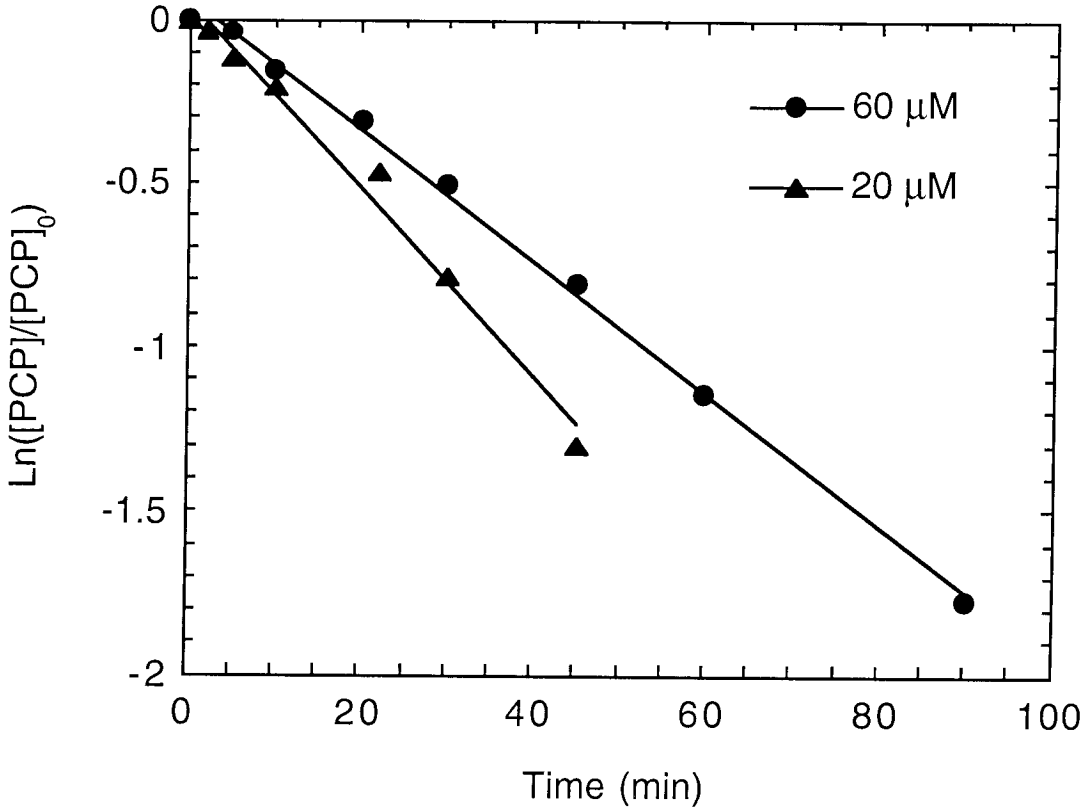

Figure 5.2: First-order plot of [PCP] degradation by sonication at 500 kHz.

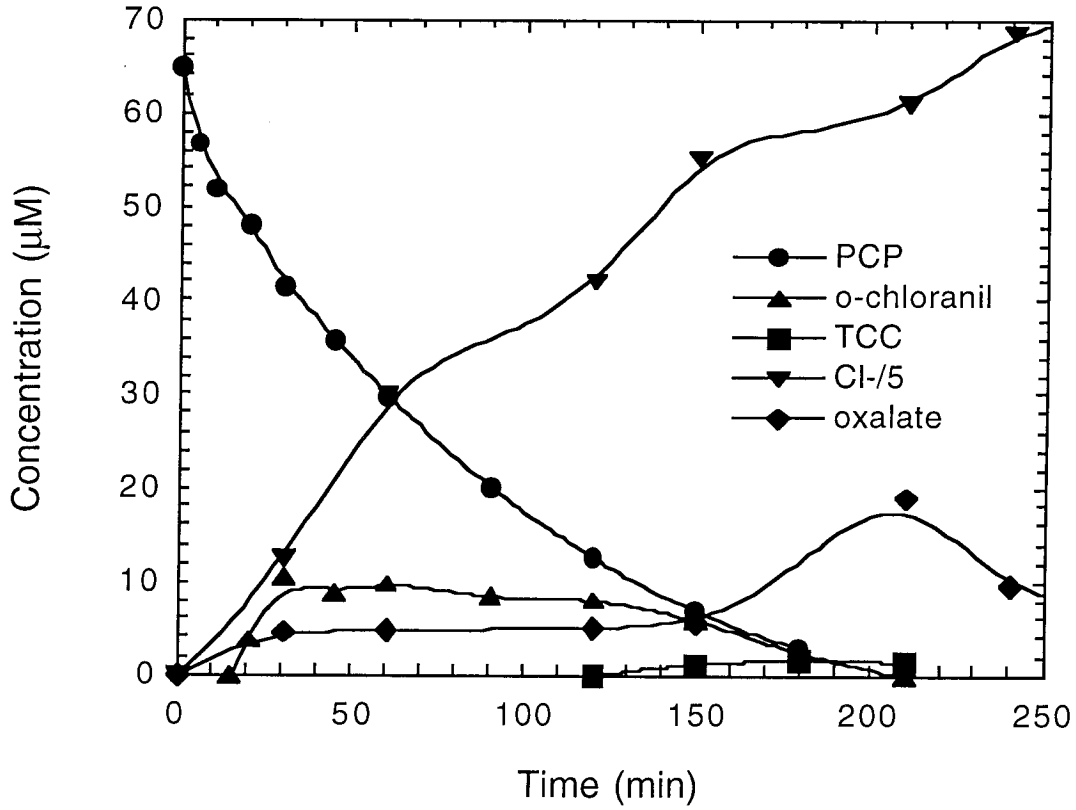

Figure 5.3: Degradation of 60 μM PCP and intermediates formed by sonication with O_2 in the 20 kHz Tube Resonator.

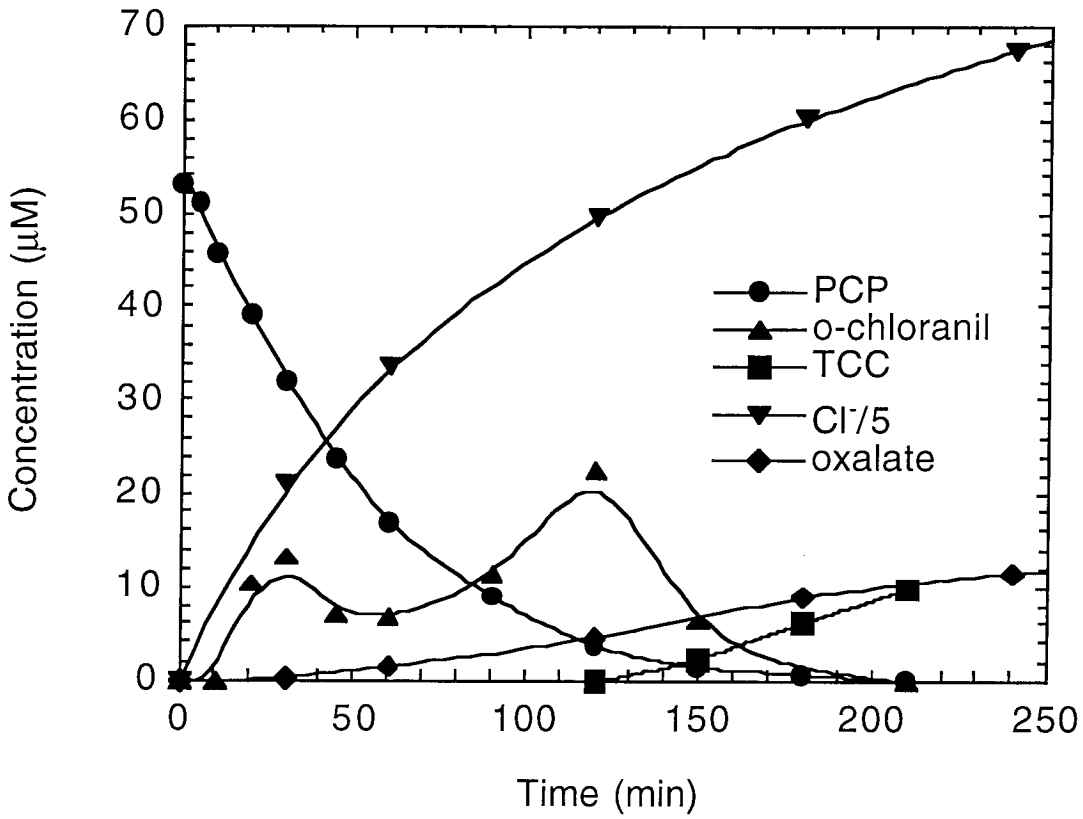

Figure 5.4: Degradation of 60 μM PCP and intermediates formed by sonication with O_2 at 500 kHz.

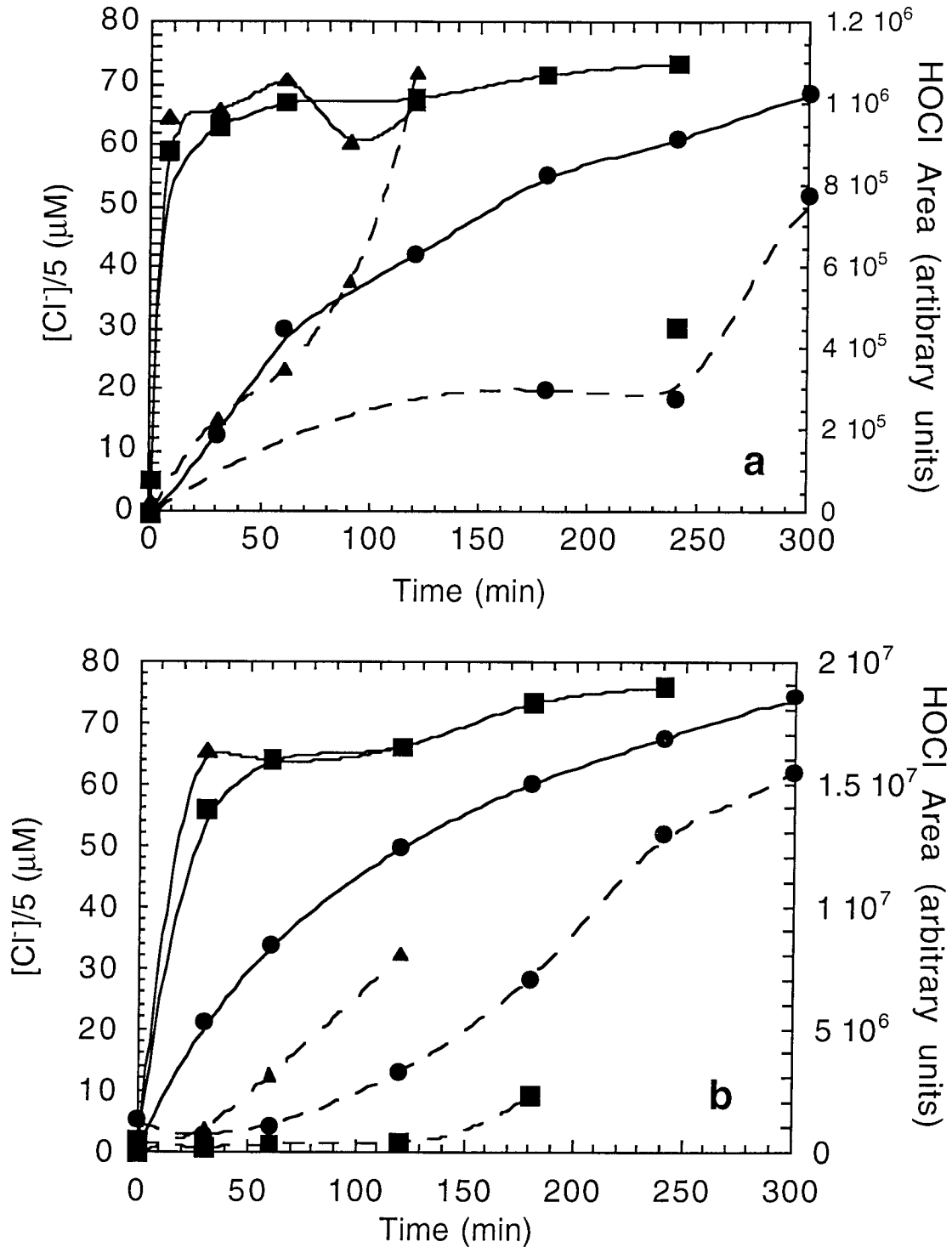

Figure 5.5: Cl^- (solid line) and HOCl (dashed line) formation from 60 μM PCP destruction by sonication with O_2 (circles), ozonation (squares), and sonolytic ozonation (triangles) in the 20 kHz Tube Resonator (a), and 500 kHz Orthoreactor (b).

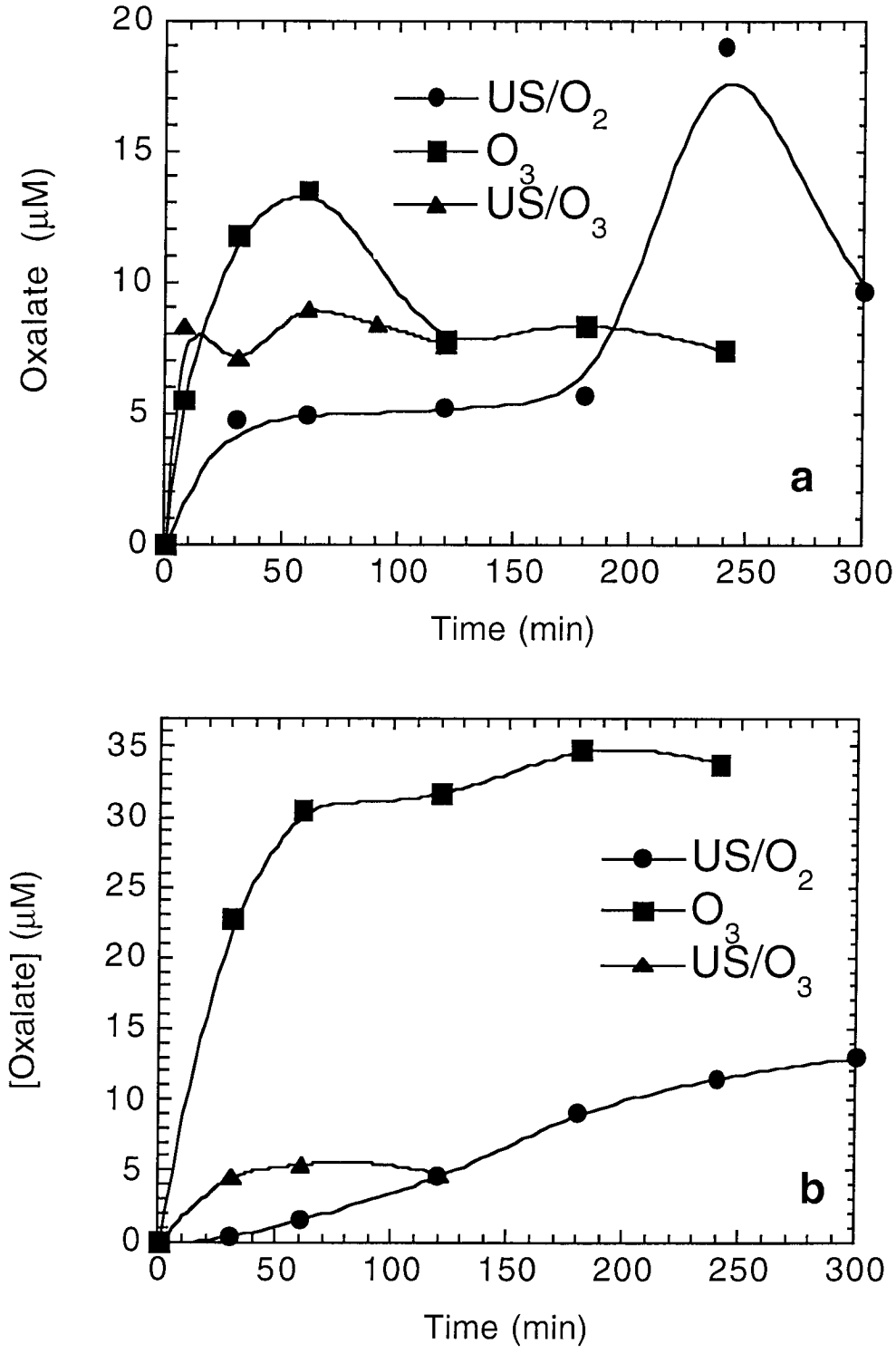

Figure 5.6: Formation of oxalate from 60 μM PCP destruction by sonication with O_2, ozonation, and sonolytic ozonation in the 20 kHz Tube Resonator (a), and 500 kHz Orthoreactor (b).

Chapter 6

A New Advanced Oxidation Process: Degradation of Triethanolamine and COD Reduction in Wastewater by Photoactivated Periodate

---

(*Water Environment Research,* **1997**,69,1112-1119)

ABSTRACT: The rapid reduction of the chemical oxygen demand (COD) of an industrial wastewater is achieved using a novel oxidant, periodate (IO_4^-), coupled with UV irradiation. The wastewater is characterized by a high COD, low total suspended solids (TSS), variable triethanolamine (TEA) concentrations and ppm levels of iron (Fe) and zinc (Zn). The use of periodate and ultraviolet irradiation with either aqueous TEA solutions or real wastewater is shown to be effective in reducing the COD to acceptable levels. The optimal pH for COD degradation is determined to be pH 7.6 due to the combined effects of pH on the speciation of TEA and IO_4^-. Increasing the $[IO_4^-]_0/[TEA]_0$ ratio increased the degradation rate up to an apparent saturation value. Irradiation with a 1000 W Hg(Xe) lamp increased the pseudo first-order degradation rate constant of COD by a factor of 5.5 for synthetic TEA solutions and 2.3 for the industrial wastewater as compared to irradiation with a 1000 W Xe lamp.

KEYWORDS: chemical oxygen demand, oxidation, ozone, periodate, triethanolamine, ultraviolet irradiation, wastewater

Introduction

The reduction of COD in high strength industrial wastewaters by biological treatment is often expensive and land intensive. In addition, many industrial chemicals are toxic to microorganisms.

Advanced oxidation processes (AOPs) are applicable to the degradation of a wide range of pollutants and are especially useful as pre-treatment steps before biological treatment, for the degradation of wastewaters that are resistant to biodegradation, and as a post-treatment process to minimize the toxic effects on receiving waters (Eckenfelder, 1989). Most AOPs rely on the generation of hydroxyl radical (Legrini et al., 1993). However, other chemical oxidation techniques may result in faster wastewater treatment than the more traditional AOPs, such as UV/O_3, UV/H_2O_2, $H_2O_2/Fe(II)$, and TiO_2/UV (Hoffmann et al., 1995).

Triethanolamine is used in the manufacture of surface active agents, waxes, polishes, detergent builders, herbicides, demulsifiers, cement additives, and cutting oils (Kroschwitz and Howe-Grant, 1991). Alkanolamines, in general, are good inhibitors of the corrosion of ferrous metals. They are widely used in coolant systems, lubricating oils, metal working fluids, petroleum antifouling applications and in drilling. TEA is often used to coat stainless steel to prevent high-temperature oxidation (Kroschwitz and Howe-Grant, 1991). It is also an effective complexing agent of metal ions such as iron and zinc (Perrin, 1979).

Although the general organic chemistry of alkanolamines is known, the redox and autooxidation chemistry of TEA is not well established. This is understandable, in part, since TEA is often used as an antioxidant or free-radical trap to retard the autooxidation of a variety of materials.

TEA is known to be oxidized slowly by a variety of oxidizing agents including hydrogen peroxide (Jones and Burns, 1925), sodium hypochlorite (Price et al., 1947),

periodate (Fluery et al., 1949), potassium permanganate (Mata-Pérez and Pérez-Benito, 1984), hydroxyl radical (Schwarz, 1982), chromate (Antelo et al., 1977), persulfate (Hagopian et al., 1972), photocatalytic Pt/TiO_2 (Malinka and Kamalov, 1994), and microorganisms (Frings et al., 1994; Williams and Callely, 1982). The reported oxidation products and intermediates include: formaldehyde, acetaldehyde, monoethanolamine, diethanolamine, hydroxyacetaldehyde, acetate, formate, and ammonia.

Periodic acid (H_5IO_6) or periodate (IO_4^-) is a well-known oxidant in organic chemistry (Buist, 1972; Dryhurst, 1970; Jackson, 1944). It is highly reactive with respect to the oxidation of 1,2-diols and 1,2-ketones. It is also very active with respect to the oxidation of a wide range of other organic compounds such as ketoacids, carbohydrates, carboxylic acids, sugars, amines, aldehydes, and aminoalcohols such as TEA. Dark reaction of periodate with glycols and related compounds involves the formation of a cyclic periodate complex (Dryhurst, 1970). Periodate has a fairly high oxidation potential as shown in Table 6.1, where the 2-electron reduction product of periodic acid is iodate (IO_3^-) (Latimer, 1952).

Periodate reactions are known to become less selective with respect to specific functional groups with increasing temperature or by the addition of light (Dryhurst, 1970). In order to enhance oxidation and to exploit the loss of substrate selectivity, the use of UV light with periodate was investigated. The photolysis of periodate and periodic acid has been studied over a wide range of pH and a large number of photochemical reactions involving periodate have been proposed (Kläning et al., 1981; Kläning and Sehested, 1978; Wagner and Strehlow, 1982). For example, the following mechanism for the photolysis of periodate has been suggested by Wagner and Strehlow (1982):

$$IO_4^- \xrightarrow{h\nu} IO_3\bullet + O\bullet^- \qquad (1)$$

$$O\bullet^- + H^+ \longleftrightarrow OH\bullet \qquad (2)$$

$$OH\bullet + IO_4^- \longrightarrow OH^- + IO_4\bullet \quad (3)$$

$$2\ OH\bullet \longrightarrow H_2O_2 \quad (4)$$

$$2\ IO_4\bullet \longleftrightarrow I_2O_8 \quad (5)$$

$$I_2O_8 + H_2O \longrightarrow IO_3^- + IO_4^- + 2\ H^+ + O_2 \quad (6)$$

$$2\ IO_3\bullet \longleftrightarrow I_2O_6 \quad (7)$$

$$I_2O_6 + H_2O \longrightarrow IO_4^- + IO_3^- + 2\ H^+ \quad (8)$$

$$IO_4^- \xrightarrow{h\nu} IO_3^- + O(^3P) \quad (9)$$

$$O_2 + O(^3P) \longrightarrow O_3 \quad (10)$$

$$O_3 + IO_3\bullet \longrightarrow IO_4\bullet + O_2 \quad (11)$$

The photolytic decomposition mechanism involves a number of highly reactive radical and non-radical intermediates such as $IO_3\bullet$, $\bullet OH$, IO_3^-, O_3, and $IO_4\bullet$. Therefore, the photoassisted oxidation of organic substrates by periodate most likely occurs via free radical pathways. This mechanism indicates possible regeneration of IO_4^- through radical chain reactions. Studies of $UV/TiO_2/O_2$ systems with added IO_4^- show that oxidation of a wide variety of organic compounds occurs very rapidly when compared to $UV/TiO_2/O_2$ oxidation alone (Grätzel et al., 1990; Halmann, 1992; Martin et al., 1995; Pelizzetti et al., 1991).

The detailed interrelationship among the various oxidation states and their intermediates during photolytic oxidation in the UV/IO_4^- system is shown schematically in

Fig. 6.1 (Barat et al., 1971; Buxton and Sellers, 1985; Kläning et al., 1981; Mezyk and Elliot, 1994; Wagner and Strehlow, 1982; White, 1992). The mechanism follows a free-radical chain decomposition pathway and shows possible regeneration to iodate. The diagram indicates that hypoiodous acid, iodine, iodide and hydrogen peroxide are formed. HOI, I_2, and H_2O_2 are important products since they are effective oxidants and are used in the disinfection of water (White, 1992). Redox half-reactions for various iodine species are shown in Table 6.1.

The principal objectives of our investigation were to selectively destroy TEA and its associated COD. Initial studies by more traditional methods such as oxidation by hydrogen peroxide, ozone, and sonication were ineffective. Focus then shifted to explore photoassisted oxidation with periodate and to determine the optimal reaction conditions with respect to pH, $[IO_4^-]_o/[TEA]_o$, and light intensity. Experiments were performed on industrial wastewater to evaluate the practical effectiveness of this treatment technology.

Methodology

Reagents. All chemicals were of reagent grade. Triethanolamine (Baker, pK_a = 7.8), periodic acid (Aldrich), lithium hydroxide (Aldrich), barium hydroxide octahydrate (Sigma), perchloric acid (EM Science), sodium hydroxide (Mallinckrodt), and 30% hydrogen peroxide (EM Science) were used as received. Milli-Q UV Plus water (R = 18.2 MΩ-cm) was used for the preparation of aqueous solutions.

Oxidation Studies. Sonications were performed with a 20 kHz direct immersion ultrasonic probe (Sonics and Materials, model VCX 400). Complete experimental details of typical sonications is found in Hua et al., 1995. The pH of these systems was initially adjusted to pH 9 or 10 with NaOH. Initial TEA concentrations were 0.005 or 0.05 M as indicated in Table 6.2. For H_2O_2 or O_3 combined with ultrasound, the oxidant was added upon initiation of sonication. Ozone was generated from oxygen gas with an OREC model O3V10-O ozone generator with ~2% ozone v/v in gas phase. O_3 was

continually bubbled through the reaction vessel at a flow rate of 70 mL/min. Concentrated H_2O_2 was added to TEA solutions to obtain initial concentrations as shown in Table 6.2.

Periodate Studies. Reactions as a function of pH were conducted by adjusting 0.3 M H_5IO_6 solutions and wastewater or 5 mM TEA to pH 1, 4, 7.6, or 9 with 4.0 N LiOH or 5.0 N $HClO_4$. For this study LiOH was used to allow for a larger investigation of the pH effect. KIO_4 as well as $Na_2H_3IO_6$ are relatively insoluble limiting the use of both NaOH and KOH over a broad pH range. The reaction components were added together at the start of the experiment to obtain the desired concentration of 0.1 M H_5IO_6 and 3.3 mM TEA or dilution of the wastewater by 2/3 to obtain an irradiated volume of 180 mL. The initial ionic strength (μ) was approximately 0.2 M. Irradiations were performed with a 1000 Watt Xe arc lamp (Oriel Corp.) at 20 °C except selected experiments which were performed on a 1000 Watt Hg(Xe) arc lamp (Oriel Corp.) at 20 °C. Potassium ferrioxalate was used as an actinometer (Calvert and Pitts, 1966; Rabek, 1982); the incident light intensity was 0.2 μeinsteins/cm^{2}sec and 8 μeinsteins/cm^2/sec for the Xe and Hg(Xe) lamps respectively. Infrared irradiation was controlled by a 10 cm water filter and by cooling the reaction vessel with a recirculating constant temperature bath (Haake Co., model A81) at 20 °C. The pH was controlled with a model ABU 80 autoburette and model TTT 80 titrator (Radiometer). The oxidation kinetics in the absence of light were conducted in well-mixed amber jars under the same initial conditions.

Periodate experiments involving ozone were conducted with the same initial conditions but with an irradiated volume of 60 mL and without temperature or pH control. Ozone was generated from oxygen gas with an OREC model O3V10-O ozone generator with ~2% ozone v/v in gas phase as determined by the Indigo Method (Bader and Hoigné, 1981). Gas was bubbled into the reactor at a rate of 25 mL/min.

At selected time intervals, 2.5 mL aliquots of the reaction mixture were extracted from the irradiation vessel. To precipitate periodate, 2.5 mL of a 0.15 M barium hydroxide solution were added to each sample aliquot. The suspensions were then filtered with maxi-

clean IC/Ag 1.5 mL cartridges (Alltech) to remove I^- and 0.45 μm Teflon syringe filters (Gelman) to remove any remaining particles.

Analysis. Analysis of TEA was performed on a capillary electrophoresis chromatograph (Dionex, model CES I). Cations were separated by applying a positive voltage across a 375 μm O. D. x 75 μm I.D. x 70 cm bare silica interior capillary (Dionex). A solution of 30 mM creatinine and 4 mM hydroxyisobutyric acid pH adjusted to 4.8 with glacial acetic acid was used as the buffer. Detection of eluent peaks was by reverse UV absorption at 220 nm. To release TEA bound with Fe(II), Fe(III), and Zn(II), 0.1 M EDTA (Aldrich) was added to wastewater samples approximately 24 hours before analysis. The technique of standard addition was employed to determine TEA concentrations in the wastewater.

COD was measured with High-Range COD vials provided by Hach (COD ≤ 1500 ppm). COD vials with 2 mL aliquots were digested for 2 hours at 150 °C. The absorbance of the digested COD vials was then taken with an HP 8452a diode array spectrophotometer (Hewlett Packard) at a wavelength of 600 nm.

Analysis of the metals in the wastewater was performed using ICP-MS (Perkin-Elmer, Elan 5000). Samples were prepared by adding 1 mL of sample to 9 mL of ~5% HNO_3 and filtering before analysis.

Total suspended solids was measured following the standard methods procedures (Greenberg and Clesceri, 1992). TSS measurements were not taken immediately upon receipt of wastewater. For comparison purposes, the relative concentrations of TSS in the wastewaters were not expected to change considerably over time. Light absorbance of raw wastewater samples were measured with an HP 8452a diode array spectrophotometer.

Results and Analysis

Periodate Speciation. The speciation of periodate as a function of pH was calculated (Westall, 1979) in order to determine the dominant periodate species as a

function of pH (Fig. 6.2). As shown in equations 12-14 periodate has three pK_a's; it dimerizes (eqn 16); and it is sensitive to dehydration (eqn 15) (Buist, 1972):

$$H_5IO_6 \longleftrightarrow H_4IO_6^- + H^+ \qquad pK_{a1} = 1.64 \qquad (12)$$

$$H_4IO_6^- \longleftrightarrow H_3IO_6^{2-} + H^+ \qquad pK_{a2} = 8.36 \qquad (13)$$

$$H_3IO_6^{2-} \longleftrightarrow H_2IO_6^{3-} + H^+ \qquad pK_{a3} = 12.2 \qquad (14)$$

$$H_4IO_6^- \longleftrightarrow IO_4^- + 2\,H_2O \qquad K_D = 40 \qquad (15)$$

$$H_3IO_6^{2-} \longleftrightarrow H_2I_2O_{10}^{4-} + 2\,H_2O \qquad K_X = 141\ M^{-1} \qquad (16)$$

Figure 6.2 shows the variation of five species and their relative concentrations as a function of pH for a concentration of 0.1 M total periodate. Over a wide pH range the dehydrated periodate species dominates. Above pH 9.5, the dimer becomes the major species.

Oxidation of TEA. Initial experiments were focused on the oxidative degradation of TEA by a variety of techniques such as sonolysis with ozone or hydrogen peroxide, UV/TiO_2 photocatalysis, ozone alone, and hydrogen peroxide alone. These preliminary studies indicated that ultrasound with ozone or ozone alone were the most effective methods for the destruction of TEA. The extents of TEA degradation after 60 min by each of these methods are given in Table 6.2. TEA oxidation was incomplete indicating that COD loss would be slight and hence was not measured. Although these experiments were performed at a high TEA concentration, sonication at a concentration similar to the concentration of periodate experiments did not increase the extent of degradation considerably.

Even though these processes were somewhat effective with respect to TEA oxidation, they proved to be ineffective at reducing the COD of the wastewaters of interest.

At this point, periodate, which is known to oxidize TEA effectively at pH 7.6 (Fluery et al., 1949) was explored as an alternative oxidant. Dark reactions for the oxidation of TEA by IO_4^- are shown in Fig. 6.3. As predicted by Fluery (1949), the optimal pH for the oxidation of TEA by IO_4^- was pH 7.6. A plausible explanation for this pH optimum is that triethanolamine is more readily oxidized in its deprotonated form (pK_a = 7.8) while the active oxidizing species is the dehydrated periodate, IO_4^-. Deprotonated TEA is oxidized in the dark by periodate but only to formaldehyde and ammonia (Dryhurst, 1970):

$$N(CH_2CH_2OH)_3 + 3\ IO_4^- \longrightarrow 6\ HCOH + NH_3 + 3\ IO_3^- \qquad (17)$$

Therefore, the COD associated with TEA was not reduced significantly via oxidation with periodate alone.

Experiments with Reagent Grade TEA. 5 mM was chosen as a representative TEA concentration since it has a theoretical COD = 1500 mg/L, which is similar to the COD value of the actual wastewater. However, the measured COD was approximately 1200 mg/L. This discrepancy was due to the inability of dichromate to oxidize the amine group to nitric acid (Greenberg and Clesceri, 1992). 5 mM was the concentration before dilution with 0.3 M periodate. Reaction concentrations were $[TEA]_o$ = 3.3 mM and $[IO_4^-]_o$ = 0.1M.

The variation of the first-order degradation rate constant, k_{obs}, was examined at pH 1, 4, 7.6 and 9. Degradation of both TEA and its corresponding COD were followed. With a pH stat, the pH was held constant by the addition of strong acid or base during the course of the reaction. At pH 7.6 and 9, the pH of the solution increased during photooxidation in the absence of added H^+. At lower initial pH values, H^+ was produced initially; the pH dropped, then rose slightly but did not exceed the initial pH values. This behavior indicates the possibility of different reaction mechanisms at high and low pH. The apparent rates of photooxidation of TEA and COD followed pseudo first-order kinetics at constant pH, T and μ as follows:

$$-\frac{d[TEA]}{dt} = k_{obs\ TEA}\,[TEA] \tag{18}$$

$$-\frac{d[COD]}{dt} = k_{obs\ COD}\,[COD] \tag{19}$$

where the corresponding integrated solutions are:

$$\ln\frac{[TEA]_t}{[TEA]_o} = -k_{obs\ TEA}\,t \tag{20}$$

$$\ln\frac{[COD]_t}{[COD]_o} = -k_{obs\ COD}\,t \tag{21}$$

Figure 6.4 illustrates the variation of k_{obs} with pH when 3.3 mM TEA was photooxidized by 0.1 M periodate. The destruction of TEA occurred much faster than the COD reduction. Similarly, TEA present in the wastewater was expected to be destroyed much faster than the reduction of the corresponding COD. The observed first-order rate constant for TEA degradation, $k_{obs\ TEA}$, increases with pH. The rate of reduction of the COD reaches an apparent maximum at pH 7.6. A plausible explanation for this behavior is that TEA reacts much faster in its deprotonated form. In addition, the reactive periodate intermediates may react more quickly with TEA at a lower pH. Since pH 7.6 was the optimal pH examined for the reduction of COD further parametric investigations were performed at this pH.

The effect of $[IO_4^-]_o/[TEA]_o$ ratios on the rates of oxidation was noted as shown in Fig. 6.5. The $[IO_4^-]_o/[TEA]_o$ ratio is a molar ratio defined as: molar ratio ≡ (moles/L)/(moles/L) = M/M. In the absence of IO_4^-, there was no photooxidation of TEA. The molar extinction coefficients at 222 nm are $\varepsilon_{\lambda=222nm} = 1 \times 10^4\ M^{-1}cm^{-1}$ (Wagner and Strehlow, 1982) for periodate and $\varepsilon_{\lambda=222nm} = 400\ M^{-1}cm^{-1}$ for TEA, respectively. The

relatively low extinction coefficient for TEA indicates that it does not photolyze as readily as periodate. As the $[IO_4^-]_o/[TEA]_o$ ratio increases, $k_{obs\ TEA}$ increases rapidly until it reaches an apparent saturation value. However, at high concentrations $k_{obs\ TEA}$ decreases.

Photooxidation of the COD associated with the synthetic TEA solutions represented by $k_{obs\ COD}$ is also negligible in the absence of IO_4^-. $k_{obs\ COD}$ increases linearly up to a $[IO_4^-]_o/[TEA]_o$ ratio of 37.5. $k_{obs\ COD}$ is approximately 0.1 of $k_{obs\ TEA}$. This is expected since the TEA is oxidized to other organic compounds which also exert a COD. The stoichiometric oxidation of TEA to CO_2 by periodate is 15:1 $[IO_4^-]_o$:$[TEA]_o$. Although a maximum rate is obtained with a ratio of 37.5:1 in a practice a lower ratio of perhaps 17.5:1 $[IO_4^-]_o$:$[TEA]_o$ with longer irradiation times could be used. However, periodate combined with sunlight oxidations of formaldehyde and formic acid are known to be more rapid when excess periodate is employed (Head and Hughes, 1952).

The proposed mechanism for IO_4^- photolysis (Wagner and Strehlow, 1982) involves the formation of I_2O_6 and I_2O_8 dimers from the self reactions of IO_3• and IO_4•. These dimers hydrolyze to form non-radical species. Formation of stable species from radicals is inhibitory to the photo-induced free radical chain oxidation. This chain termination effect is observed at high $[IO_4^-]_o$. Therefore, it is necessary to optimize $[IO_4^-]_o/ [TEA]_o$ in order to obtain a maximum rate and extent of oxidation. Given these constraints, a $[IO_4^-]_o/[TEA]_o = 30$ was chosen for the wastewater experiments. This corresponds to $[IO_4^-]_o/[COD]_o \sim 1.3 \times 10^{-4}$ M/(mg/L) which is more relevant for the wastewater.

To examine the effect of different light sources, irradiations were performed utilizing a mercury-xenon lamp. For these experiments, the pH was held constant at 7.6 with initial conditions as above ($[TEA]_o = 3.3$ mM and $[IO_4^-]_o = 0.1$M). Figure 6.6 shows a 5.5 fold increase in $k_{obs\ COD}$ with the Hg(Xe) lamp. The reaction rate was expected to increase, therefore, $k_{obs\ TEA}$ was not measured for these experiments due to the rapid degradation of TEA. A xenon lamp has a relatively flat irradiance over the range of 300-800 nm with an exponential decay in irradiance down to 250 nm. However, a mercury-

xenon lamp has a much stronger irradiance in the 200-300 nm UV region. This was verified by considerably higher light flux measurements using ferrioxalate actinometry which measures the light absorbance over the 254-480 nm wavelength range. IO_4^- has a maximum absorbance at 222 nm indicating that the Hg(Xe) lamp photolyzes IO_4^- much more efficiently than the Xe lamp. For a IO_4^-/UV process to be used in the field the light source would be a key consideration.

Characterization of the Wastewater. The wastewater samples used to evaluate the effectiveness of this technique were taken as grab samples from an axle and brake manufacturing facility. The samples were taken from similiar waste streams at two different factilities over a several month period of time. The waste stream comes from periodic floor washing in the metal working area on the manufacturing floor. Samples of industrial wastewater were analyzed for critical parameters to observe the day to day variability in the wastewater. As shown in Table 6.3, the pH varies from 6.8 to 8.1 with a relatively high conductivity. The TEA concentrations vary by more than an order of magnitude and the metal concentrations show considerable variation in the ppm range. TSS measurements vary somewhat but were all low. The measured COD remains relatively constant despite the wide variations in other parameters. TEA was expected to be a main component of this stream and consequently was the only measured organic compound. However, oil, grease, surfactants, ethylene glycol, and degradation products of TEA such as monoethanolamine and diethanolamine are also present. UV/VIS spectral analysis shows similar broad absorption over a wide range of the UV region. Wastewater sample #6 was taken from a nanofiltration retentate. Due to its high TSS, sample #6 was filtered prior to irradiation.

Experiments with Wastewater. Values of k_{obs} were determined for the degradation of the COD in the wastewater at pH 7.6 using 0.1 M IO_4^- and UV irradiation with the Xe lamp. Table 6.3 shows the rate constants for actual wastewater samples. The observed rates of degradation of COD are slower with real wastewater than with homogeneous solutions of TEA. Neither oxidation of the wastewater by IO_4^-, nor

photolysis alone reduced the COD of the wastewater. Slower rates of degradation may be due to a variety of effects, such as the presence of a wide range of organic compounds and metals other than those measured, higher ionic strengths of the wastewaters, stronger UV absorbances of the wastewaters than synthetic solutions, and the presence of free radical traps such as carbonate. Between 58% and 82% of the COD was destroyed in three hours of photooxidation depending on the particular wastewater sample. The observed rate constants do not appear to correlate with any measured parameter except TSS. This effect is more likely due to the oxidation and dissolution of organic solids during the reaction than to surface effects. Samples were filtered before COD analysis removing the organic COD of the TSS. Thus, the IO_4^-/UV system appears to be applicable to a wide range of organic wastewaters.

The correlation of pH with k_{obs} was not seen with the wastewater. Fig. 6.7 shows that for the photooxidation of the wastewater at pH 7.6 and 9, the k_{obs} values are only 20% greater than k_{obs} at pH 1. Since TEA is only a minor component in the waste streams, the degradation rates were very similar over the pH range investigated. The mixture of a variety of compounds minimized any effect of protonation of a single compound in the wastewater.

Degradation of wastewater sample #5 with the Hg(Xe) lamp showed a similar rate enhancement as in the synthetic TEA experiments. The values of $k_{obs\ COD}$ were 0.0068 and 0.016 min^{-1} for the Xe and Hg(Xe) lamps respectively. This corresponds to a 2.3 fold increase in $k_{obs\ COD}$ which is a smaller enhancement than for TEA solutions. Since the wastewater absorbs light more strongly in the UV range of interest than TEA solutions, the effect of increasing the light intensity in this wavelength region is diminished due to a smaller portion of photons reaching IO_4^-.

The addition of ozone to the IO_4^-/UV system was also investigated. The experiments were carried out in a 60 mL reactor without temperature (T = ~40 °C), or pH control (pH increased to ~9). Since O_3 has been observed to form in the IO_4^-/UV system and it is thought to participate in the propagation of the periodate radicals, it was expected

to have some effect on the overall reaction. However, as shown in Fig. 6.8 the coupled IO_4^-/O_3/UV oxidations of wastewater were only somewhat more effective than either IO_4^- /UV or IO_4^-/O_3. The irradiated reaction rates are considerably faster than in Table 6.3 due to the lack of temperature control and the smaller irradiation volume. Ozone at pH 7.6 is unstable and generates hydroxyl radical. Therefore, these experiments also suggest a role for hydroxyl radical as indicated in eqns. 1-11. UV irradiation of IO_4^- appears to have a greater effect than addition of OH• indicating that either reaction of periodate with OH• is relatively slow or reaction of the intermediate IO_4• with reductants is slow. According to the mechanism of eqns. 1-11, removal of hydroxyl radical would allow the I(VI) radical species, IO_3•, to predominate.

Discussion

Ultraviolet irradiation in combination with IO_4^- is an effective approach for the degradation of TEA and elimination of its associated COD. Optimal conditions for the destruction of COD in synthetic TEA solutions were found at pH 7.6 with $[IO_4^-]_o/[TEA]_o$ = 30. The Hg(Xe) lamp was found to be 5.5 times more effective than the Xe lamp.

The IO_4^-/UV process has been demonstrated to be effective in reducing the COD levels in a variety of wastewaters. Degradation of COD appears to be correlated with the TSS even though this correlation could be an artifact of the analysis technique. Again, use of a lamp with stronger light intensity in the UV region increased the effectiveness of the system. Ozone addition to the IO_4^-/UV system increased reaction rates only slightly.

We suggest, that based on our results, the IO_4^-/UV system should serve as an excellent AOP for a wide variety of wastewaters. This reaction system appears to be promising since: (1) its reaction rates are considerably faster for the degradation of TEA than with other AOPs employing H_2O_2, O_3, sonolysis with H_2O_2, or with O_3; (2) at similar COD levels but variable TEA concentrations high reactivity is observed; and (3) with iodine in the I(VII) (i.e., IO_4^-, $H_4IO_6^-$) state, periodate serves as an 8-electron

oxidant. Further investigations of this system are necessary to determine the effect of parameters such as ionic strength. Determination of various iodine species formed during irradiation would be beneficial in understanding the reduction pathway of periodate.

Since the IO_4^-/UV system depends on the availability of photoactivated periodate, the wastewater matrices should have relatively low intrinsic extinction coefficients. On the other hand, this limitation could be overcome by filtration before photolysis.

At the present time, there are no discharge requirements or drinking water standards for iodine species. This is due mainly to the small usage of iodine in water or wastewater treatment. Also, Iodine and iodide are believed to be relatively low in toxicity. No toxicity data have been reported for hydroiodic acid, iodate or periodate. Due to the cost of periodate and to limit the introduction of iodine species into natural water systems it would be beneficial to recover the iodine species from the wastewater using ionic exchange and electrochemically regenerate it to periodate.

Conclusions

The IO_4^-/UV system is demonstrated to be effective in the oxidation of TEA and its associated COD as well as COD reduction of a real wastewater. A pH of 7.6 and a $[IO_4^-]_o/[TEA]_o$ ratio of 30 were determined to be optimal conditions for rapid TEA degradation. At pH 7.6, the COD of TEA solutions was reduced by 90% in 3 hours using a Xe lamp and 90% in 30 min with a Hg(Xe) lamp. The COD reduction of the wastewater varied from 58% to 82%. Reduction pathways of periodate involve free-radical chain reactions with reactive species regeneration via UV irradiation. This system was found to degrade TEA faster than other AOP systems investigated. Degradation of wastewater samples occurred at a significant rate in the $IO_4^-/h\nu$, system, while the wastewater was relatively resistant to other AOPs. Therefore, further research into the applicability of the $IO_4^-/h\nu$ system as a new AOP is warranted.

Acknowledgments

Credits. We are appreciative of the efforts of Sayuri Desai for her contributions to preliminary experimental work. This research was funded by Eaton Corporation (Milwaukee, WI) and the Advanced Research Projects Agency, ARPA, and the Office of Naval Research, ONR, (Grant NAV 5HFMN N00149J1901) of the Department of Defense.

Authors. L. Weavers is a Ph.D. candidate and M. R. Hoffmann is the James Irvine Professor of Environmental Chemistry at the California Institute of Technology. I. Hua is an Assistant Professor of Environmental Engineering and Hydraulics at Purdue University. Correspondence should be addressed to Dr. M. R. Hoffmann, Environmental Engineering Science, W. M. Keck Laboratories, California Institute of Technology, Pasadena, CA 91125. e-mail: mrh@cco.caltech.edu.

References

Antelo, J. M., et al. (1977) Kinetic Study of the Oxidation of Ethanolamines with Chromium (VI) in Acetic Acid. *Acta. Cient. Compostelana,* **14**, 375.

Bader, H., and Hoigné, J. (1981) Determination of Ozone in Water by the Indigo Method. *Water Res.,* **15**, 449.

Barat, F., et al. (1971) Transient Species in the Pulse Radiolysis of Periodate Ion in Neutral Aqueous Solutions. *Chem. Commun.,* **17**, 847.

Buist, G. J. (1972) The Oxidation of Organic Compounds by Non-metallic Anions. In *Comprehensive Chemical Kinetics.* C. H. Bamford and Tipper, C. F. H. (Eds.), Elsevier, Amsterdam, Vol. 6, 435.

Buxton, G. V., and Sellers, R. M. (1985) Radiation-induced Redox Reactions of Iodine Species in Aqueous Solution. *J. Chem. Soc., Faraday Trans. I,* **81**, 449.

Calvert, J. G., and Pitts, J. N. (1966) Photochemistry. John Wiley and Sons, New York.

Dryhurst, G. (1970) Periodate Oxidation of Diol and Other Functional Groups. Analytical and Structural Applications. Pergamon Press, New York.

Eckenfelder, W. W. (1989) Industrial Water Pollution Control. 2nd ed. Mc Graw-Hill, New York.

Fluery, P., et al. (1949) Action de L'acide Periodique Sur Les Composés Aminés. *Bull. Soc. Chim.,* **18**, 88.

Frings, J., et al. (1994) Fermentative Degradation of Triethanolamine by a Homoacetogenic Bacterium. *Arch . Microbiol.,* **162**, 103.

Grätzel, C. K., et al. (1990) Decomposition of Organophosphorus Compounds on Photoactivated TiO_2 Surfaces. *J. Mol. Catal.,* **60**, 375.

Greenberg, A. E., and Clesceri, L. S. (Ed.) (1992) Standard Methods For the Examination of Water and Wastewater. 18th Ed. APHA, AWWA, and WEF, Baltimore.

Hagopian, R. M., et al. (1972) On the Mechanism of the Oxidation of Triethyl-, Diethanol-, Ethyldiethanol-, and Triethanol Amines by Potassium Persulfate in Aqueous Solutions. *Arm. Kim. Zh.,* **25**, 644.

Halmann, M. (1992) Photodegradation of Di-*n*-butyl-*ortho*-phthalate in Aqueous Solution. *J. Photochem. Photobiol. A: Chem.,* **66**, 215.

Head, F. S. H. and Hughes, G. (1952) The Oxidation of Simple Organic Substances by Sodium Metaperiodate in Solutions Exposed to Daylight. *J. Chem. Soc.*, 2046.

Hoffmann, M. R., et al. (1995) Environmental Applications of Semiconductor Photocatalysis. *Chem. Rev.,* **95**, 69.

Hua, I., et al. (1995) Sonolytic Hydrolysis of p-Nitrophenyl Acetate: The Role of Supercritical Water. *J. Phys. Chem.,* **99**, 2335.

Jackson, E. L. (1944) Chapter 8: Periodic Acid Oxidation. In *Organic Reactions.* R. Adams et al. (Eds.), John Wiley & Sons, New York, Vol. 2, 341-375.

Jones, L. W., and Burns, G. R. (1925) Trihydroxy-triethylamine Oxide and Substituted Hydroxylamines with Hydroxy-ethyl Radicals. *J. Am. Chem. Soc.*, **47**, 2966.

Kläning, U. K., et al. (1981) Laser Flash Photolysis and Pulse Radiolysis of Iodate and Periodate in Aqueous Solution. *J. Chem. Soc., Faraday Trans. I,* **77**, 1707.

Kläning, U. K., and Sehested, K. (1978) Photolysis of Periodate and Periodic Acid in Aqueous Solution. *J. Chem. Soc., Faraday Trans. I,* **74**, 2818.

Kroschwitz, J. L., and Howe-Grant, M. (Ed.) (1991) Encyclopedia of Chemical Technology. 4th Ed. Wiley-Interscience, New York, Vol. 2, 1-26.

Latimer, W. M. (1952) Oxidation Potentials. 2nd ed. Prentice-Hall, Englewood Cliffs.

Legrini, O., et al. (1993) Photochemical Processes for Water Treatment. *Chem. Rev.*, **93**, 671.

Malinka, E. A., and Kamalov, G. L. (1994) Influence of pH and Surface Complexes on the Rate of Hydrogen Evolution from Photocatalytic Systems Pt/TiO_2-electron Donor. *J. Photochem. Photobiol. A: Chem.*, **81**, 193.

Martin, S. T., et al. (1995) Chemical Mechanism of Inorganic Oxidants in the TiO_2/UV Process: Increased Rates of Degradation of Chlorinated Hydrocarbons. *Environ. Sci. Techol.*, **29**, 2567.

Mata-Pérez, F., and Pérez-Benito, J. (1984) Permanganate Ion Oxidation of Amines. *Z. Phys. Chem. N. Folge,* **141**, 213.

Mezyk, S. P., and Elliot, A. J. (1994) Pulse Radiolysis of Iodate in Aqueous Solution. *J. Chem. Soc. Faraday Trans.*, **90**, 831.

Pelizzetti, E., et al. (1991) Enhancement of the Rate of Photocatalytic Degradation on TiO_2 of 2-Chlorophenol, 2,7-Dichlorodibenzodioxin and Atrazine by Inorganic Oxidizing Species. *New J. Chem.*, **15**, 351.

Perrin, D. D. (Ed.) (1979) Stability Constants of Metal-Ion Complexes, Part B Organic Ligands. Pergamon Press, Elmsford, 465-466.

Price, C. C., et al. (1947) Hydrolysis and Chlorination of Three ß-Chloroethylamines. *J. Org. Chem.*, **12**, 308.

Rabek, J. F. (1982) Experimental Methods in Photochemistry and Photophysics, Part 2. Wiley-Interscience, New York.

Schwarz, H. A. (1982) Chain Decomposition of Aqueous Triethanolamine. *J. Phys. Chem.*, **86**, 3431.

Wagner, I., and Strehlow, H. (1982) Flash Photolysis in Aqueous Periodate-Solutions. *Ber. Bunsenges. Phys. Chem.*, **86**, 297.

Westall, J. (1979) MICROQL: A Chemical Equilibrium Program in BASIC. Swiss Federal Institute of Technology, EAWAG, Dubendorf, Switzerland.

White, G. C. (1992) The Handbook of Chlorination and Alternative Disinfectants. 3rd ed. Van Nostrand Reinhold, New York.

Williams, G. R., and Callely, A. G. (1982) The Biodegradation of Diethanolamine and Triethanolamine by a Yellow Gram-negative Rod. *J. Gen. Microbiol.,* **128**, 1203.

Table 6.1: Reduction potentials of selected iodine species.

Redox half-reaction	E° (volts)
$H_5IO_6 + H^+ + 2\ e^- \leftrightarrow IO_3^- + 3\ H_2O$	+1.60
$IO_3^- + 6\ H^+ + 5\ e^- \leftrightarrow \frac{1}{2} I_2 + 3\ H_2O$	+1.20
$HOI + H^+ + 2\ e^- \leftrightarrow I^- + H_2O$	+0.99
$I_2 + 2\ e^- \leftrightarrow 2\ I^-$	+0.54

Table 6.2: Oxidation of TEA by selected methods.

Experiment	$[TEA]_0$ (M)	Reaction Conditions	% degraded in 60 minutes
20 kHz probe sonication	0.005	pH 10	12
20 kHz probe sonication	0.05	pH 10	9
ozonation	0.05	constant sparge, pH 10	92
oxidation with H_2O_2	0.05	0.8 M H_2O_2, pH 9	44
20 kHz sonication with O_3	0.05	constant sparge, pH 10	93
20 kHz sonication with H_2O_2	0.05	25 mM H_2O_2, pH 9	67
oxidation with IO_4^-	0.003	0.1 M IO_4^-, pH 7.6	98
UV irradiation and IO_4^-	0.003	0.1 M IO_4^-, pH 7.6	100*

* Complete degradation of TEA occurs after 10 minutes.

Table 6.3: Wastewater characteristics and pseudo-first-order rate constants (k_{obs}) for the degradation of COD.

Sample No.	pH_o †	Conductivity (mS/cm)	TSS (mg/L)	COD (mg/L)	TEA (mM)	Fe (ppm)	Zn (ppm)	k_{obs} (min^{-1})
1	6.8	4.5	61	1400	0.88	3.5	0.3	
2	7.5	10.6	43	1300	0.43	4.4	0.8	0.0049
3	7.8	8.0	11	1120	0.04	5.0	0.3	0.0090
4	7.2	1.9	86	1250	0.03	11.7	0.2	0.0056
5	8.1	7.5	4	1300	0.46	3.2	0.7	0.0068
6 *	7.9	10.3	174	4900	0.19	36.3	3.5	0.0072

† pH_o is the pH of the wastewater upon receipt. All wastewater experiments except Figure 6.6 were conducted at pH 7.6.

* Irradiation was done after filtration and a three-fold dilution.

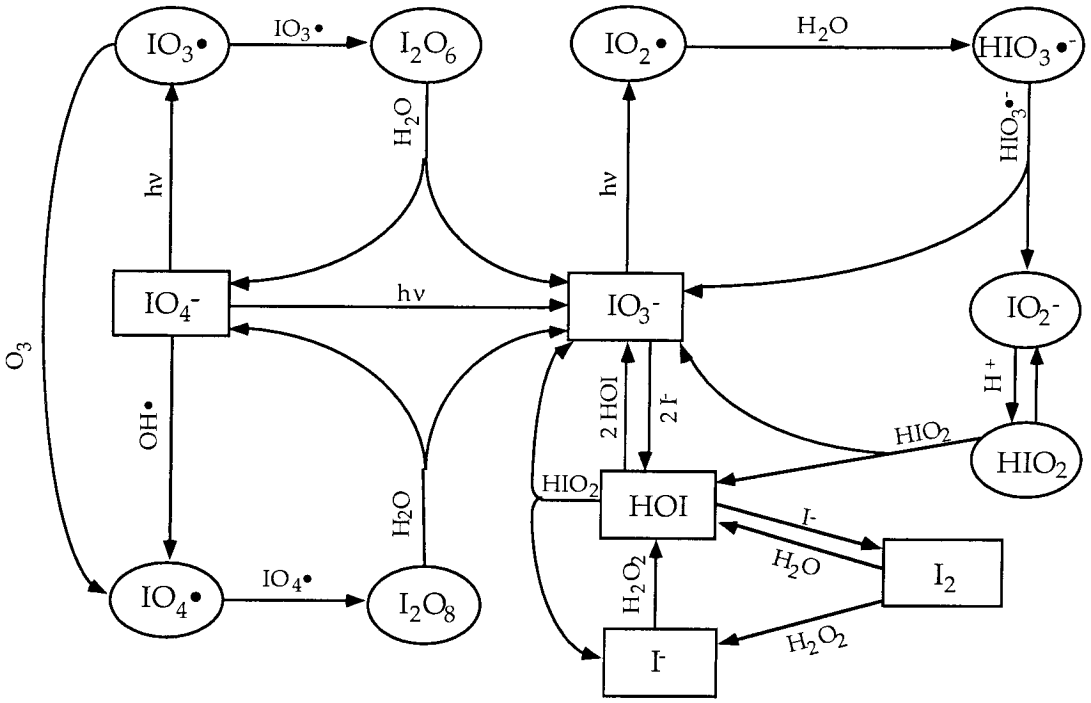

Figure 6.1: Diagram of possible reduction pathway of IO_4^- to I^- based on radiolysis and UV irradiation studies of iodine species.

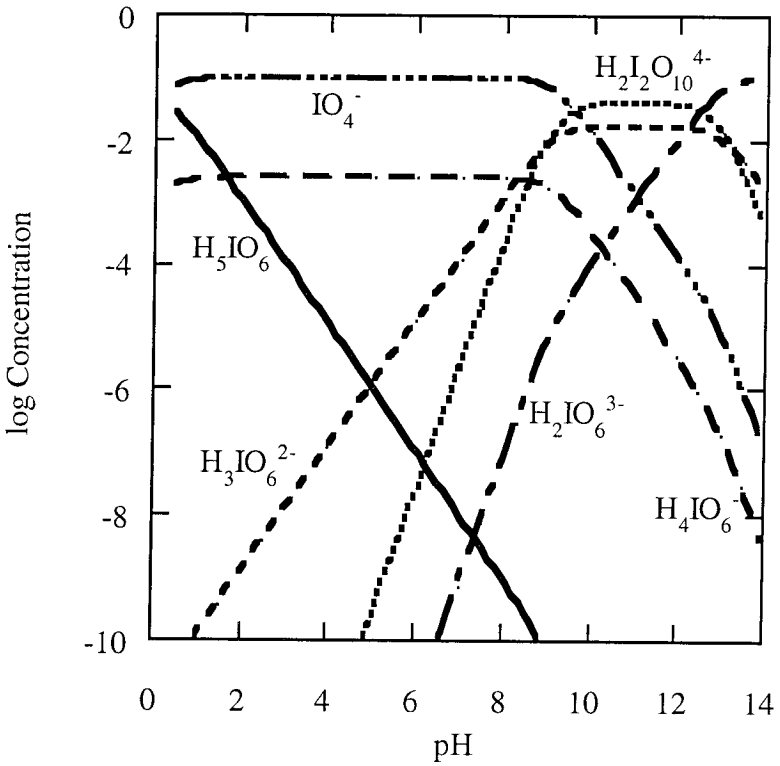

Figure 6.2: Speciation diagram of 0.1 M periodate.

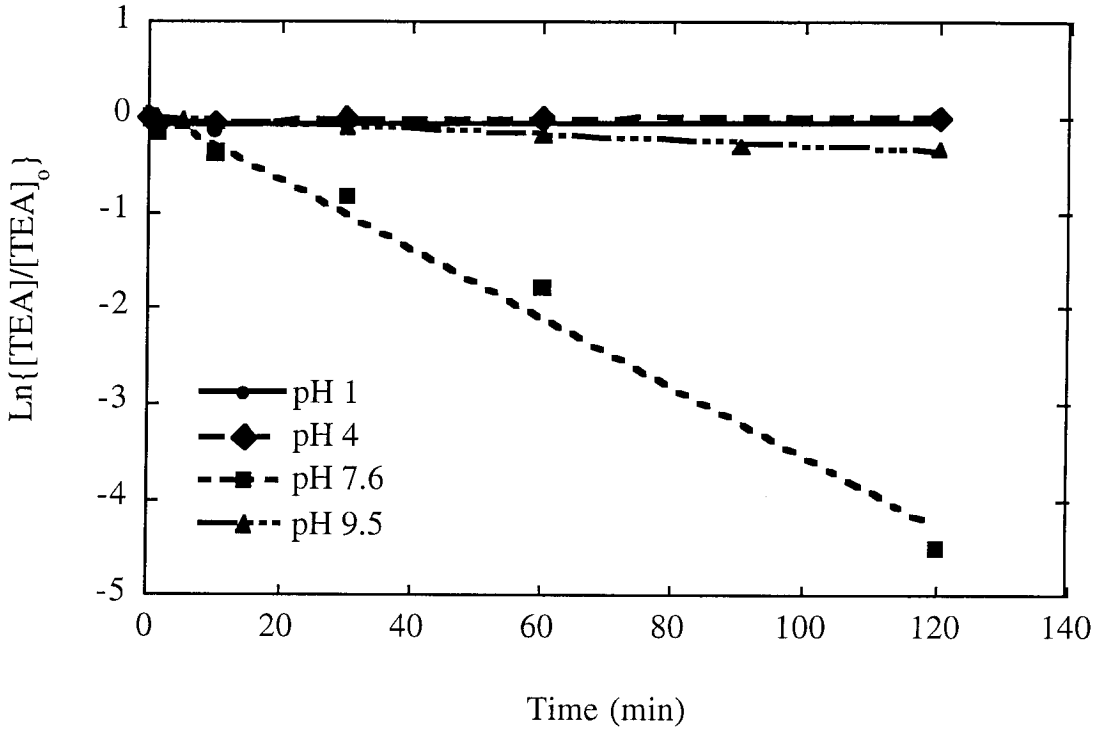

Figure 6.3: Oxidation of $[TEA]_0$ = 3.3 mM by $[IO_4^-]_0$ = 0.1 M in the absence of ultraviolet light at four pH values. The observed first-order rate constants were 0.0003, 0.0005, 0.04, and 0.003 min^{-1} at pH 1, pH 4, pH 7.6, and pH 9 respectively.

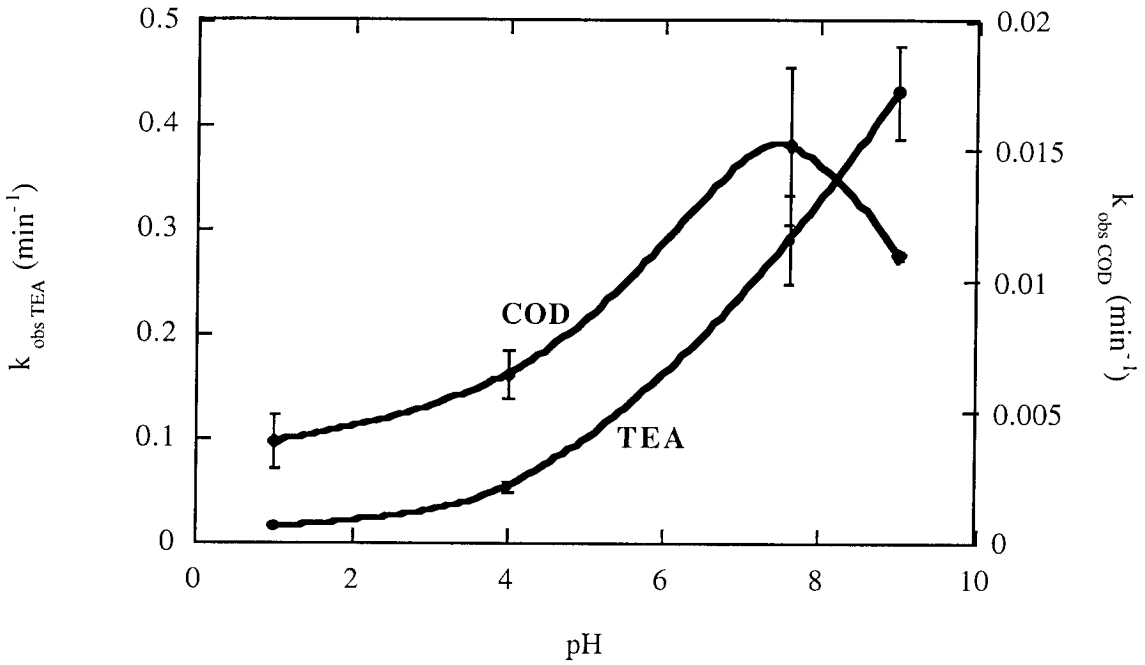

Figure 6.4: Effect of pH on the observed first-order rate constants for the degradation of $[TEA]_o$ = 3.3 mM and associated COD with UV light and $[IO_4^-]_o$ = 0.1 M. Three sets of experiments were conducted at each pH.

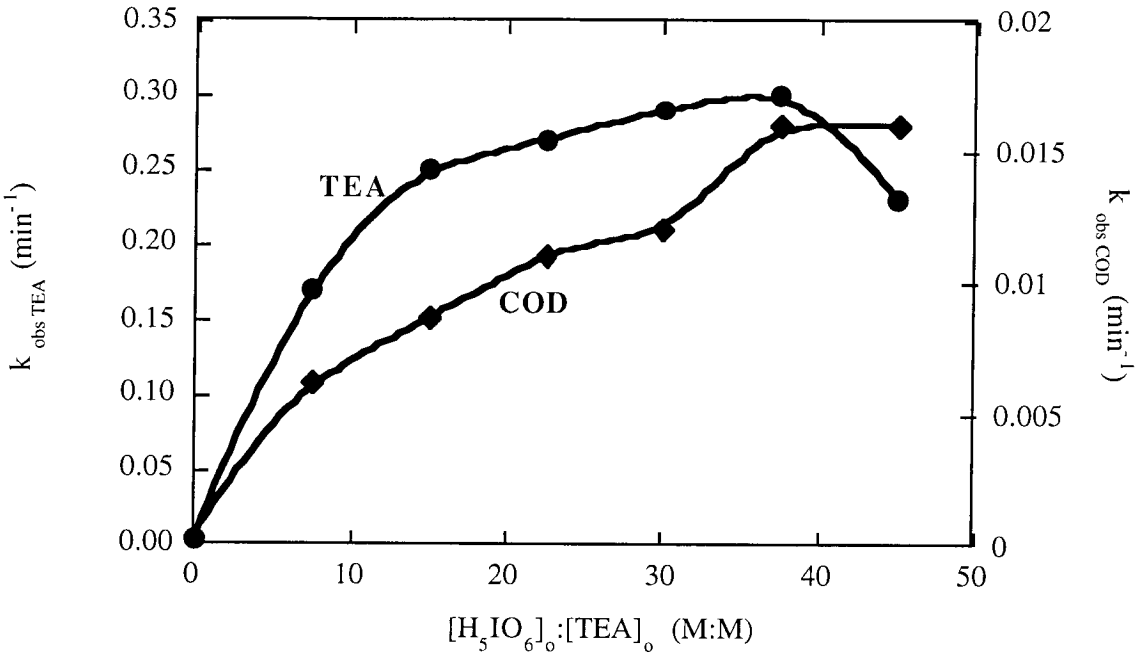

Figure 6.5: Effect of $[IO_4^-]_o$:$[TEA]_o$ on the first-order rate constants for TEA degradation ($k_{obs\ TEA}$) and associated COD ($k_{obs\ COD}$) at pH 7.6. $[TEA]_o$ = 3.3 mM and $[IO_4^-]_o$ was varied from 0 to 0.15 M.

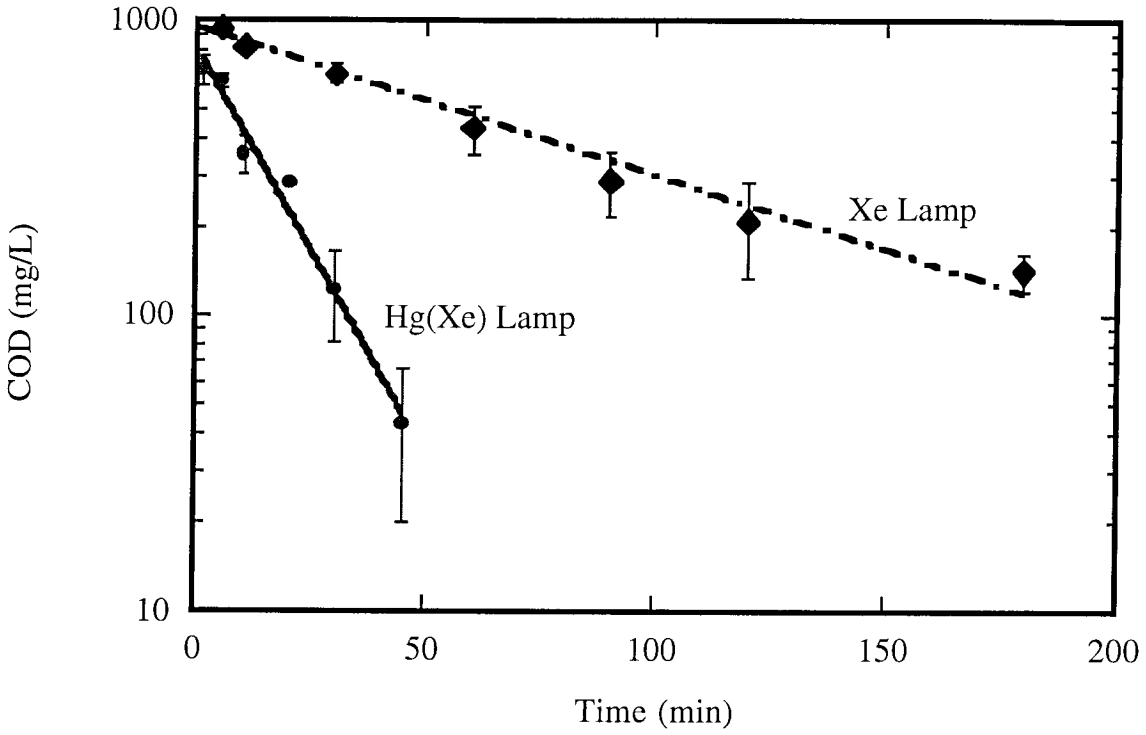

Figure 6.6: Effect of increased light intensity on the degradation of COD associated from $[TEA]_o$ = 3.3 mM with $[IO_4^-]_o$ = 0.1 M at pH 7.6. The observed first-order rate constants were k = 0.063 and 0.012 min^{-1} for Hg(Xe) and Xe lamps respectively.

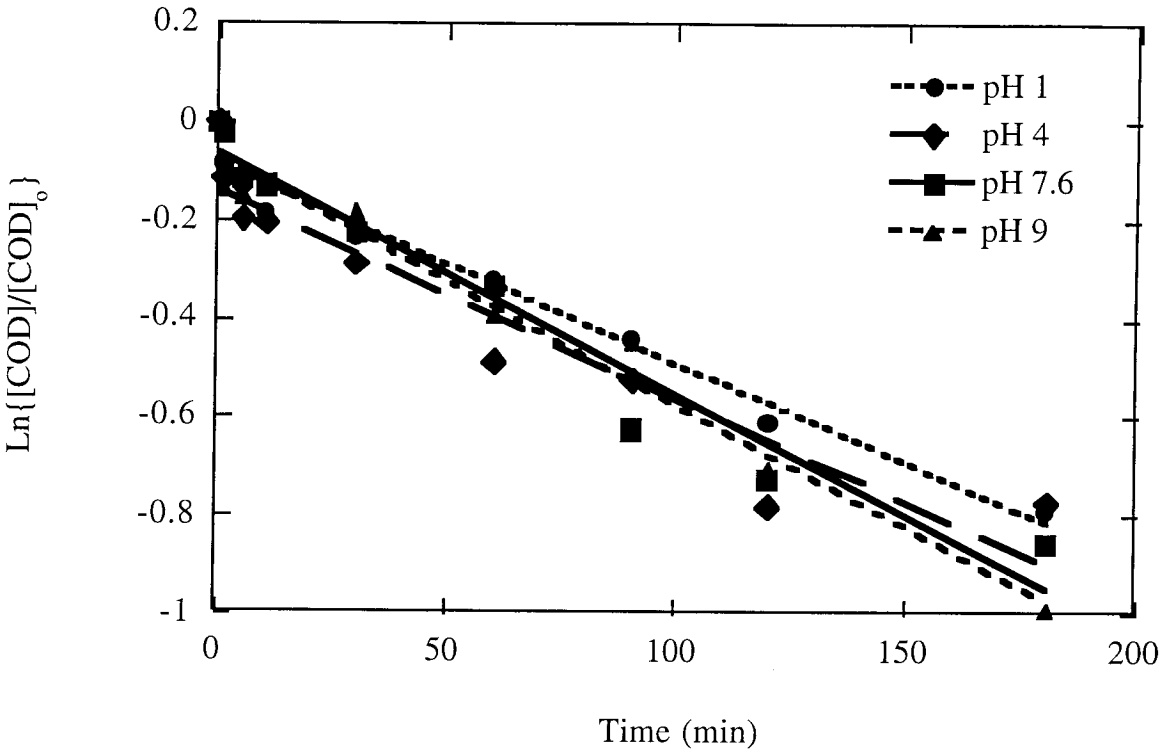

Figure 6.7: Effect of pH on $k_{obs\ COD}$ for the photoassisted degradation of the COD in wastewater sample #2 with UV irradiation and $[IO_4^-]_o = 0.1$ M. The observed first-order rate constants were 0.0040, 0.0042, 0.0049, and 0.0050 min^{-1} at pH 1, pH 4, pH 7.6, and pH 9 respectively.

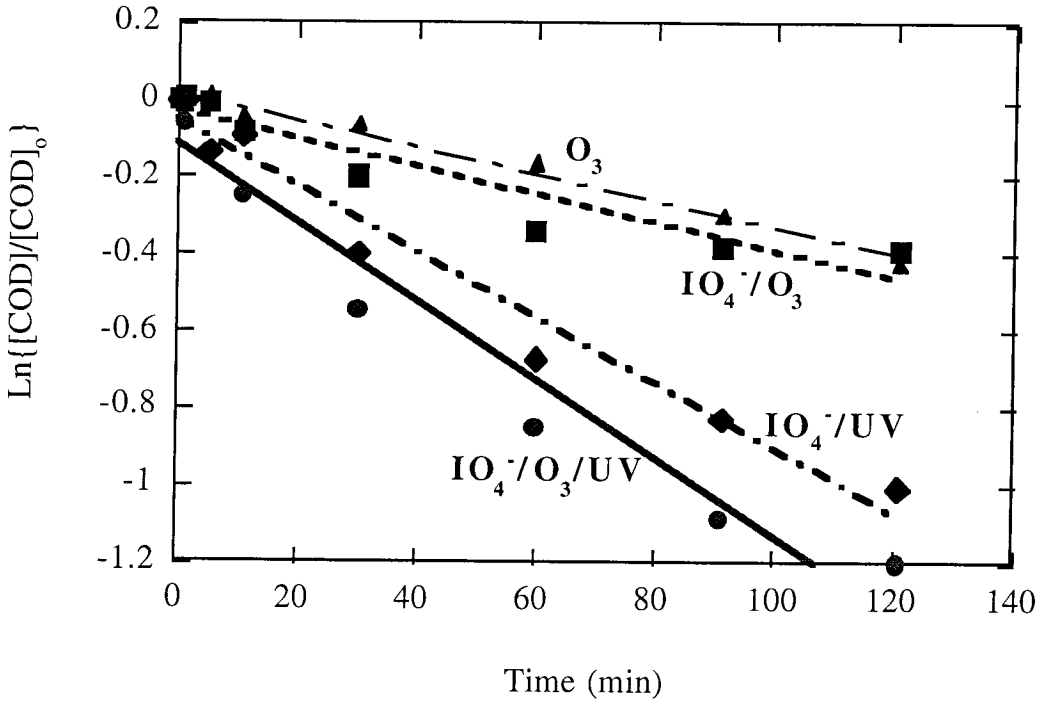

Figure 6.8: The observed first-order kinetics of degradation of wastewater sample #1 at pH 7.6 with ozone ($k_{obs\ COD}$ = 0.0034 min^{-1}); ozone with 0.1 M periodate ($k_{obs\ COD}$ = 0.0036 min^{-1}); UV light with 0.1 M periodate ($k_{obs\ COD}$ = 0.0085 min^{-1}); and UV light with 0.1 M periodate and ozone ($k_{obs\ COD}$ = 0.010 min^{-1}).

Chapter 7

Conclusions

An exploration of the chemical and physical mechanisms for enhancement of AOPs (Advanced Oxidation Processes) was performed in this thesis. In chapters 3-5 mechanisms for the enhancement of the coupling of sonolysis and ozonolysis were investigated. For example, in chapter 3, it was determined that the apparent enhancement in reactivity due to the combination of ultrasound with ozone results from thermolytic decomposition of ozone in the acoustic cavitation bubbles. The relative enhancement effects for organic compound degradation by sonolytic ozonation increased with the reported degradation rate constants with ozone and with the Henry's Law constant of the specific compounds. Retardation by sonication combined with ozone at 500 kHz was correlated with increasing degradation rate constants with ozone.

In chapter 4, the effects of ultrasound on the mass transfer of O_3 into aqueous solution were examined. It was determined that mass transfer was enhanced due to the sonolytic decomposition of ozone in the cavitation bubbles. Small mechanical effects affecting increased mass transfer were observed at 20 kHz due to acoustic streaming.

The degradation of cyclohexene by sonication, ozonation, and the combination of sonication with ozonation demonstrated that large diffusing gas bubbles containing O_3 (*e.g.*, 1000 μm) are not directly influenced by ultrasound. Ozone in a diffusing gas bubble must first diffuse into aqueous solution before entering a cavitation bubble. This indicates that gaseous ozone does not need to be added directly in the presence of ultrasound in order to achieve positive synergistic effects.

The degradation of pentachlorophenol (PCP) at pH 7 did not result in enhanced degradation by sonication combined with ozonation over the individual sonication and ozonation experiments due to the rapid reaction rate constant for the reaction of PCP with O_3. The reduction of TOC by sonolytic ozonation was more rapid at both frequencies than the linear combination of individual control experiments. Intermediate products observed during the degradation of pentachlorophenol indicated that the reaction proceeded via OH radical addition to the aromatic ring.

In this thesis a range of compounds, which reacted at varying rates O_3 was explored as shown in Figure 7.1. If a substrate is not reactive with O_3, it is much easier to observe enhancement than if a substrate reacts more rapidly with O_3. If a compound reacts with O_3 at the diffusing gas bubble interface, it is not beneficial to combine the two treatment systems. As ozone is allowed to diffuse into solution and into a cavitation bubble, the enhancement or antagonism increases. The antagonism is a trade-off with k_{O3} and k_{US}, depending on the reaction rates. At 20 kHz, as k_{O3} is increased, the synergism decreases. However, at 500 kHz, the antagonism first increases with k_{O3}, then peaks at a moderate reaction rate constant with O_3, and then subsequently decreases. It is expected that as k_{O3} is decreased further, the apparent enhancement at both frequencies will continue to increase. At 500 kHz the enhancement should become positive. Depending on the physicochemical parameters for the compounds such as the Henry's Law constants (H), the octanol water partitioning coefficients (K_{OW}), and the second-order reaction rate constants with OH radical (k_{OH}) these trends could be altered. As shown in Figure 7.2 and 7.3, the effects of H (Pa m^3 mol^{-1}) and K_{OW} (M/M) on the degradation rate of a compound by sonication are illustrated. As both H and K_{OW} increase, the observed degradation rate constant tends to increase.

The IO_4^-/UV system was demonstrated to be effective for the oxidation of triethanolamine (TEA) and its associated COD, as well as COD reduction in an industrial wastewater. A pH of 7.6 and a $[IO_4^-]_o/[TEA]_o$ ratio of 30 were determined to be optimal conditions for rapid TEA degradation. At pH 7.6, the COD of TEA solutions was reduced by 90% in 3 hours using a Xe lamp and 90% in 30 min with a Hg(Xe) lamp. Reduction pathways of periodate involve free-radical chain reactions with reactive species regeneration via UV irradiation. This system was found to degrade TEA faster than other AOP systems investigated. Degradation of wastewater samples occurred at a significant rate in the IO_4^- /hν, system, while the wastewater was relatively resistant to other AOPs. Therefore, further research into the applicability of the IO_4^-/hν system as a new AOP is warranted.

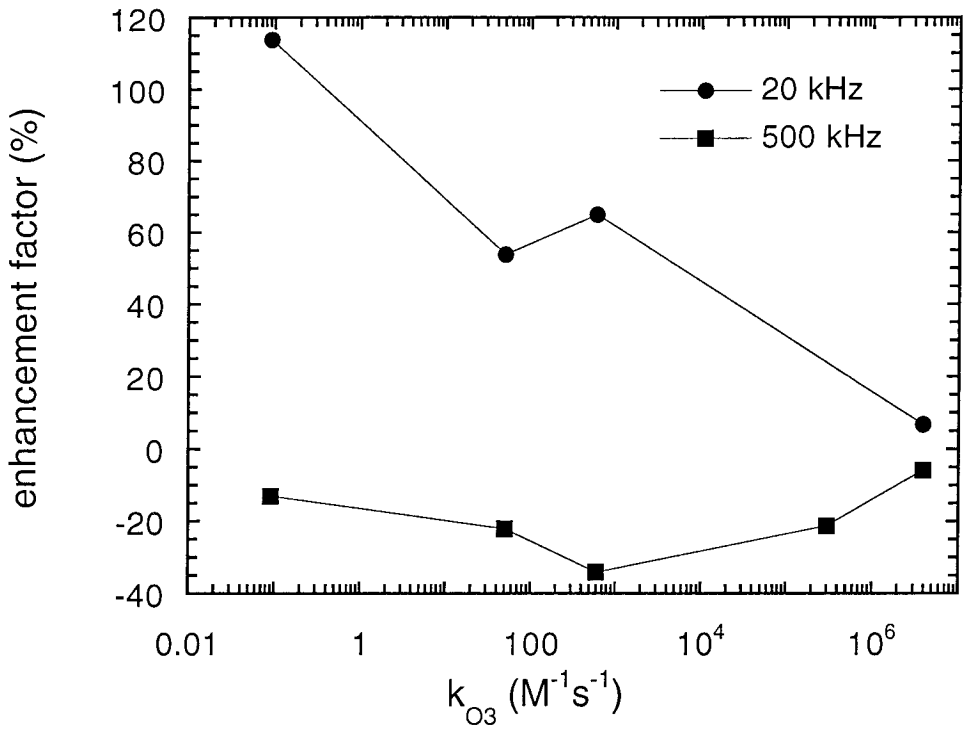

Figure 7.1 Enhancement of combination of sonication with ozonation vs the reported second-order reaction rate constant of the compound with O_3.

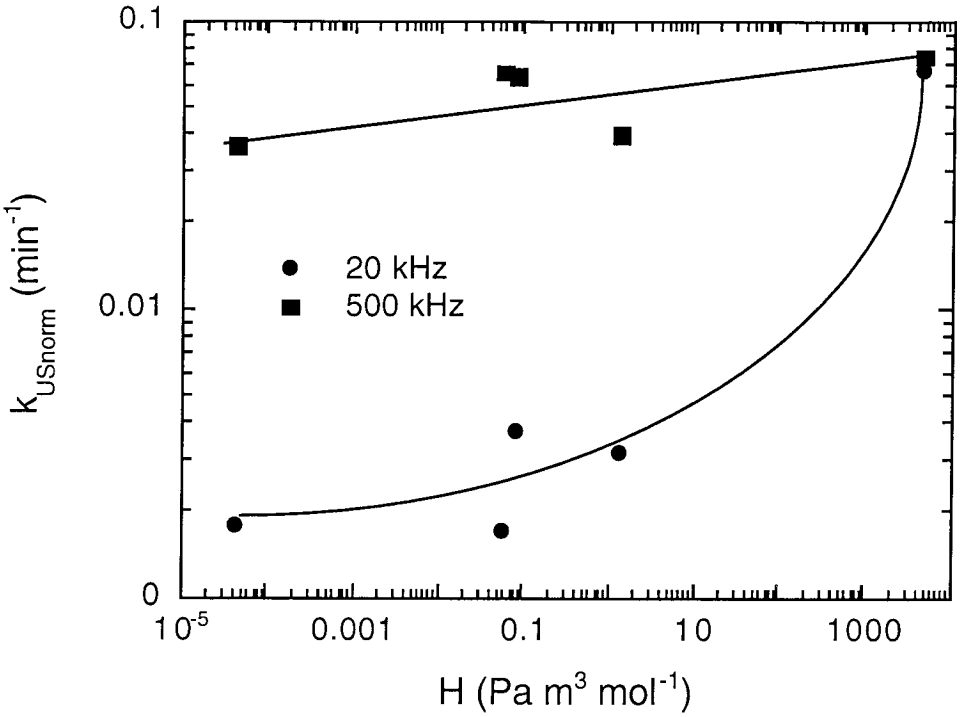

Figure 7.2 Normalized degradation rate constant for sonication vs the Henry's Law constant of the compound at both 20 and 500 kHz ultrasonic frequency.

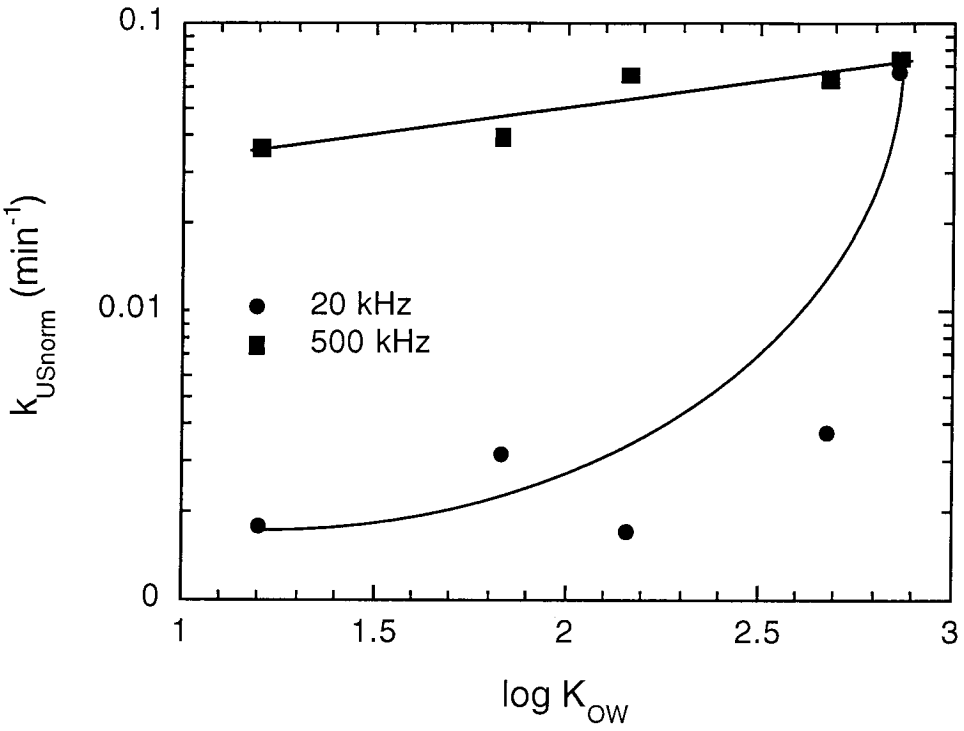

Figure 7.3 The normalized degradation rate constant for sonication at both 20 and 500 kHz ultrasonic frequency vs the octanol water partitioning coefficient.

Appendix A

Model of a Single Collapsing Sonochemical Bubble

NOMENCLATURE

A	preexponential factor in Arrhenius equation
A_s	surface area of the bubble
$\bar{c}$	mean speed of the molecule
[C]	concentration of species C in the bubble
C_{V_i}	molecular specific heat of species i,
E_a	activation energy
f	linear frequency of ultrasound
H	chemical component in the bubble, hydrogen atom
H_2	chemical component in the bubble, hydrogen
H_2O	chemical component in the bubble, water
HO_2	chemical component in the bubble, hydroperoxyl radical
H_2O_2	chemical component in the bubble, hydrogen peroxide
ΔH_{form_i}	heat of formation of species i
k	Arrhenius reaction rate constant
k_B	Boltzman constant
KE	kinetic energy of the collapsing bubble
n	total number of molecules in the bubble
n_i	number of molecules of species i
n_{i0}	number of molecules of species i initially
O, $O(^3P)$	chemical component in the bubble, atomic oxygen
O_2	chemical component in the bubble, oxygen
O_3	chemical component in the bubble, ozone
OH	chemical component in the bubble, hyroxyl radical
p_0	hydrostatic pressure exerted on the bubble
P_A	acoustic pressure amplitude

P_m	external pressure on the bubble (assumed constant)
PE	potential energy of the collapsing bubble
Q	energy consumed by gas-phase chemical reactions
R	radius of the bubble
R_0	initial radius of bubble before expansion cycle
R_{max}	maximum radius obtained at the end of the expansion cycle
$\Re$	universal gas constant
SE	surface energy of the bubble
T	temperature in the bubble
T_0	initial bubble temperature
UE	internal energy of gas in the bubble
V	volume of gas in the bubble
α	mass accommodation coefficient
ß	rate coefficient function for non-Arrhenius behavior
σ	surface tension of water
ν_C	escape rate of species from gaseous bubble
ρ	density of the liquid
ω	circular frequency of ultrasound
χ_i	mole fraction of species i

INTRODUCTION

As shown in Chapters 3, 4, and 5 sonochemistry leads to the rapid destruction of a variety of organic compounds. At 20 kHz, the addition of ozone to ultrasound leads to more rapid destruction of the parent substrate when the compound reacts rather slowly with ozone. In the case that the substrate reacts quickly with ozone, the linear combination of separate experiments is approximately equal to the combined sonolytic ozonation rate constant. At 500 kHz, antagonism is observed with compounds that react more slowly with ozone.

Previous models have been developed to investigate the causes and conditions for sonochemistry and sonoluminescence. A liquid-phase kinetic model assuming a constant flux of OH radical into solution was created to understand the sonochemical oxidation of H_2S (1). Two studies to explain gas-phase sonochemistry have been conducted. Both of these studies assumed thermodynamic equilibrium at the end of collapse. Prasad Naidu et al. (2) investigated a 20 kHz collapse and imposed the end of the bubble collapse to occur when the speed of the wall of the bubble equals that of sound in the liquid due to the formation of shock waves. They also used a polytropic approximation to determine the temperature rise upon collapse. Sochard et al. (3) modeled the collapse of bubbles at 20 and 500 kHz. They accounted for mass transfer and varying temperatures in the bubble in order to model the bubble past a Mach number of 1, and determined that 20 kHz ultrasound should yield more radicals than 500 kHz but offered no explanation for the conflicting experimental evidence.

Recently, two chemical models have been developed to gain insight into mechanisms of sonoluminescence. Kamath and Prosperetti (4) used a kinetic model to determine free-radical formation during low excitation amplitude collapse. Another model was developed to estimate the temperature at collapse based on the formation and recombination of atomized species (5). However, they did not account for the energy

consumed by chemical reactions. To date sonochemical models have failed to include the chemistry associated with the solvent vapor or the effect of chemical reactions on cavitational bubble collapse.

The objective of this chapter is to determine if the bubble collapses at 20 and 500 kHz in the presence of O_3 are different resulting in synergism in one case and antagonism in the other. It is also interesting to recall that the loss of TOC is accelerated in all cases. The pathway of destruction of a substrate to CO_2 will most likely include compounds which do not react with O_3. Therefore, the enhanced loss of TOC indicates that substrates which do not react with O_3 will be accelerated in any case. By investigating, the formation of oxidizing species from the bubble collapse, we will gain insight into the mechanism of synergism or antagonism. This could help in determining optimum reaction conditions for adding O_3 to ultrasound.

DESCRIPTION OF THE MODEL

A full model sonochemical action would deal with cavitational cloud collapse, asymmetric collapse, and bubble-bubble interactions. However, in this study a single bubble was modeled. Although many differences exist between the behavior of a single bubble and bubble clouds, the analysis of a single bubble will provide the basis of bubble cloud characteristics. In order to determine the collapse of the bubble, its energy balance was assumed to be given by:

$$\Delta KE + \Delta UE + Q = \Delta PE + \Delta SE \qquad (1)$$

where KE is the kinetic energy of the collapsing bubble, UE is the internal energy of gas in the bubble, Q is the energy consumed by gas-phase chemical reactions, PE is the potential energy of the collapsing bubble, and SE is the surface energy of the bubble. Expressing

the energy equation in terms of the bubble radius, R, and assuming the gas in the bubble is ideal, it becomes:

$$2\pi\rho R^3\left(\frac{dR}{dt}\right)^2 + (T-T_0)\sum_i n_i C_{V_i} + \sum_i \Delta H_{form_i}(n_i - n_{i0}) = \frac{4}{3}\pi P_m(R_{max}^3-R^3) + 4\pi\sigma(R_{max}^2-R^2) \qquad (2)$$

where ρ is the density of the liquid, T is the temperature in the bubble, T_0 is the initial bubble temperature, n_i is the number of molecules of species i, n_{i0} is the number of molecules of species i initially, C_{V_i} is the molecular specific heat of species i, ΔH_{form_i} is the heat of formation of species i, P_m external pressure on the bubble (assumed constant), R_{max} is the maximum radius obtained at the end of the expansion cycle, and σ is the surface tension of water.

The bubble temperature was assumed to be uniform and was determined by equating the thermal energy of the gas and energy consumed by reactions to the work done compressing the bubble:

$$(T-T_0)\sum_i n_i C_{V_i} + \sum_i \Delta H_{form_i}(n_i - n_{i0}) = \int_0^t \frac{3}{R} nk_B T \frac{dR}{dt'}\,dt' \qquad (3)$$

where k_B is the Boltzman constant and n is the total number of molecules in the bubble. Therefore, the polytropic approximation is no longer needed nor is it applicable. Changing amounts of gas species are followed during collapse rather than assuming a polytropic constant throughout collapse.

Bubbles were assumed to grow during the expansion cycle isothermally (6), and reach R_{max} which assumes a vaporous collapse and is dependent on the density of the

liquid, the applied frequency ($\omega = 2\pi f$), and the hydrostatic (p_0) and acoustic (P_A) pressure but is independent of the initial radius (7):

$$R_{max} = \frac{4}{3\omega}(P_A - p_0)\left(\frac{2}{\rho P_A}\right)^{1/2}\left(1 + \frac{2}{3p_0}(P_A - p_0)\right)^{1/3} \qquad (4)$$

During the compression cycle, heat transfer to the liquid was neglected, however, loss of vapor from the bubble was allowed using a mass accommodation coefficient of 0.001 (7). Also, to determine the effect of mass transfer of a species, mass transfer was performed on selected runs assuming free radicals have a strong affinity for water. The escape rate was determined by calculating the number of molecules striking the surface of the bubble per unit time per unit volume (8):

$$\nu_C = \frac{1}{4}\alpha[C]\bar{c}\frac{A_s}{V} \qquad (5)$$

where α is the mass accommodation coefficient, [C] is the concentration of species C in the bubble, $\bar{c}$ is the mean speed of the molecule, A_s is the surface area of the bubble, and V is the volume of gas in the bubble.

A series of 40 equations of the species O_3, O_2, H_2O, OH, O, H, H_2, HO_2, and H_2O_2 were considered as shown in Table A.1 (9-15). Organic species were omitted from the reaction mechanism since even a simple compound such as CH_3OH along with all of the intermediates produced would complicate the mechanism considerably. However, in most cases organic contaminants will be present in small concentrations compared to other species. Rate constants as a function of temperature were determined from Arrhenius parameters as follows:

$$k = A\,T^{\beta}\exp\left(-\frac{E_a}{\Re T}\right) \qquad (6)$$

where E_a is the activation energy, and $\Re$ is the universal gas constant. Table A.1 lists reduced activation energies ($E_a/\Re$) in units of Kelvin. Rate equations and Arrhenius parameters were taken from the latest NIST compliation of combustion studies and were validated over a range from 300 to at least 2500 K.

A chemical kinetics program using a Gear method to solve the system of differential equations was implemented (16). Differential equations for R, chemical species, and mass transfer were solved numerically.

RESULTS

Figures A.1 and A.2 show the collapse of a bubble when chemical reactions are included and also when reactions are neglected. Figure A.1 displays a "soft" collapse at f = 20 kHz, P_A = 2 atm, and an initial radius of R_0 = 41 μm before the expansion cycle. If reactions are neglected, the bubble collapses quicker, and the bubble wall continuously accelerates during bubble implosion. However, when reactions are included, the bubble wall accelerates until the internal energy change of the gas balances the compression work in the imploding bubble and the bubble slows and is eventually stopped due to chemical reactions. A collapse at 500 kHz with initial radius of 1.5 μm and P_A = 2 atm resulted in a similar "soft" collapse.

On the other hand, Figure A.2 demonstrates the condition where a bubble is not influenced greatly by the chemical reactions. The bubble still requires longer to collapse, but the bubble wall continues to accelerate as it collapses. In this case the bubble is influenced by an acoustic pressure amplitude of 11 atm with the same initial radius as in Figure A.1. This bubble collapse would be considered to be inertially controlled, and therefore, a transient collapse.

The addition of 1% O_3 to the O_2 bubble with chemical reactions is shown in Figure A.3. Although the shape of the bubble collapse is identical in both cases, the temperature of the bubble with O_3 is slightly lower due to the additional chemical reactions occurring with O_3.

Figure A.4 shows the major chemical species produced from the collapse of the bubble in Figure A.1. OH is produced in the largest quantity followed by O, HO_2, H and H_2. Radical species are produced only in the last 30 ns when the temperature increases rapidly. The collapse of this bubble with 1% O_3 is shown in Figure A.5. Since O_3 has a lower activation energy as shown in Table A.1, it pyrolizes at a lower temperature, and hence earlier in the collapse than H_2O vapor or O_2. O from O_3 decomposition forms and decays before the end of the collapse and before significant OH is formed. OH formation is increased slightly in the presence of O_3.

Starting with the same initial bubble radius, $R_0 = 41$ μm but with a higher pressure amplitude, $P_A = 11$ atm, the bubble collapses more violently and results in a different ratio of species. Figure A.6 shows that H_2 is the major product in this bubble. The collapse time is much longer than with a smaller pressure amplitude but the chemical reactions occur only in the last 10 ns. With the addition of O_3, it appears that OH and H_2 formation is less than without O_3 as shown in Figure A.7. Also, in this bubble, H_2O is more than an order of magnitude larger than O_2, whereas at $P_A = 2$ atm, O_2 was larger than H_2O. O_2 is produced in the final stages of collapse rather than consumed and 27% of the water is consumed.

In Figure A.8, the collapse of a larger bubble at $P_A = 11$ atm, results in similar species to Figure A.4. The time scale of formation of the species is longer than in Figure A.6, ≈50 ns. Upon the addition of O_3 (Figure A.9), significant improvement in the amount of OH is observed, $n_{OH} = 5 \times 10^{14}$ without O_3 to $n_{OH} = 1.5 \times 10^{15}$ with O_3. Approximately 50% of the H_2O is consumed and about 20% of the O_2.

At 500 kHz the bubble collapse is very rapid. The generation of radicals occurs in less than 1 ns as seen in Figure A.10. Again OH is formed in the largest amount followed by O. In Figure A.11, OH production is slightly improved upon addition of O_3, and the pyrolysis of O_3 occurs closer to the end of the collapse. The n_O peak occurs 3 ns from the end of collapse compared to 500 ns from the end at 20 kHz with $P_A = 11$ atm.

As mentioned above, previous gas-phase sonochemical models used equilibrium calculations to determine chemical species upon collapse. Table A.2 tabulates the chemical species produced by kinetic analysis as opposed to assuming thermodynamic equilibrium. Under all conditions examined, equilibrium was not attained. Since bubble collapse is likely to occur asymmetrically for violent collapses at 20 kHz, equilibrium calculations were also performed at Mach 1 of the liquid. Although shock waves will form even earlier than Mach 1 for a bubbly mixture, Mach 1 will give an indication of the equilibrium conditions before the end of the collapse and was also used as the stopping point in Prasad Naidu et al. (2) calculations. At Mach 1, the bubble appears to be even farther from equilibrium than at the end of the collapse. This is plausible since at the end of collapse the bubble decelerates and the temperature levels off allowing it to approach equilibrium.

A range of initial bubble radii were investigated to determine the effect of the ratio R_{max}/R_0 on the formation of the major oxidizing species, OH and O. Figure A.12 shows that an R_{max}/R_0 ratio of 5 to 8 is optimal for the production of oxidizing radicals. Below $R_{max}/R_0 = 5$, the percentage of OH and O in the bubble rapidly decreases and at $R_{max}/R_0 = 2$, $\chi_{OH} + \chi_O$ reaches zero. At high R_{max}/R_0, the percent of OH and O asymptotically levels off to $\approx$10 %.

The addition of varying amounts O_3 to the bubble was examined at both 20 and 500 kHz as shown in Figures A.13, and A.14. At 20 kHz, the $\chi_{OH} + \chi_O$ peaks grow, decay, and then grow again dramatically at the end of the collapse. A larger fraction of O_3 results in a larger $\chi_{OH} + \chi_O$ at the end of the collapse, however, a smaller χ_{O_3} does not have as dramatic a decay in $\chi_{OH} + \chi_O$ as a larger χ_{O_3}. At 500 kHz the oxidizing species increase

due to O_3 pyrolysis and continue to increase as water vapor is pyrolized due to the shorter time scale of collapse.

Tables A.3 and A.4 show $\chi_{OH} + \chi_O$ at the end of bubble collapse for a variety of bubble sizes and χ_{O_3}. $R_0 = 41$ μm stimulated by 20 kHz and $P_A = 2$ atm results in an increase of oxidizing species whereas at $P_A = 11$ atm the oxidizing species are decreased. At the higher pressure amplitude, Mach 1 is broken so it may not be practical to reach this condition at $P_A = 11$ atm. At Mach 1 nearly an order of magnitude enhancement is observed in oxidizing species production. At $R_{max}/R_0 = 2.3$ the largest enhancement in $\chi_{OH} + \chi_O$ production is observed at both pressure amplitudes and both frequencies. The addition of O_3 to the bubble results in a 1.3 fold increase at 20 kHz and $P_A = 2$ atm, a 3.7 fold increase at 20 kHz and $P_A = 11$ atm, and a 2880 fold increase at 500 kHz and $P_A = 2$ atm. At R_{max}/R_0 above 3.4 the addition of O_3 appears to be detrimental to the production of oxidizing species.

The effect of mass transfer of species other than gases was also investigated. As shown in Table A.4, it does not have an affect on the formation of oxidizing species at 500 kHz. However, at 20 kHz, since the collapse time is much longer, effects of mass transfer are seen. Contrary to intuition, the fraction of oxidizing species is reduced with mass transfer both with and without O_3. However, the percentage increase of $\chi_{OH} + \chi_O$ from $\chi_{O_3} = 0.0$ to $\chi_{O_3} = 0.01$ is 1.9% with mass transfer compared to 0.7% without mass transfer. Therefore, it appears that the longer time scales for collapse at 20 kHz allow free radicals from O_3 pyrolysis to escape to the liquid.

DISCUSSION

Flynn examined the energy dissipation and maximum temperature of the collapse as a function of R_{max}/R_0 (17). In the region $2\ R_0 \leq R_{max} \leq 3\ R_0$ a transition was observed which has been considered to be the transition from stable to transient (inertial) cavitation.

For $R_{max}/R_0 \geq 2$ to 3, the bubble undergoes explosive growth and violent collapse. The collapse occurs in such a manner as to concentrate the kinetic energy of implosion significantly. Below R_{max}/R_0 of 2 the energy dissipation dominates the collapse. The lower threshold transient cavitation is dependent on P_A and bound by the Blake threshold (7):

$$P_B = p_0 + \frac{8\sigma}{9}\sqrt{\frac{3\sigma}{2R_B^2(p_0 + \frac{2\sigma}{R_B}}} \qquad (7)$$

where P_B is the acoustic pressure required to generate transient cavitation of the bubble R_B. However, the reason the bubble does not cavitate is a result of the growth phase rather than the collapse. From equation 7 we see that at very small bubble sizes, surface tension inhibits growth. Due to the nature of our model we could not observe the effects of reaching the Blake threshold. However, the Blake radius will be approximately 0.3 μm at 20 and 500 kHz with $P_A = 2$ and at 20 kHz and $P_A = 11$ the Blake radius will be 0.05 μm. R_{max} is a function of the frequency, resulting in a larger expansion at a lower frequency. Therefore, the size range of bubbles available for growth is much smaller at 500 kHz than at 20 kHz, although the number density and size distribution of bubbles in the presence of ultrasound is not well understood but expected to be biased to the smaller sizes.

Previous investigations of bubble dynamics observed the "best" bubbles to be those which had the largest expansion ratio due to the violent nature of the collapse, and hence the higher temperatures observed (7,18). In this study, although higher temperatures were observed with the largest R_{max}/R_0 ratio, these were not the "best" bubbles in producing OH and O radicals. Without O_3, the optimal bubble size ranged from 6 to 8, however, at this size range the effect of O_3 was detrimental to the additional formation of oxidizing species at $R_{max}/R_0 = 6$ to 8. The maximum increase in oxidizing species occurred with a smaller expansion ratio.

The cavitation growth cycle was assumed to be relatively slow allowing the H_2O vapor pressure to remain equilibrated with liquid H_2O. Therefore, changing R_{max}/R_0 also resulted in different ratios of H_2O to gas. The bubble $R_0 = 41$ μm in Figures A.4 to A.7 show dramatically different ratios of H_2O to O_2 and O_3. In Figure A.5, the concentration of gas is slightly larger than H_2O, however, in Figure A.7 n_{O_2} is 50 fold smaller than n_{H_2O}. It is apparent that 1% O_3 in O_2 gas will have negligible impact with a large R_{max}/R_0.

The initiation of O_3 decomposition with temperature results in atomic oxygen and O_2 gas formation as follows:

$$O_3 \xrightarrow{M} O(^3P) + O_2 \qquad (8)$$

Since this initiation occurs at a lower temperature than H_2O and O_2 decomposition, radical concentrations before the very end of collapse are the result of O_3 pyrolysis only and the major reactions with $O(^3P)$ are:

$$O(^3P) + H_2O \longrightarrow 2\ OH \qquad (9)$$

$$O_3 + O(^3P) \longrightarrow 2\ O_2 \qquad (10)$$

To have the largest benefit from O_3 addition, reaction 9 should be maximized. It is also important to maximize this pathway if O_3 reacts with the substrate directly in the liquid-phase, since cavitation bubbles could reduce that pathway which would result in observed antagonism in the combined system. The percent excess O_2 in Tables A.3 and A.4 show the percent O_2 formed in excess of reaction 8:

$$\%\ \text{excess}\ O_2 = \frac{n_{O_2\ max} - n_{O_2 i}}{n_{O_3 i}} - 0.5 \qquad (11)$$

A larger percent means that reaction 10 is dominant over reaction 9. It appears that larger R_{max}/R_0 results in less O_2 formation although $\chi_{OH} + \chi_O$ is smaller with O_3 than without O_3 present. Also, at 500 kHz the % excess O_2 is approximately 50% in all cases. As χ_{O_3} is increased from 0.01 to 0.06, the % excess O_2 also increases. At larger R_{max}/R_0 the fraction of H_2O overwhelms the gas concentration, increasing the reaction rate of equation 9, but also minimizing the effect of O_3 at the end of collapse. Similarly, as the concentration of O_3 is increased in the bubble, the reaction rate of equation 10 is increased. Bubbles which are not optimal without O_2 appear to show more enhancement with O_3 than the optimal bubbles. In some cases this is clearly due to very little OH and O produced with O_2 alone, however, in other bubbles, O_3 must be altering the temperature in the bubble and chemical reactions so that production is increased or decreased more than if O_3 were efficiently producing OH and O.

In Chapters 3, 4, and 5 more enhancement was observed at 20 kHz than at 500 kHz. This was most obvious in Chapter 3 with the degradation of nitrobenzene, 4-nitrophenol, and 4-chlorophenol. At 20 kHz, the P_A applied was approximately 11 atm while $P_A = 2$ atm was used for the degradation of pentachlorophenol. In the absence of O_3, 20 kHz required considerably more energy to degrade the same amount of substrate although n_{OH} produced in a bubble was approximately 10^{12} and 10^{14} molecules at $P_A = 2$ and 11 atm, respectively, whereas $n_{OH} \approx 10^8$ molecules at 500 kHz. There are 25 compression and rarefaction cycles at 500 kHz for every cycle at 20 kHz so the 500 kHz bubble could produce $n_{OH} \approx 10^9$ molecules per 20 kHz bubble. Also, $P_A = 11$ atm was less effective than $P_A = 2$ atm at 20 kHz. This requires at least one of the following to occur: more active cavitation bubbles are formed at a lower pressure amplitude and higher frequency since smaller bubbles are needed to reach the optimal R_{max}/R_0, or since the collapse is more violent at $P_A = 11$ atm resulting in a higher Mach number of the bubble wall, it collapses asymmetrically before it attains such high mole fractions of OH than the

single bubble model produced. Also, this would account for the significant increase in substrate destruction upon the addition of O_3 seen in Chapter 3. As shown for the bubble $R_0 = 41$ μm excited at $P_A = 11$ atm, no enhancement is seen if the bubble is collapsed to the theoretical end. However, at Mach 1 an order of magnitude increase in $\chi_{OH} + \chi_O$ is observed. It is also possible that bubbles growing by rectified diffusion may compress enough in the compression phase of the ultrasonic wave to increase the bubble temperature so that O_3 is decomposed. At 20 kHz, a larger fraction of bubbles is growing by rectified diffusion per unit time than at 500 kHz due to the larger resonant radius at 20 kHz.

Although this model is for a single bubble, whereas in an ultrasonic reactor a bubble cloud exists, the model reveals that at high amplitude the bubble collapses much harder and most likely does not maintain its spherical shape. At low amplitude a spherical collapse is possible and could be the reason for the observed accelerated rates in degradation reactions at 500 kHz over 20 kHz with O_2. However, the addition of shock waves to the model and modeling a bubble through many cycles would give more insight into the transfer of chemical species out of the bubble. Heat transfer is another variable that could control the temperature of many collapses. More research is also needed on the bubble size distribution in an ultrasonic reactor. The size of the bubble plays a key role in the mole fractions of species produced and the effectiveness of O_3 in the bubble.

CONCLUSIONS

Modeling a single bubble showed that chemical reactions slow down the end of the collapse due to the energy required to form radical species. However, the influence of chemical reactions on the bubble dynamics was only significant at small R_{max}/R_0. In the absence of O_3, the optimal bubble in producing oxidizing species was between R_{max}/R_0 of 6 to 8 which is lower than Flynn's optimal bubble. Upon the addition of O_3, the maximum enhancement in oxidizing species was found at R_{max}/R_0 of 2 to 3. However, the smallest

amount of excess O_2 was found at the highest R_{max}/R_0 due to the larger fraction of H_2O in the bubble. It is plausible that at 20 kHz and P_A = 11 atm the bubble collapses asymmetrically before the theoretical end of the collapse. This would result in a considerable increase in the oxidizing species with O_3 present in the bubble since the rapid formation of free radicals would not have occurred and is the reason for the larger enhancement due to O_3 observed at 20 kHz and high amplitude as opposed to 500 kHz.

It should be noted that this model does not include physical components of the gas such as thermal conductivity and heat losses of the bubble by radiation. The concept of the contents of the bubble forming a super critical liquid resulting in the loss of an interface are also neglected. However, some insight is gained into the possiblity of chemistry affecting bubble collapse were observed.

ACKNOWLEDGMENT

Professor A. J. Colussi contributed enormously to the model development. Conversations with Prof. Brennen, Fabrizio D'Auria, Alistar Preston, and Douglas Varela gave insight into understanding the bubble dynamics. Financial support provided by Defense Advanced Research Projects Agency (DARPA), Office of Naval Research (ONR), and Electrical Power Research Institute (EPRI) is gratefully acknowledged.

REFERENCES

1. Kontronarou, A.; Hoffmann, M. R. In *Advances in Chemistry Series* vol. 244; American Chemical Society: 1995; pp 233-251.

2. Prasad Naidu, D. V.; Rajan, R.; Kumar, R.; Gandhi, K. S.; Arakeri, V. H.; Chandrasekaran, S., *Chem. Eng. Sci.,* **1994**, *49*, 877-888.

3. Sochard, S.; Wilhelm, A. M.; Delmas, H., *Ultrasonics Sonochemistry,* **1997**, *4*, 77-84.

4. Kamath, V.; Prosperetti, A.; Egofopoulos, F. N., *J. Acoust. Soc. Am.,* **1993**, *94*, 248-260.

5. Bernstein, L. S.; Zakin, M. R.; Flint, E. B.; Suslick, K. S., *J. Phys. Chem.,* **1996**, *100*, 6612-6619.

6. Leighton, T. G., *Ultrasonics Sonochemistry,* **1995**, *2*, S123-S136.

7. Leighton, T. G. *The Acoustic Bubble*; Academic Press: London, 1994.

8. Seinfeld, J. H. *Atmospheric Chemistry and Physics of Air Pollution*; Wiley-Interscience: New York, 1986.

9. Heimer, J. M.; Coffee, T. P., *Combust. Flame,* **1979**, *35*, 117.

10. Hippler, H.; Rahn, R.; Troe, J., *J. Phys. Chem.,* **1990**, *93*, 6560.

10. Hippler, H.; Rahn, R.; Troe, J., *J. Phys. Chem.*, **1990**, *93*, 6560.

11. Atkinson, R.; Baulch, D. L.; Cox, R. A.; R. F. Hampson, J.; Kerr, J. A.; Troe, J., *J. Phys. Chem. Ref. Data,* **1989**, *18*, 881.

12. Masten, D. A.; Hanson, R. K.; Bowman, C. T., *J. Phys. Chem.*, **1990**, *94*, 7119.

13. Baldwin, R. F.; Walker, R. W., *J. Chem. Soc. Faraday Trans. 1,* **1979**, *75*, 140.

14. Tsang, W.; Hampson, R. F., *J. Phys. Chem. Ref. Data,* **1986**, *15*, 1087.

15. Warnatz, J. In *Combustion Chemistry*; W. C. Gardiner, Ed.; Springer-Verlag: New York, 1984; pp 197-360.

16. Curtis, A. R.; Sweetenham, W. P. FASCIMILE, United Kingdom Atomic Energy Authority Harwell: Oxfordshire, 1987.

17. Flynn, H. G., *J. Acoust. Soc. Am.*, **1975**, *58*, 1160-1170.

18. Roy, R. A. In *NATO Advanced Study Institute on Sonochemistry and Sonoluminescence*; Leavenworth, WA, 1997.

Table A.1: Chemical equations and Arrhenius parameters.

Reaction	A ‡ (cm^3 /molec/s)	β	E_a (K)	Ref.
$O_3 + M \rightarrow O_2 + O + M$	7.15e-10		11172	9
$O_3 + O \rightarrow O_2 + O_2$	8.0e-12		2060	11
$O_3 + H \rightarrow OH + O_2$	1.4e-10		480	11
$O_3 + OH \rightarrow HO_2 + O_2$	1.9e-12		1000	11
$O_3 + HO_2 \rightarrow OH + O_2 + O_2$	1.4e-14		600	11
$O_2 + M \rightarrow O + O + M$	3.01e-6	-1	59429	14
$O_2 + O + M \rightarrow O_3 + M$	4.0e-32	-1		10
$O_2 + H + M \rightarrow HO_2 + M$	1.77e-29	-1		14
$O_2 + H \rightarrow OH + O$	5.85e-8	-0.7	8589	12
$O_2 + OH \rightarrow O + HO_2$	3.7e-11		26500	14
$O_2 + H_2 \rightarrow H + HO_2$	2.4e-10		28500	14
$O_2 + H_2O_2 \rightarrow HO_2 + HO_2$	9.0e-11		20000	14
$H_2O + M \rightarrow H + OH + M$	5.8e-9		52900	14
$H_2O + O \rightarrow OH + OH$	7.60e-15	1.30	8605	14
$H_2O + H \rightarrow OH + H_2$	1.03e-16	1.9	9265	14
$OH + M \rightarrow O + H + M$	4.0e-9		50000	14
$OH + OH + M \rightarrow H_2O_2 + M$	1.6e-23	-3		14
$OH + OH \rightarrow O + H_2O$	3.5e-16	1.4	-200	14
$OH + O \rightarrow O_2 + H$	7.49e-10	-0.5	30	14
$OH + H + M \rightarrow H_2O + M$	6.11e-26	-2		14
$OH + H \rightarrow O + H_2$	8.1e-21	2.8	1950	14
$OH + HO_2 \rightarrow H_2O + O_2$	2.4e-8	-1		14
$OH + H_2O_2 \rightarrow H_2O + HO_2$	2.9e-12		160	14
$OH + H_2 \rightarrow H_2O + H$	1.06e-17	2	1490	14
$O + O + M \rightarrow O_2 + M$	5.21e-35		-900	14
$O + H + M \rightarrow OH + M$	1.3e-29	-1		14
$O + HO_2 \rightarrow OH + O_2$	2.9e-11		-200	14
$O + H_2O_2 \rightarrow OH + HO_2$	1.6e-17	2	2000	14
$O + H_2 \rightarrow OH + H$	2.49e-17	2	3801	15
$H + H + M \rightarrow H_2 + M$	1.5e-29	-1.3		14
$H + HO_2 \rightarrow OH + OH$	2.8e-10		440	14
$H + HO_2 \rightarrow H_2 + O_2$	1.1e-10		1070	14
$H + HO_2 \rightarrow H_2O + O$	9.12e-11		914	13
$H + H_2O_2 \rightarrow H_2O + OH$	4.11e-11		2000	14
$H + H_2O_2 \rightarrow HO_2 + H_2$	8e-11		4000	14
$HO_2 + M \rightarrow H + O_2 + M$	2e-5	-1.18	24363	14
$HO_2 + HO_2 \rightarrow H_2O_2 + O_2$	3e-12			14
$HO_2 + H_2 \rightarrow H + H_2O_2$	5e-11		13100	14
$H_2O_2 + M \rightarrow OH + OH + M$	2.14e9	-4.86	26795	14
$H_2 + M \rightarrow H + H + M$	7.59e-5	-1.4	52530	14

‡ Termolecular reactions have units (cm^6/$molec^2$/s).

Table A.2: Kinetic vs. equilibrium analysis at the end of a collapsing bubble or at Mach = 1 where indicated.

Run	n_{OH} x 10^{-11}	n_O x 10^{-11}	n_H x 10^{-11}	n_{H_2} x 10^{-11}	n_{HO_2} x 10^{-11}	$n_{H_2O_2}$ x 10^{-11}
20 kHz P_a=2 atm R_0=41 μm T=4091 K						
Kinetic	10.9	1.97	0.180	0.539	1.09	0.187
Equilib	15.1	4.01	0.606	1.33	1.93	0.324
20 kHz P_a=11 atm R_0=164 μm T=6934 K Mach=10.4						
Kinetic	4530	565	495	2200	2140	1120
Equilib	3760	434	579	2990	2850	855
20 kHz P_a=11 atm R_0=164 μm T=2662 K Mach =1.0						
Kinetic	17.7	0.0667	0.126	5.51	1.72	0.0127
Equilib	237	7.06	0.645	14.3	9.02	2.34
500 kHz P_a=2 atm R_0=1.5 μm T=4068 K						
Kinetic	6.00×10^{-4}	9.45×10^{-5}	1.03×10^{-5}	3.77×10^{-5}	5.43×10^{-5}	5.07×10^{-6}
Equilib	8.35×10^{-4}	1.88×10^{-4}	1.53×10^{-5}	3.98×10^{-5}	8.13×10^{-5}	9.49×10^{-6}

Table A.3: Comparison of O_3 addition to oxidizing mole fraction at 20 kHz

R_0 (μm)	P_A (atm)	R_{max}/R_0	χ_{O_3}	$\chi_{OH}+\chi_O$*	% excess O_2
41	2	3.1	0.0	9.48	-
41	2	3.1	0.01	9.55	73.19
41	2	3.1	0.02	9.72	83.02
41	2	3.1	0.04	9.98	89.81
41	2	3.1	0.06	10.32	92.40
41‡	2	3.1	0.0	9.31	-
41‡	2	3.1	0.01	9.49	73.04
55	2	2.3	0.0	1.198	-
55	2	2.3	0.01	1.54	84.78
5	2	25.3	0.0	9.92 (1.74)	-
5	2	25.3	0.01	4.33 (1.74)	49.70
0.7	2	181	0.0	9.789 (1.69)	-
0.7	2	181	0.01	4.06 (1.69)	50.06
390	11	2.3	0.0	7.36	-
390	11	2.3	0.01	27.02 (13.9)	92.83
41	11	21.9	0.0	10.77 (0.0008)	-
41	11	21.9	0.01	10.6 (0.007)	51.97
41‡	11	21.9	0.0		-
41‡	11	21.9	0.01		50.70

*values in parenthesis are mole fractions at Mach = 1.

‡ including mass transfer of oxidants to liquid

Table A.4: Comparison of O_3 addition to oxidizing mole fraction at 500 kHz

R_0 (μm)	P_A (atm)	R_{max}/R_0	χ_{O_3}	$\chi_{OH}+\chi_O$*	% excess O_2
1.5	2	3.4	0.0	6.43	-
1.5	2	3.4	0.01	6.84	50.80
1.5	2	3.4	0.02	7.09	52.38
1.5	2	3.4	0.04	7.15	57.27
1.5	2	3.4	0.06	7.94	62.36
1.5‡	2	3.4	0.0	6.43	-
1.5‡	2	3.4	0.01	6.83	50.80
2.2	2	2.3	0.0	0.0004	-
2.2	2	2.3	0.01	1.15	53.10
0.7	2	7.24	0.0	18.2 (7.76)	-
0.7	2	7.24	0.01	18.27 (7.75)	50.06

*values in parenthesis are mole fractions at Mach = 1.

‡ including mass transfer of oxidants to liquid

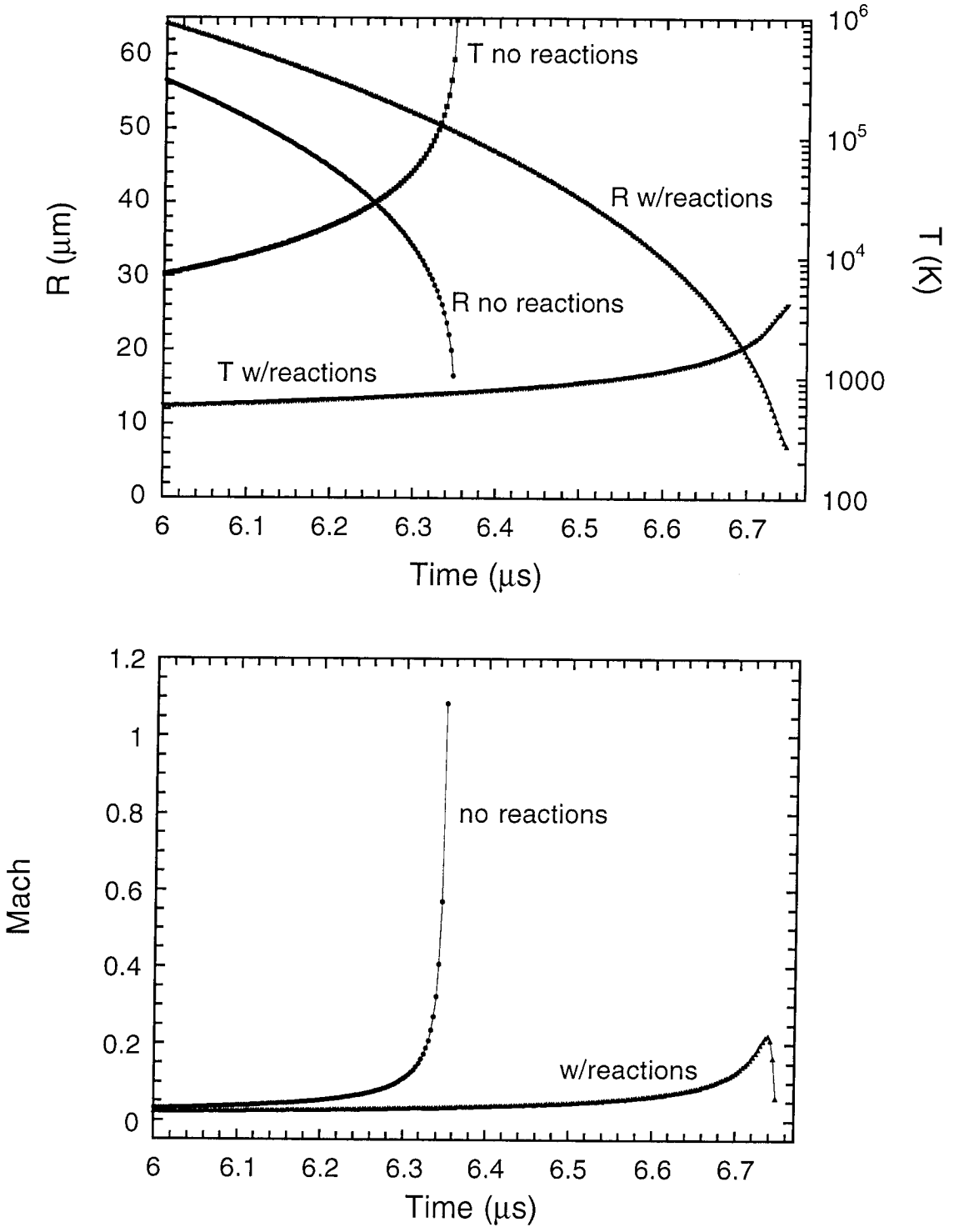

Figure A.1: (a) The collapse of an oxygen containing bubble and temperature produced initially at R_0=41 μm with and without considering chemical reactions at 20 kHz and P_A=2 atm. (b) The Mach number of the imploding bubble wall.

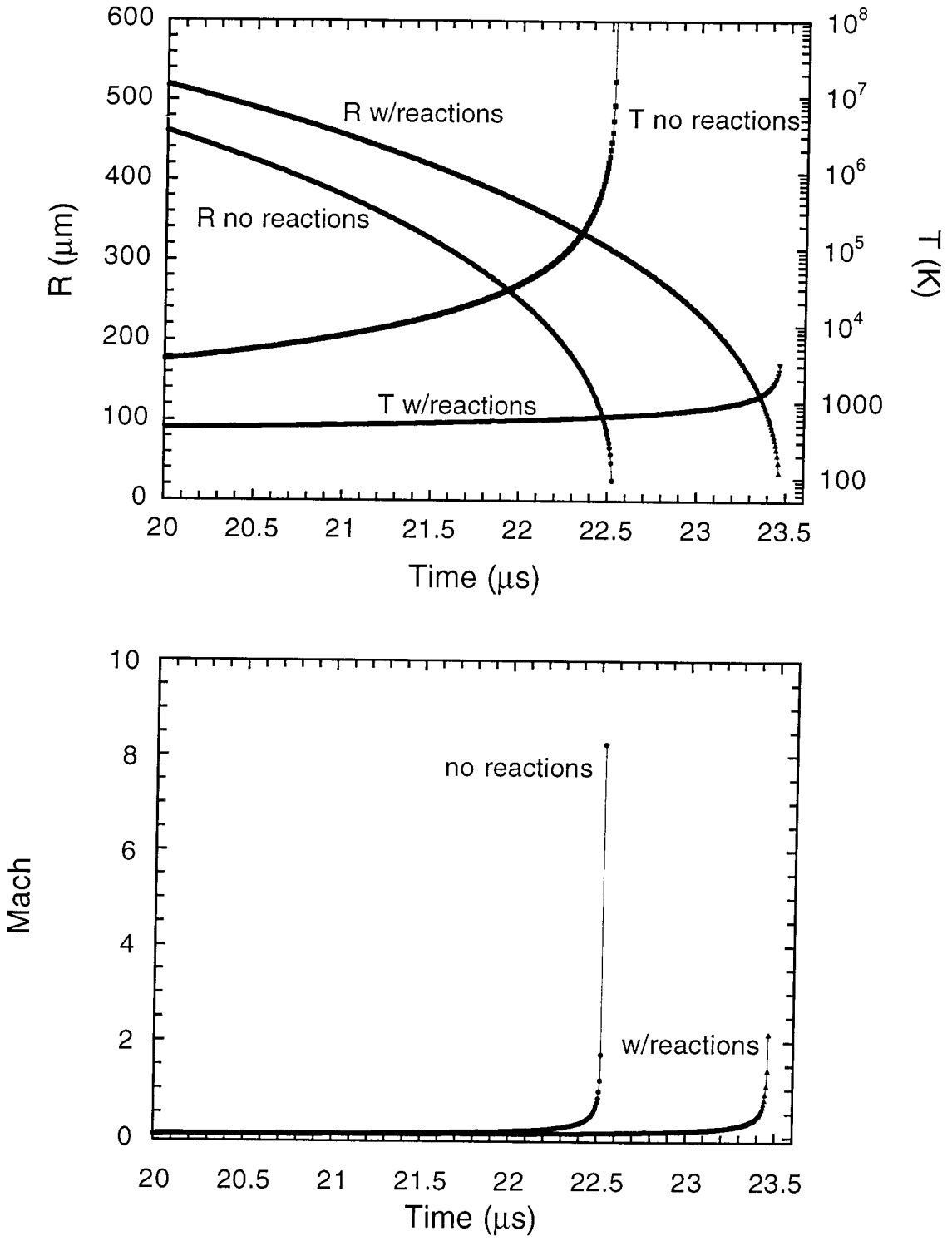

Figure A.2: (a) The collapse of an oxygen containing bubble and temperature produced initially at R_0=41 μm with and without considering chemical reactions at 20 kHz and P_A=11 atm. (b) The Mach number of the imploding bubble wall.

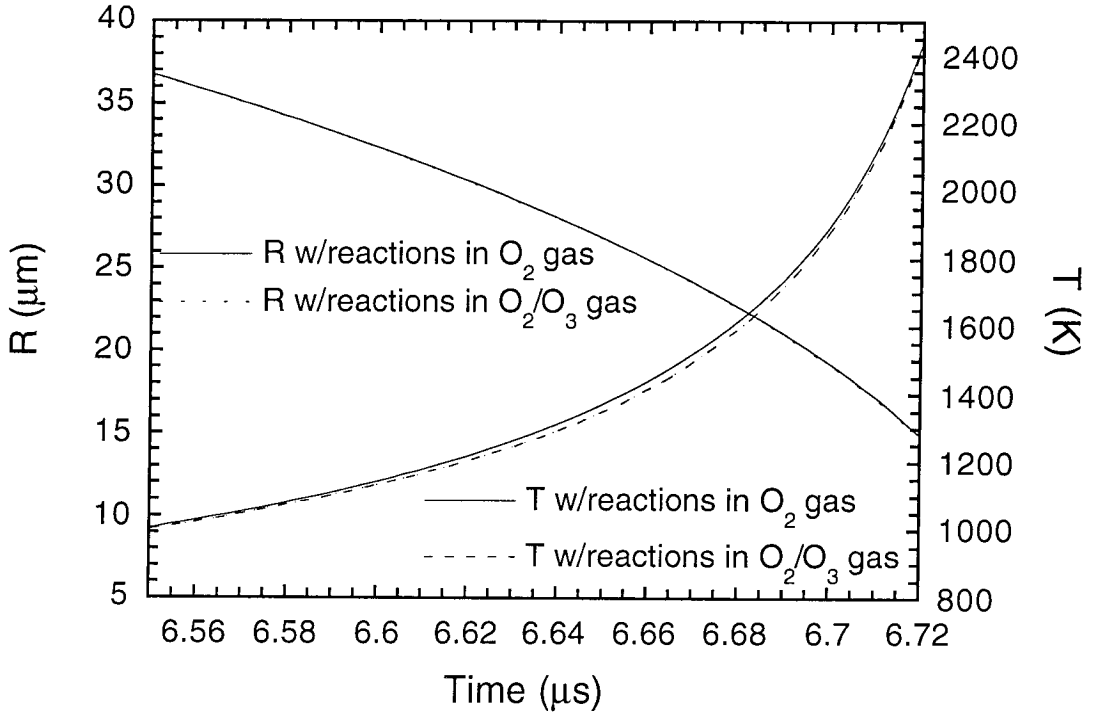

Figure A.3: The collapse of an oxygen and oxygen/ozone bubble and temperature produced initially at R_0=41 μm influenced at 20 kHz and P_A=2 atm and considering chemical reactions.

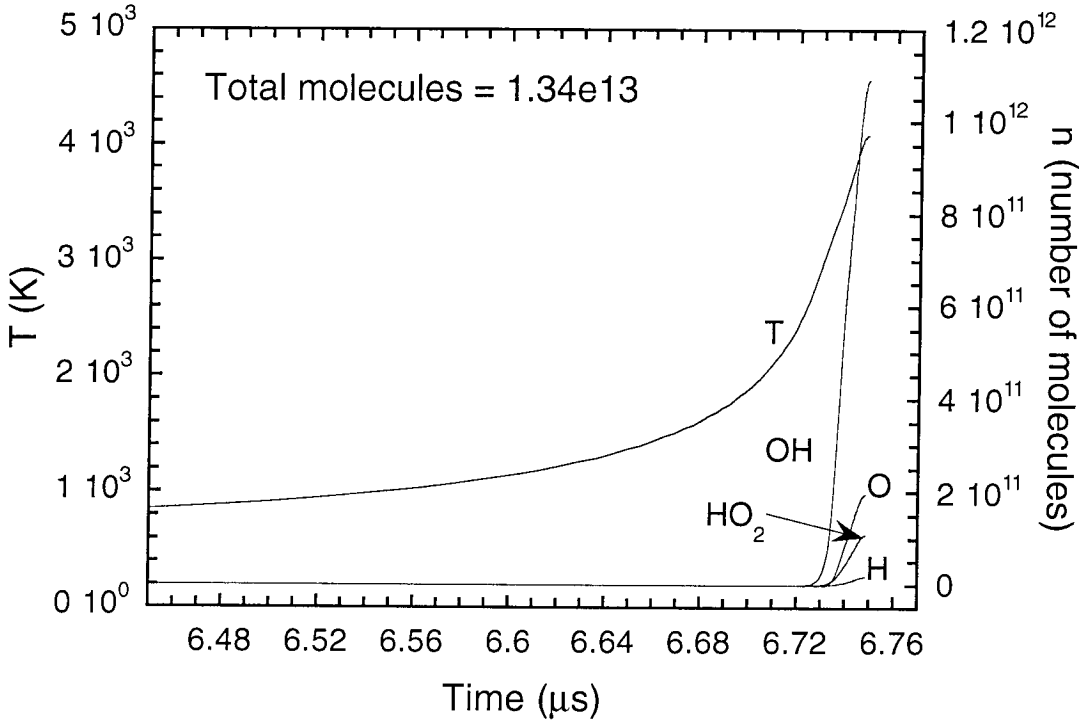

Figure A.4: The temperature and chemical species produced from the collapse of an oxygen bubble initially at R_0=41 μm, influenced by P_A=2 atm and 20 kHz.

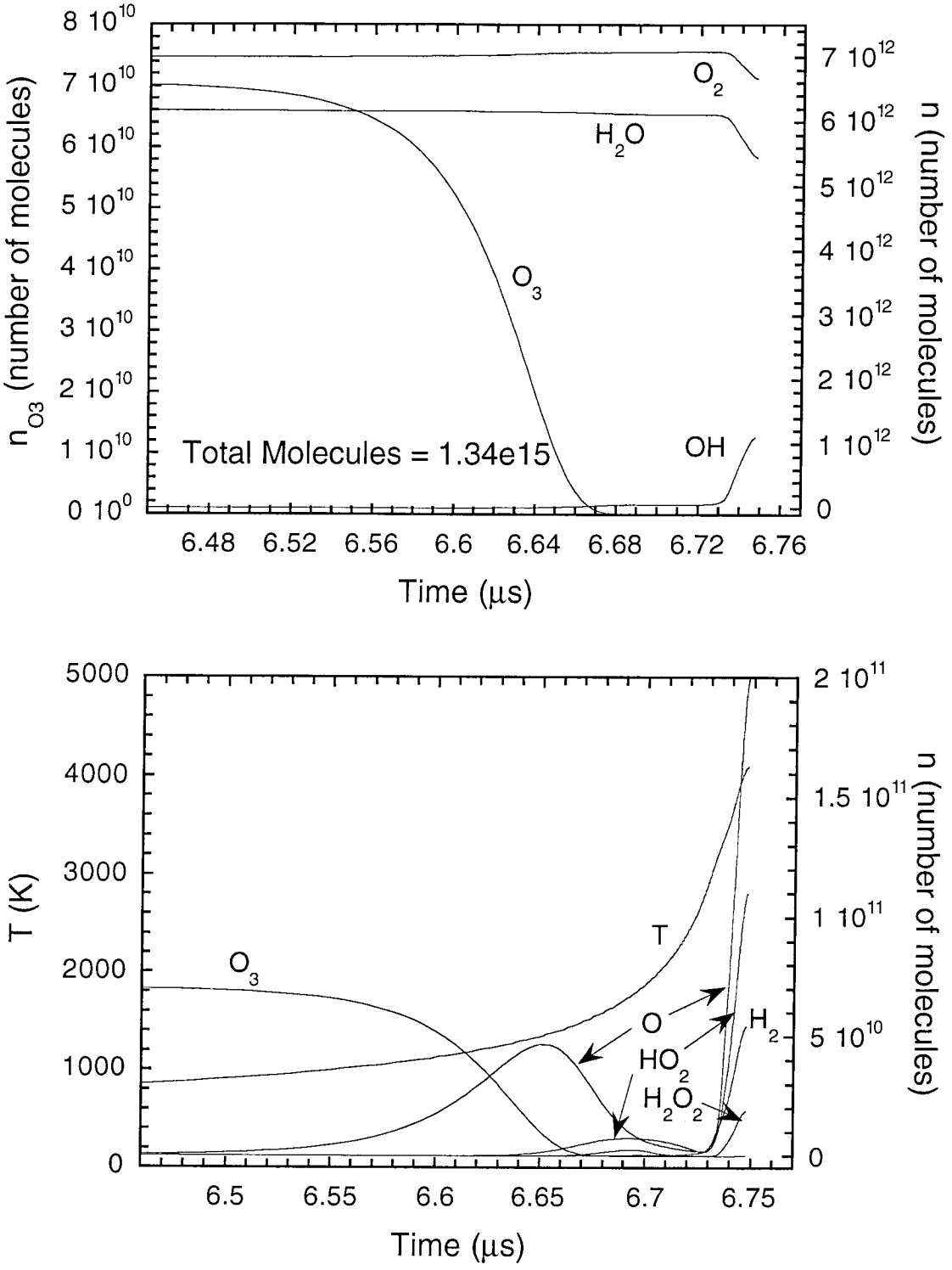

Figure A.5: The temperature and chemical species produced from the collapse of an oxygen bubble with 1% O_3, initially at R_0=41 μm, influenced by P_A=2 atm and 20 kHz.

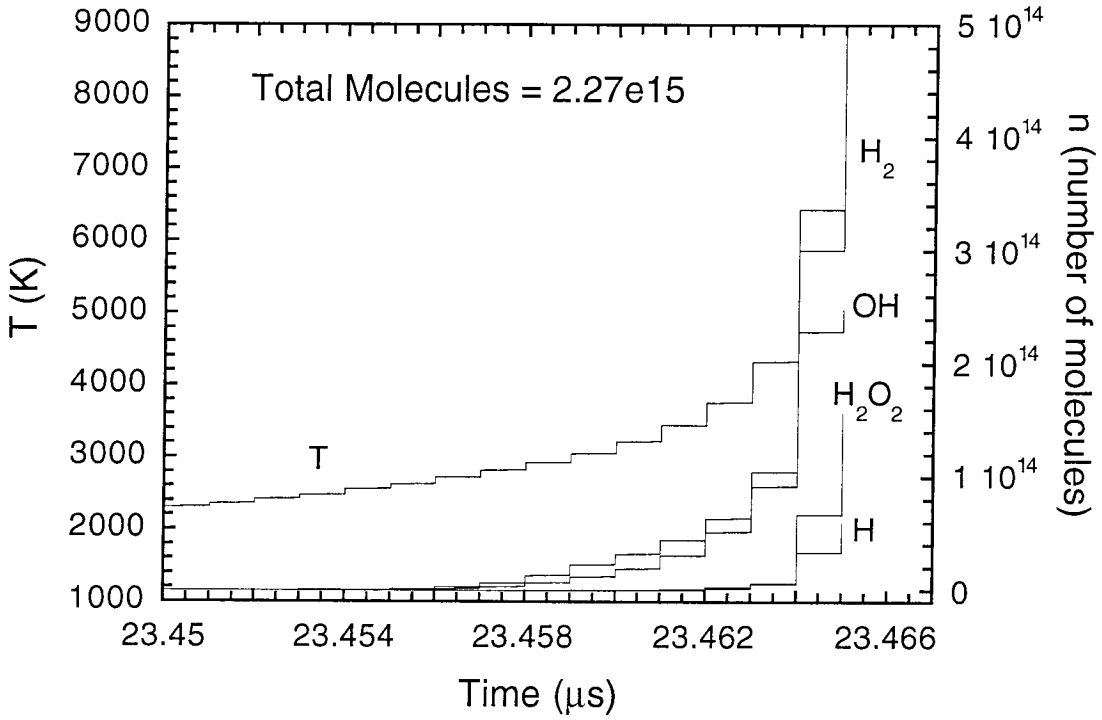

Figure A.6: The temperature and chemical species produced from the collapse of an oxygen bubble initially at R_0=41 μm, influenced by P_A=11 atm and 20 kHz.

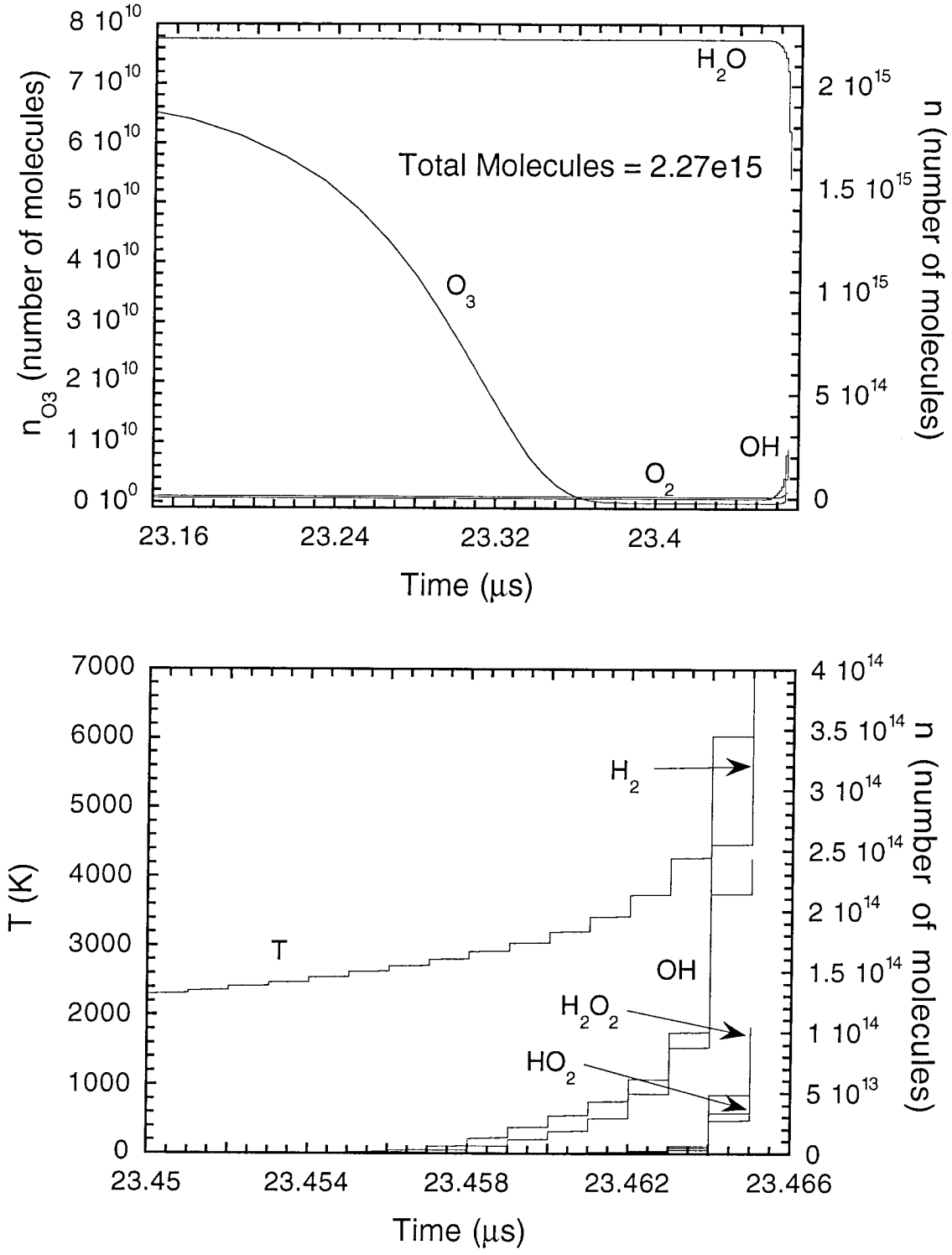

Figure A.7: The temperature and chemical species produced from the collapse of an oxygen bubble containing 1% O_3, initially at R_0=41 μm, influenced by P_A=11 atm and 20 kHz.

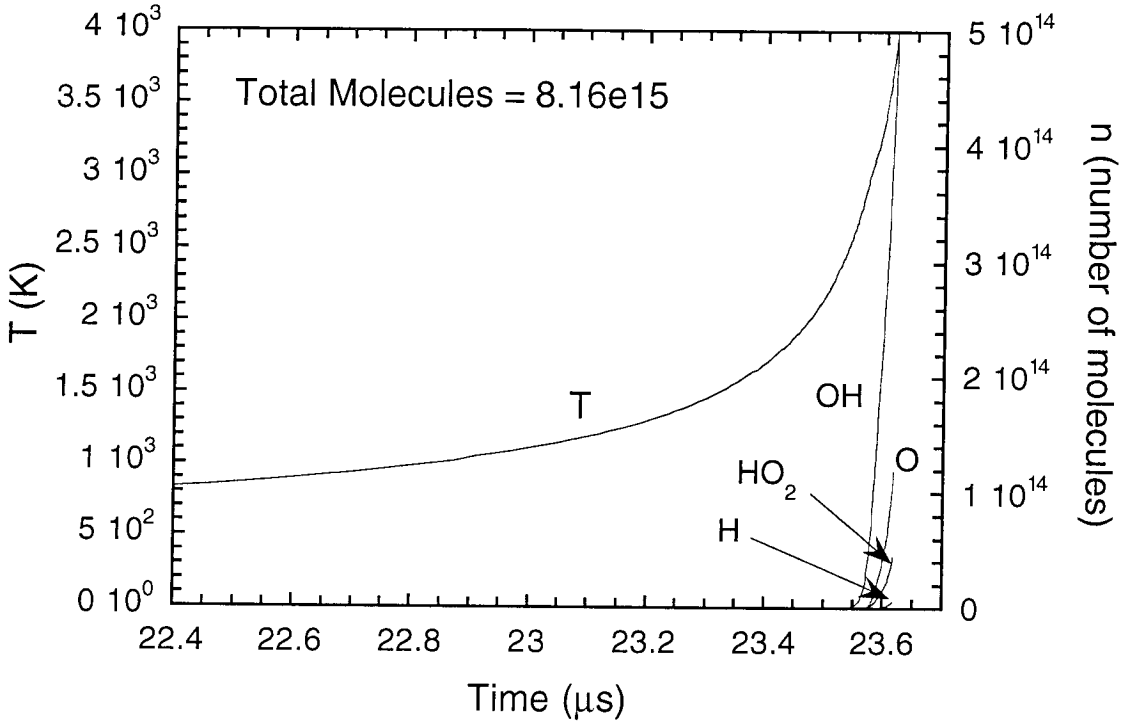

Figure A.8: The temperature and chemical species produced from the collapse of an oxygen bubble initially at R_0=390 μm, influenced by P_A=11 atm and 20 kHz.

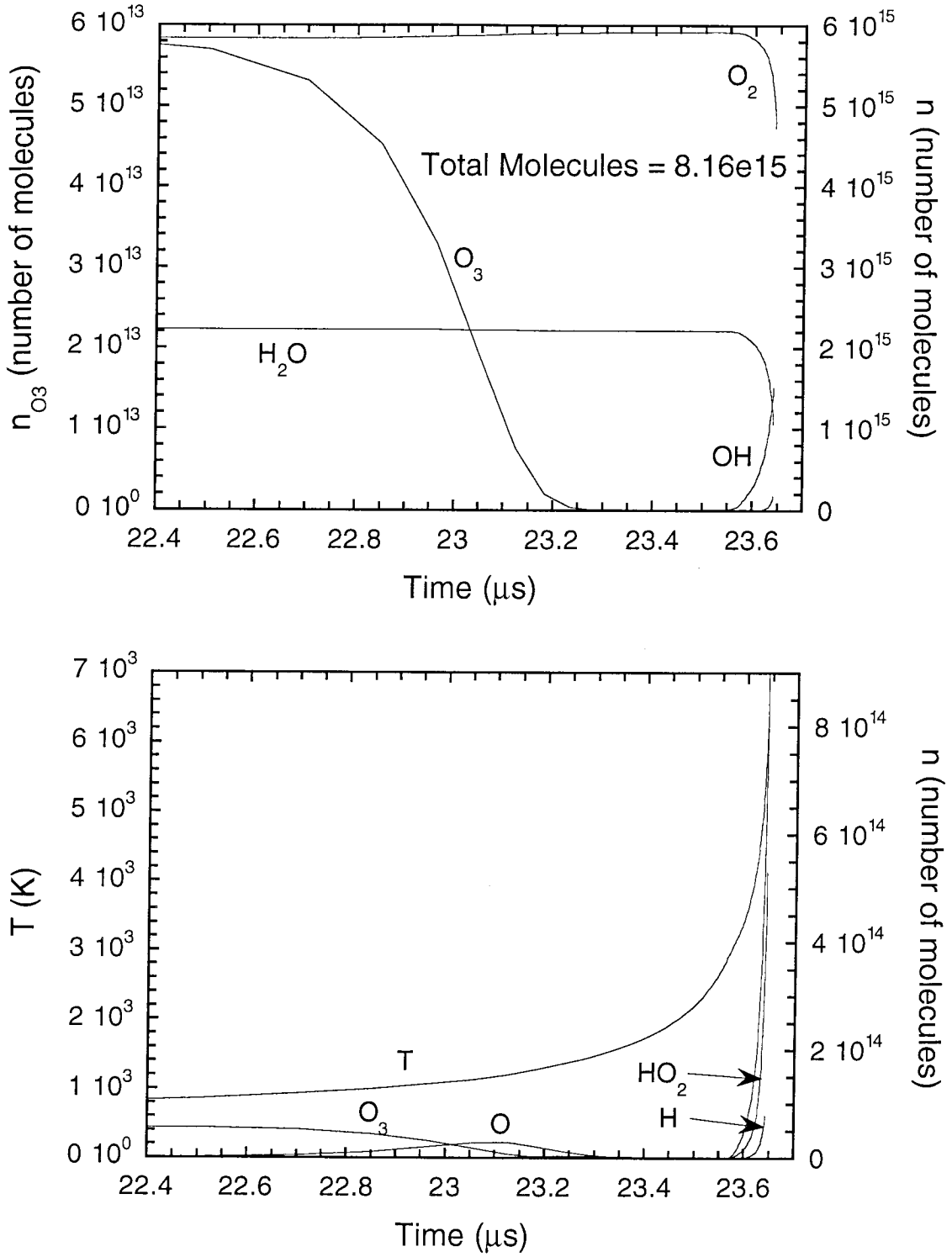

Figure A.9: The temperature and chemical species produced from the collapse of an oxygen bubble containing 1% O_3, initially at R_0=390 μm, influenced by P_A=11 atm and 20 kHz.

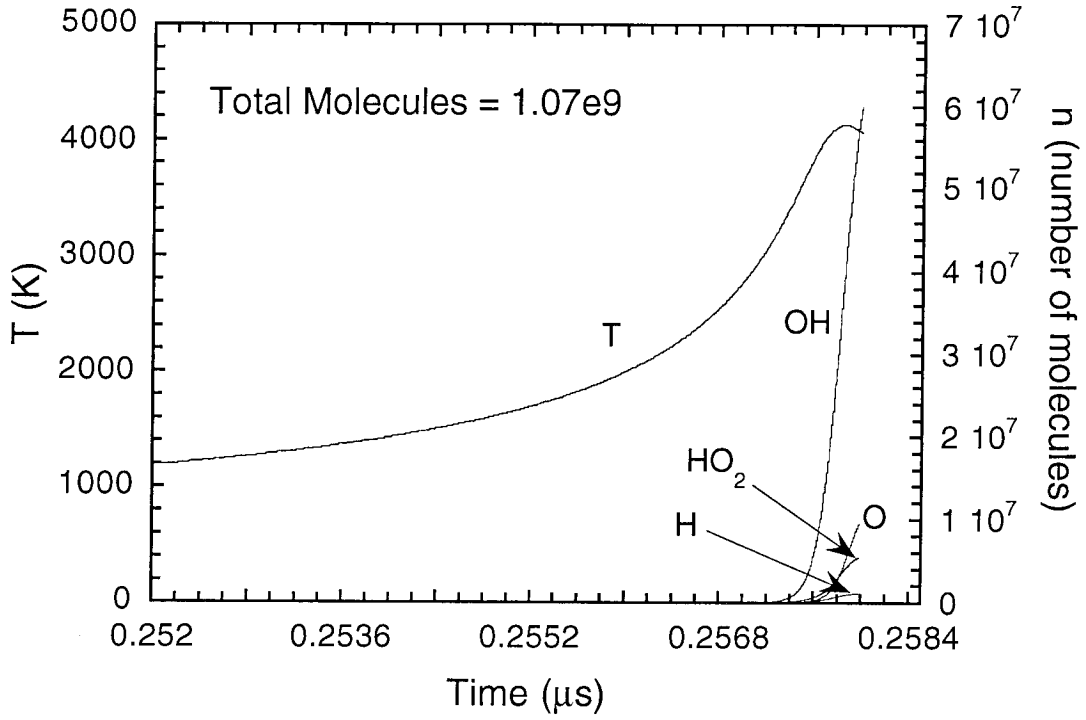

Figure A.10: The temperature and chemical species produced from the collapse of an oxygen bubble initially at R_0=1.5 μm, influenced by P_A=2 atm and 500 kHz.

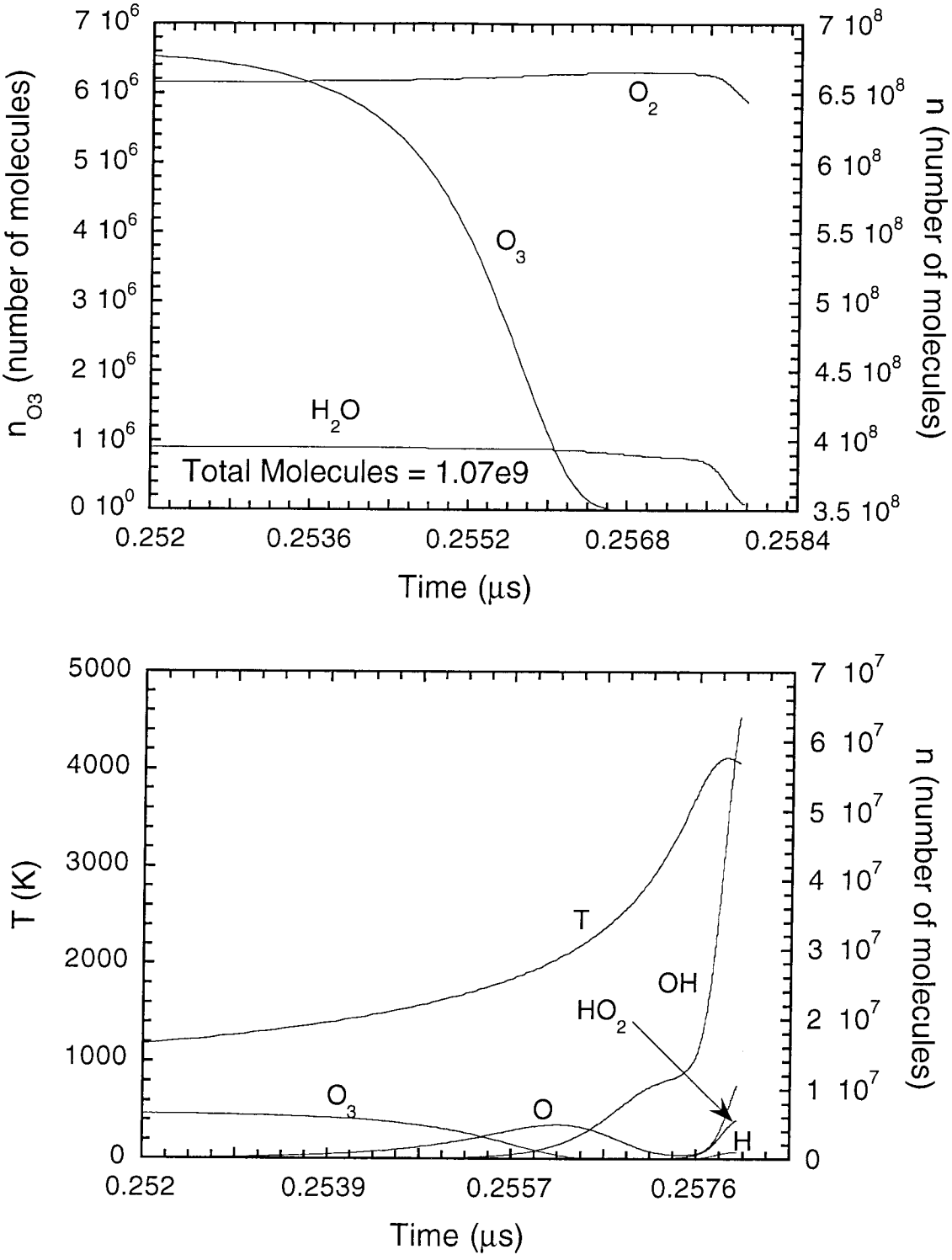

Figure A.11: The temperature and chemical species produced from the collapse of an oxygen bubble containing 1% O_3, initially at R_0=1.5 μm, influenced by P_A=2 atm and 500 kHz.

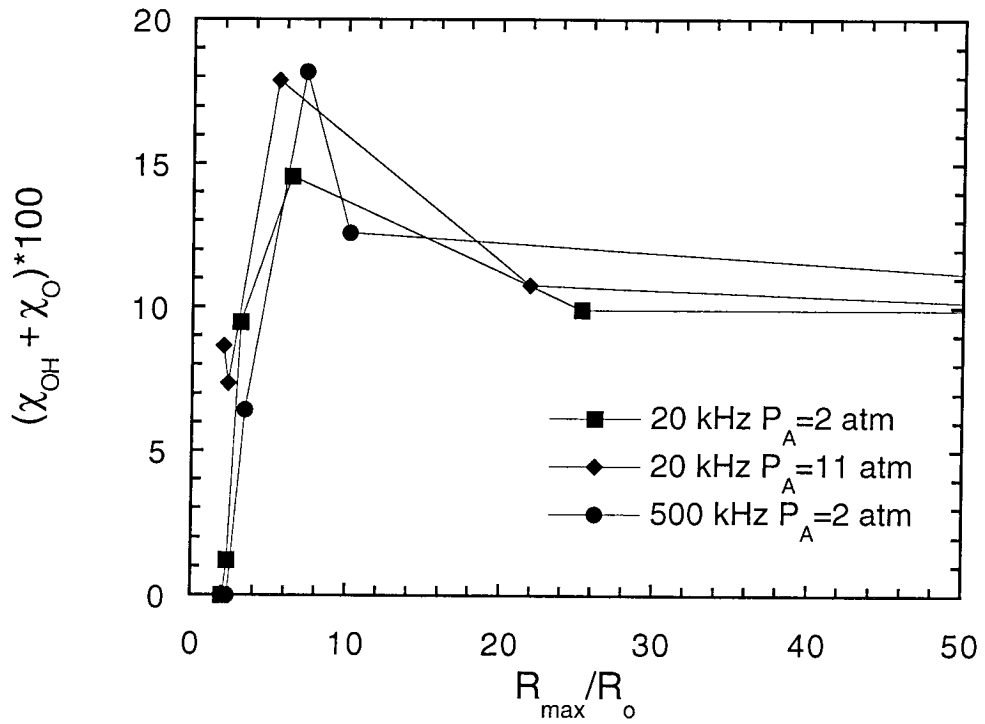

Figure A.12: The mole fraction of OH and O produced as a function of the expansion ratio at 20 kHz and P_A=11 atm, 20 kHz and P_A=2 atm and 500 kHz and P_A=2 atm.

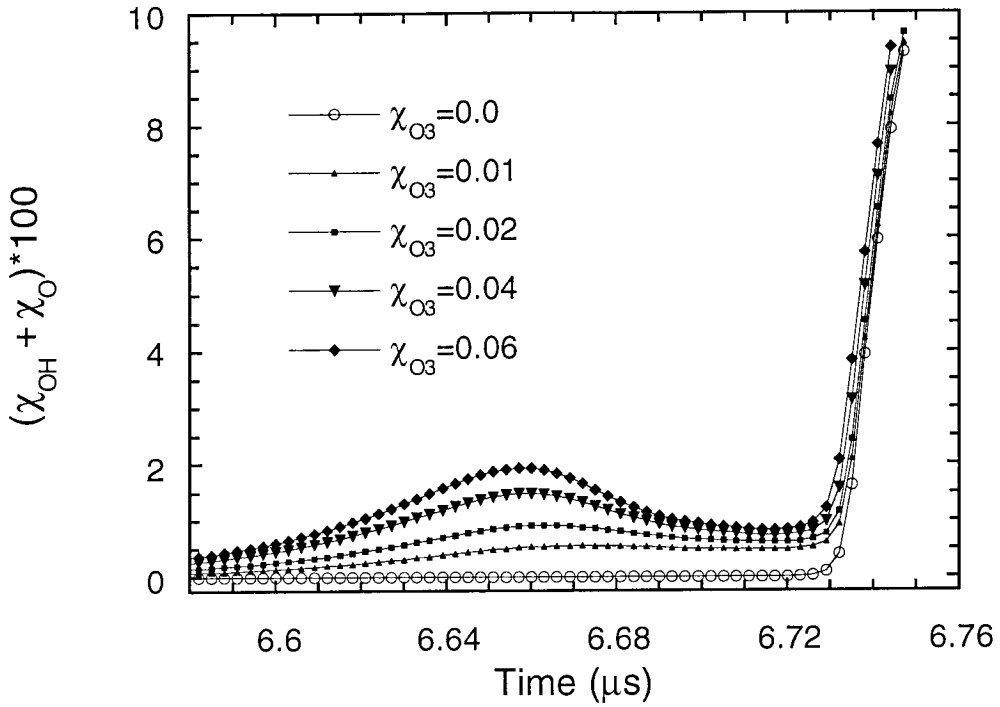

Figure A.13: The mole fraction of OH and O produced in a collapsing bubble initially at R_0=41 μm and influenced by P_A=2 atm at 20 kHz for various mole fractions of O_3.

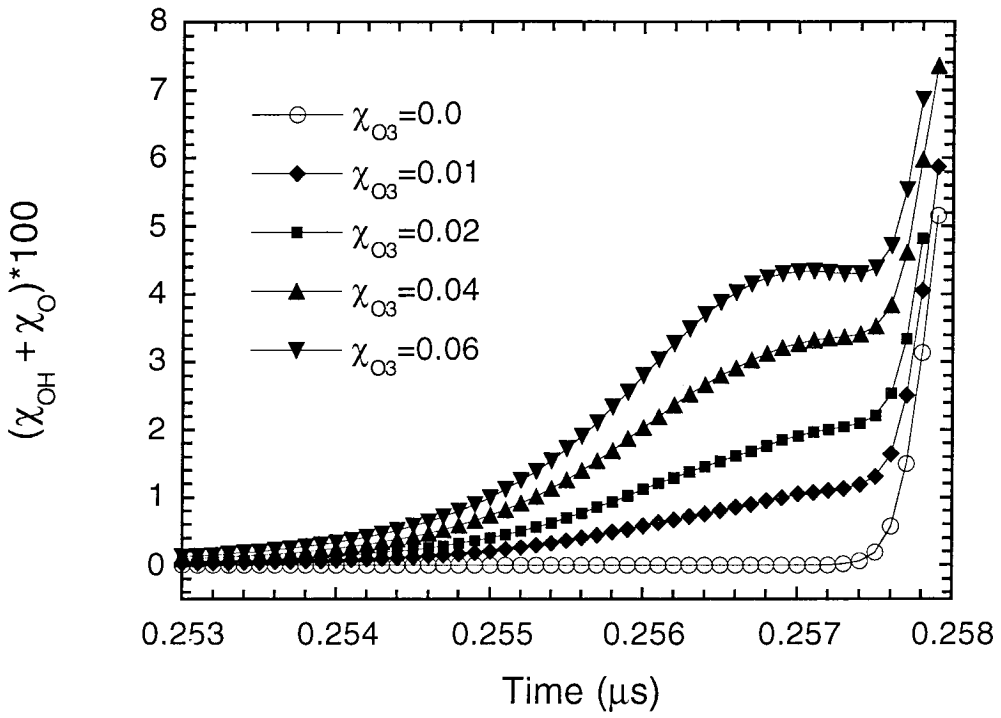

Figure A.14: The mole fraction of OH and O produced in a collapsing bubble initially at R_0=1.5 μm and influenced by P_A=2 atm at 500 kHz for various mole fractions of O_3.